SCREENING INFANT'S DEVELOPMENTAL ASPECTS OF LEARNING DURING STANDING BY MEASURING PRESSURE DISTRIBUTION BENEATH THE FEET

A THESIS SUBMITTED TO
THE GRADUATE SCHOOL OF NATURAL AND APPLIED SCIENCES
OF
MIDDLE EAST TECHNICAL UNIVERSITY

BY

ELMIRA POURREZA

IN PARTIAL FULFILLMENT OF THE REQUIREMENTS
FOR
THE DEGREE OF DOCTOR OF PHILOSOPHY
IN
ENGINEERING SCIENCES

AUGUST 2022

Approval of the thesis:

SCREENING INFANT'S DEVELOPMENTAL ASPECTS OF LEARNING DURING STANDING BY MEASURING PRESSURE DISTRIBUTION BENEATH THE FEET

submitted by **ELMIRA POURREZA** in partial fulfillment of the requirements for the degree of **Doctor of Philosophy in Engineering Sciences Department, Middle East Technical University** by,

Prof. Dr. Halil Kalıpçılar
Dean, Graduate School of **Natural and Applied Sciences** _____

Prof. Dr. Murat Dicleli
Head of Department, **Engineering Sciences** _____

Assist. Prof. Dr. Senih Gürses
Supervisor, **Engineering Sciences, METU** _____

Examining Committee Members:

Prof. Dr. Ayşen Tezcaner
Engineering Sciences, METU _____

Assist. Prof. Dr. Senih Gürses
Engineering Sciences, METU _____

Assist. Prof. Dr. Serdar Arıtan
Sports Sciences, Hacettepe University _____

Prof. Dr. Murat Zinnuroğlu
Internal Medicine, Gazi University _____

Assist. Prof. Dr. Murat Perit Çakir
Cognitive Science, METU _____

Date:10.08.2022

I hereby declare that all information in this document has been obtained and presented in accordance with academic rules and ethical conduct. I also declare that, as required by these rules and conduct, I have fully cited and referenced all material and results that are not original to this work.

Name, Surname: Elmira Pourreza

Signature :

ABSTRACT

SCREENING INFANTS DEVELOPMENTAL ASPECTS OF LEARNING DURING STANDING BY MEASURING PRESSURE DISTRIBUTION BENEATH THE FEET

Pourreza, Elmira
Ph.D., Department of Engineering Sciences
Supervisor: Assist. Prof. Dr. Senih Gürses

August 2022, 150 pages

This study investigates developmental changes in active usage of a contact surface and pressure distribution beneath infants' foot during learning of upright posture. We started studying longitudinally on 22 female and 22 male infants at their 12.5th months (1st trimester, T1) and kept on screening the same subjects at every three months (19 females and 12 males at 15.5th months (T2), 17 females and 7 males at 18.4th months (T3)), in Gazi University Hospital, Social Pediatrics Department. Each trial was fulfilled by an infant standing on a pressure pad placed on top of a force plate to collect the pressure distribution data beneath the feet for 15 sec at T1, and 25-sec at T2 and T3 and was repeated at least three times. Data collection sessions were also recorded with the camera. We expected to monitor the developmental changes at an infant's standing experience during their 2nd-year epoch through time-frequency domain analysis metrics on the overall CoPx and CoPy signals.The stabilogram plots showed noticeable shrinkage both in AP and ML directions. The phase plane plots showed shrinkage of the pattern in both CoPx and CoPy signals, and the amplitude of the frequency density function estimates and the frequency spectrum of CoP de-

creased significantly by time from T1 to T3. In the next part of the study, the image processing analysis have been done on pressure pad matrices. Time and frequency domain metrics of contact area, weight, pressure, and moment arms of front, mid, and hind regions of each foot have been estimated. In the frequency domain metrics there were significant shifts of the power of pressure distribution and moment arms to the lower frequencies due to the trimesters. We observed high frequency pressure vibration at the Mid foot at all trimesters. Further, we revealed higher frequency manifestations of moment arm at Fore foot in regional CoPx, which may be pointing to the role of the Fore foot as the controller and Mid foot as the load transmitter. Moreover, nonlinear dynamic analyses have been performed and led us to calculate the characteristic metrics of the m-dimensional attractor dynamics constructed in phase-space by estimating critical τ (time-delay operator) from the CoPx signal through S-average displacement method. Further, Approximate Entropy (ApEn) metric was calculated by using critical τ estimates, which showed an increase in ApEn, from T1 to T3. These metrics, which define the characteristics of the developmental stages of motor learning, will help to illuminate the evolution of upright stance.

Keywords: Postural Control, Infant Biomechanics, Spatiotemporal Evolution, Infant's Foot Development, Quiet Stance

ÖZ

BEBEKLERDE "AYAKTA DİK DURUŞ" GELİŞİMİNİN AYAK ALTI BASINÇ DAĞILIMININ İNCELENEREK İZLENMESİ

Pourreza, Elmira
Doktora, Mühendislik Bilimleri Bölümü
Tez Yöneticisi: Dr. Öğr. Üyesi. Senih Gürses

Ağustos 2022 , 150 sayfa

Bu çalışma, dik duruşun öğrenilmesi sırasında bir temas yüzeyinin aktif kullanımındaki gelişimsel değişiklikleri ve bebeklerin ayağının altındaki basınç dağılımını araştırmaktadır. 12 aylık yaşlarında (1. trimester, T1) 22 kız ve 22 erkek bebek üzerinde bir devamli çalışmaya başladık ve aynı denekleri her üç ayda bir (19 kadın ve 15 erkek 15.5 ayda (T2), 17 kadın ve 7 erkek 18.4 Ayda (T3), Gazi Üniversitesi Hastanesi, Sosyal Pediatri Anabilim Dalı devam ettik. Her deneme, T1'de ayakların altındaki basınç dağıtım verilerini 15 saniye boyunca ve T2 ve T3'te 25 saniye uzunluğunda bir kuvvet platform üzerine yerleştirilmiş bir basınç pedi üzerinde duran bir bebek tarafından gerçekleştirildi ve en az üç kez tekrarlandı. Veri toplama kurulumu ek olarak bebeklerin tepkilerini videoya çekmek için bir kamera içermektedir. Genel CoPx ve CoPy sinyalleri üzerindeki zaman-frekans etki alanı analizleri metrikleri aracılığıyla bir bebeğin 2. yıl döneminde ayakta durma deneyimindeki gelişimsel değişiklikleri izlemeyi umduk. Stabilogram grafikleri hem AP hem de ML yönlerinde fark edilir bir küçülme gösterdi. Faz düzlemi çizimleri, hem CoPx hem de CoPy sinyallerinde modelin küçüldüğünü gösterdi ve frekans yoğunluğu fonksiyonu tahminlerinin gen-

liği ve CoP'nin frekans spektrumu zamanla T1'den T3'e önemli ölçüde azaldı. Çalışmanın bir sonraki bölümünde, basınç pedi matrisleri üzerinde görüntü işleme analizi yapılmıştır. Her ayağın ön, orta ve arka bölgelerinin temas alanı, ağırlık, basınç ve moment kollarının zaman ve frekans alanı metrikleri tahmin edilmiştir. Frekans alanı ölçümlerinde, trimesterler nedeniyle basınç dağılımı ve moment kollarının gücünde daha düşük frekanslara doğru önemli kaymalar oldu. Tüm trimesterlerde Orta ayakta yüksek frekanslı basınç titreşimi gözlemledik. Ayrıca, bölgesel CoPx'te Ön ayakta moment kolunun daha yüksek frekanslı tezahürlerini ortaya çıkardık; bu, Ön ayağın kontrolör ve Orta ayağın yük taşıyıcısı olarak rolüne işaret ediyor olabilir. Ayrıca, doğrusal olmayan dinamik analizler gerçekleştirilmiştir ve bizi, CoPx sinyalinden S-ortalama yer değiştirme yoluyla (S-average displacement method) kritik τ (zaman gecikme operatörü) tahmin ederek faz-uzayda oluşturulan m-boyutlu çekici dinamiklerin karakteristik metriklerini hesaplamaya yönlendirmiştir. Ayrıca, kritik τ üzerinden hesaplanan Entropi (ApEn) sonuçları, T1'den T3'e bir artış gösterdi. Motor öğrenmenin gelişim aşamalarının özelliklerini tanımlayan bu metrikler, dik duruşun evrimini aydınlatmaya yardımcı olacaktır.

Anahtar Kelimeler: Postur Kontrolu, Bebek Biyomekaniği, Mekân-zamansal Evrimi, Bebek Ayağı Gelişimi, Sakin Duruş

To Vahid,

My Love, My Life, My Other Half

ACKNOWLEDGMENTS

First and foremost, I would like to express my deepest gratitude to my supervisor, Assist. Prof. Dr. Senih Gürses, assisting me with his extensive knowledge, thoughtful guidance, ample experience, and constructive feedback. I had an excellent opportunity and a great privilege to work with him. I appreciate his commitment to securing financial support for my studies and my attendance at research conferences during my study. He is genuinely a great advisor, and I am highly honored to have studied under his supervision.

I also would like to thank Prof. Dr. Ayşen Tezcaner, Assist. Prof. Dr. Serdar Arıtan, Prof. Dr. Murat Zinnuroğlu , and Assist. Prof. Dr. Murat Perit Çakir the members of my advisory committee for their kind participation and valuable comments during this research. Particularly, I would like to express my sincere appreciation to Prof. Dr. Serdar Arıtan for his continued support and valuable suggestions and comments all these years.

I owe a great deal of gratitude to Prof. Dr. Murat Zinnuroğlu, Prof. Dr. Aysu Duyan Çamurdan, NP. Gülşen Bora Taş, Dr. Birsen Muci, and NP Ayşe Dündar members of the Gazi Hospital, Physical Medicine and Rehabilitation, and Pediatric departments, for their unending support and suggestions during this work.

I also would like to thank The Scientific and Technological Research Council of Turkey (TÜBİTAK) and METU Coordinatorship of Scientific Research Projects for providing me with financial support from the TUBİTAK 121M097 project.

I am very thankful to work with the family of the Posture group, Maryam Hassanpour, Gözde Yalçın, Ekin Varlı, Mehmet Imir, and specially Berat Can Cengiz and Naci Barış Yaradanakul, for their valuable knowledge, technical assistant, endless support, and motivation. I also appreciate the support and concern of my dear friends Dr. Maryam Parsian, Dr. Naeimeh Sharghivand and Ramez Mohammadi.

Finally, but not least, my heartfelt appreciation goes to my beloved parents, Tahereh and Gholamreza, and my sister Elham. Despite their distance from me, I always felt their presence and implacable and unending love and support by my side. Also, I want to express my gratitude to my mother and father-in-law, sister, and brother-in-law, for their endless support. My special gratitude goes to my beloved husband, Vahid Ghasemnejad Berenji, for being a great supporter alongside his inexpressible love and understanding during my Ph.D. journey.

TABLE OF CONTENTS

LIST OF TABLES

TABLES

LIST OF FIGURES

FIGURES

LIST OF ABBREVIATIONS

T	Trimester
CoP	Center of Pressure
CoPx	Component of CoP on x-direction
CoPy	Component of CoP on y-direction
AP	Antero-Posterior
ML	Medio–Lateral
FP	Force Plate
PP	Pressure Pad
L	Left
R	Right
FL	Fore(Front) Left
FR	Fore Right
ML	Mid Left
MR	Mid Right
HL	Hind Left
HR	Hind Right
M	Male
F	Female
IV	Independent Variable
DV	Dependent Variable
RM	Repeated Measure
MF	Multi Factor
FFT	Fast Fourier Transform
PSD	Power Spectral Density

CFREQ	Centroidal Frequency
CFREQM	Modified CFREQ
FD	Frequency Dispersion
PF	Power Frequency
R_{xx}	Correlation function
$G_x(f)$	Power Spectral Density Function
μ_k	Spectral Moments
ξ	Phase Point
τ	Delay Vector
$S(\tau)$	Average Displacement
D	Dimension
I	Information
R	Reservoir
P	Probability
ε	Tolerance Metric
WN	White Noise
ApEn	Approximate Entropy

CHAPTER 1

INTRODUCTION

1.1 Motivation and Problem Definition

It has been recently being investigated how the pressure distribution beneath the foot points to the active usage of the foot in standing adults. Nevertheless, it offers new perspectives in postural research by introducing foot-triggered sensory-motor control strategies in quiet standing dynamics. Furthermore, the spatiotemporal evolution of physiological postural control strategies has not clearly been identified yet. Thus, we have chosen developmental aspects of the infant's postural adjustments as a media to explore learning of biped standing.

1.2 Human Posture

Human posture is defined as the individual's positioning of the trunk and limbs according to each other and their orientation in space [7]. There are a number of milestones required for the development of posture during the first 18 months of a healthy developing infant. This process begins with a situation where the body is fully supported by a surface and continues to a state that requires complex motor abilities such as strength, muscle coordination, and balance, such as sitting and standing without any support [8].

Learning to stand independently is a motor task with a high degree of difficulty [9]. The stages of child development from sitting to walking on their own represent a timetable of significant milestones in the progress of coordination and motor control [10, 11, 12]. In fact, it is possible for infants to support themselves in the stand-

ing position at approximately 8 months and stand independently at approximately 11 months [13]. Most infants start walking independently around12 months; some do not walk until 15 months, but early walking is not associated with further development in other areas [14]. The feet are crucial structures that help infants explore, interact with, and study their physical and social environments, along with changes in the central nervous system. The foot continues to change during infancy as it transforms from an organ largely utilized for reaching to one with a weight-bearing structure[15]. During this time the foot's structures and functions must adapt to the demands of weight bearing and become increasingly crucial for movement[16]. At first, infants start walking with a wide-based gait. Knees are bent and arms flex at the elbow. The whole body turns with every step; toes may be turned in or out. Feet can hit the floor flat. Subsequent improvements provide greater stability and energy efficiency. After a few months of practice, the center of gravity shifts back and the trunk remains more stable, while the knees are extended, and the arms swing to either side for balance. The toes are better aligned, and the infant can stand, turn, and lean without tipping. Moreover, between the ages of 18-24, motor development increases with the development of balance and responsiveness, with the emergence of running and stair climbing [14]. For an infant, standing up and walking means stepping into a new world where spatial constraints are removed. Posture control basically serves two purposes: The first is to maintain balance by keeping the center of pressure and the projection of the center of gravity within the support surface in the static state. Its second purpose is to serve as an interface between action and perception in dynamic conditions [17].

In 1999, Barella and Jeka conducted a study on 5 newborn infants to understand the developmental changes of standing without support. Based on the known milestones for the motor development process of newborns, they divided this process into 4 periods: 1. pulling to stand, (PS); 2. standing alone (SA); 3. walking onset, (WO); 4. 1.5 months post-walking, (PW). In this study, they examined the magnitude of the contact force applied in the process of learning the upright posture, the amount of body oscillation, and the temporal relationship between the applied force and body sway in four different developmental periods. While the infants were standing on a platform, they placed a contact surface that was asked to touch with their right hand.

The results revealed that as the standing experience increased, the force applied to the contact surface of the hand and body sways decreased. The applied force and body sways in the anteroposterior axis were consistently proportional (r $\sim$ 0.65). In the PS, SA, and WO periods body oscillations were 45 ms temporally ahead of the contact force. In contrast, in the PW period, the temporal relationship was reversed, and the applied force caused body oscillation ($\sim$ 140 ms). These results show that initially infants use surface contact as a mechanical purpose, but later for orientation information that provides posture control [9].

In addition, in a study conducted by Metcalfe and Clark in 2000, on the developmental stages of infants, it was shown that posture and movement development provide an important perspective for understanding individual development of the perception-action relationship. In this study, 13 infants were examined over time (cross-sectionally) in a quiet stance with their hands free or by lightly touching the contact surface. Average oscillation amplitude results show that infants use light touch to reduce sways ($\sim$ 28-40$\%$), as previously seen in adults [18]. In addition, when using the contact surface, movement patterns of the head and body show decreased temporal coordination ($\sim$ 25-40$\%$) and increased temporal variability compared to non-touch conditions. These findings are explained by the general conclusion that in discussing the relationship between perception and action, according to individual development, infants use somatosensory information exploratively / actively to help them develop a correct control of upright posture [19].

Accordingly, in another study [20], which investigated the relationship between quiet stance and light touch contact, they examined two types of newborns who learned to stand. First, it is the longitudinal study of infants' quiet stance during the first 9 months in the initial phase of independent walking. The second is to examine the effect of sensory mechanical conditions on infants ' posture control, such as light touch support. As a result of this study, a) with increasing walking experience, the oscillations of infants during standing upright evolve towards a lower frequency oscillation, b) walking provides a rich and dynamic sensory-motor experience and thus contributes to the development of posture control of infants, c) A light touch on a surface has been shown to stabilize the infant's posture by changing the dynamics of the swing as well as reducing the amplitude of its oscillations [20].

On the other hand, it is important to examine the information content of posture oscillation patterns during quiet stance. The posture oscillation patterns of 16 newborns (9 girls and 7 boys, average age = 11 months and 3 weeks) were compared in two experimental conditions: standing while holding a toy on a force platform and not holding it. The infants showed a lower amplitude posture swing and more complex swing patterns while holding the toy. These changes show that infants adapt their posture oscillations to make it easier to visually fix the toy in their hands. Infants exhibited posture oscillation patterns that were seen as more exploratory in nature when they simply stood. The exploratory posture oscillations that infants exhibit provide them with the opportunity to learn about the possibilities of standing upright. These results show that infants who have just started standing can control their posture depending on the task [21].

In terms of research method and measurement techniques, the evaluation of early walking patterns using plantar pressure distribution measurements of upright stance promises new perspectives. On this topic, a study was conducted on 42 children in the first year of walking [22]. In this study, plantar pressure distribution patterns were measured every 3 months with a pressure pad. During this 1-year observation, infants took several steps before reaching the platform to capture the loading pattern of the foot during natural walking. Anthropometric data of the infants showed an increase in height and body mass due to growth. In addition, they showed that there was a significant decrease in the foot shape index due to the decrease in the width of the middle foot and the increased foot length. This study shows that there are significant changes in the shape and loading characteristics of the infant's foot from standing up to the time he/she starts walking. Some infant displayed a very mature plantar pressure pattern after 1 year, while others continued to show an immature loading pattern [22].

Regarding the quiet stance paradigm, Lee I. et al. [23] conducted a study. In this study, they discussed two important approaches used in explaining the cause-effect relationship. In the traditional one, changes in postural behavior are assumed to be the result of differences in sensory information inputs. In this approach, more information reduces posture oscillation and is referred to as "information assumption" [24, 25, 26]. On the other hand, in the second approach, there is the view that changes in postural

metrics occur as a result of a facilitation provided by the active contribution of the postural system to meet new demands imposed by task manipulations [27, 28, 29, 30]. In other words, the postural system actively increases or decreases oscillation to facilitate achievement of a task (maintaining eye fixation, oscillating simultaneously with a stimulus, etc.) This approach is called the "postural facilitation assumption". With this approach, different tasks are not expected to result in different postural behaviors. Rather, the postural system changes its dynamics in order to perform a task: the system determines its behavior for a given set of task requirements [23].

In order to examine the postural oscillations discussed methodically in the above paragraph, the sensory-motor and psycho-social development of upright posture in infants must have reached a certain level of maturity [14]. However, before reaching this level, infants have been observed to exhibit a dissociated type of posture behavior compared to adults. It has been observed that infants use their feet one by one (cannot use synchronously together) before they can stand upright (biped stance) using both feet, and even use a part of their feet (mostly the back part) preferentially. Therefore, infants must have a motor repertoire [31] for achieving the characteristic patterns seen in adults' postural behaviors. In this case, the subject that needs to be investigated is how infants spend the learning process in the second year of their life from sitting without support to standing and walking without support. This process must be closely observed to understand sensory-motor control strategies in infants. To understand how the infant learns to stand and walk, we need to see its spatial and temporal evolution. Based on our previous studies, simultaneous measurement of plantar pressure distribution (distributed load system) in quiet stance is not only temporal [32, 33, 34], but can also be said that it allows the spatial distribution to be examined. The aim of this study is to illuminate the spatio-temporal evolution of quiet stance by combining these two methods. Thus, for understanding the postural dynamics and control (sensory-motor control), beside the classical engineering approach (stable equilibrium state), the modern approaches (statistical mechanics), that provides freedom based on probabilistic quasi dynamics (local instability around the equilibrium point) will also be beneficial. This modern approach obliges the dynamics of posture to be examined not only by time signals (CoP signal) but also by underfoot load distribution measurements. At the end of this research, the analysis of

the obtained data will be a powerful reference for clinical studies and will be a new way of screening postural disorders for early-stage diagnosis.

The history of the study on the relationships between the functional anatomy of the foot and the human upright posture goes back to researches in the 1950s [35, 36, 37, 38]. Recently, the relationship between the measurable distribution of pressure beneath the feet during standing and active usage of the foot has been investigated. However, revealing sensory-motor control strategies triggered by foot senses in quiet stance dynamics offers a new perspective for posture research [39]. We believed that learning upright posture should go to earlier stages in order to examine the spatiotemporal evolution of this behavioral relationship between active usage of the foot and upright posture observed in adults. For this reason, assuming that the sensory-motor and psycho-cognitive development of infants between 12 and 24 months is critical and can be examined, we decided to start a mutual study with Gazi University Faculty of Medicine, Social Pediatrics Department, which is planned to involve approximately 50 infants. Therefore, this project has a unique value in terms of sample size as well as studying the first learning phases of standing upright with longitudinal depth.

However, the limited number of studies on the role of somatosensory inputs in the postural control of infants suggests a notable gap in infant sensorimotor literature. One of the reasons for this gap may be the difficulty in designing experimental situations / conditions that enable analysis of postural development in infants. Typically, postural tasks require a quiet standing for 20-30 seconds. Obviously, this experiment is a difficult, if not impossible, task for a baby who is just trying to learn upright postural control. On the other hand, if the posture control is expected to be completed so that the required data of infant can be measured during the quiet stance, the monitoring of the developmental processes may be missed. Therefore, it is necessary to conceive an optimal data collection method and timing to monitor the spatial and temporal evolution of physiological posture control strategies.

In this study, measuring infants in critical developmental periods gets possible as a result of using the Robust Child Monitoring Appointment System together with the Social Pediatrics Department and cooperating with their families. Thus, measurements of standing upright posture from infants can be possible for a minimum of

15 seconds during data collection sessions. These measurements, being collected by a pressure pad (Tekscan® Matscan), will determine the pressure changes under the foot, for the first time in future analyzes. It is the first time to learn the dynamics of human upright posture through mapping the pressure under the foot with frame by frame and pixel by pixel method, and it will make it possible to use it for enlightening the postural control strategy. This research conducted with a larger number of participants (44 infants) compared to studies with fewer infants in the past, therefore, the richness of the findings and the reliability of the results will increase in this study with a large group of participants. Moreover, high reliability percentage will make this study a usable reference in the Children's Clinic. Thus, in order to reveal the dynamic characteristics of standing upright observed in adults and to understand how the sensory-motor control strategies are formed, we started a study that aims to observe, measure and evaluate infants from the first moment they begin to experience upright stance. The research questions we ask to achieve this goal are:

- How do infants learn to stand upright by using both feet together?

  Observing the coordination and learning process, occurring during infants first experience of quiet stance by using their feet one by one, and then using both feet together (lateralization problem).

- How does the spatiotemporal evolution of physiological upright posture dynamics occur?

- How do sensory-motor control strategies develop in quiet stance dynamics in infants?

  Since the last two questions are about how dynamic patterns that have been studied for a long time in adult posture are formed, we expect them to be discovered. However, since the first question was highlighted when the first data of this study was started to be collected and this situation is accepted a priori in adults, our answer to this question can be discussed. Therefore, the hypothesis we put at the beginning of the study was mostly directed to the answers we would give to the last two questions. The metrics of non-linear systems derived from the complex dynamics of posture oscillation seen in adults are information dimensions (entropy metrics). Moreover, how these spatial (dynamics embed-

ded in the phase-space) metrics evolved in time will be discussed in this study. Our expectation is that the information dimension will shrink over time as the transition from explorative search to exploitation is shown.

1.3 Obstacles, Contributions and Novelties

The obstacles of this study and our contributions are as follows:

- Study on the infants and its difficulties due to their young age, being dynamic, less cooperative and patient during the data collection process, and the restrain with the duration of the collected data make this investigation much more difficult

- The discontinuity of the infants during the longitudinal study also make some restrictions on the analysis

- The greatest impediment of this study was the Covid-19 pandemic, that caused the closure of the posture lab in Gazi Hospital and made us to stop the investigation before it's over. Our plan was to complete 5 trimesters (T) within the infants' first year of walking (T1:12-14 months, T2:15-17, T3:18-20, T4:21-23, T5:24-26). However, we had to stop at the beginning of T4.

- Despite all the above restrictions, this study makes its way through some significant findings regarding the newly standing infants and we could catch some of their major milestones during the transition from an unbalanced naive quiet stance toward an experienced one.

- The high number of subjects, and a strong statistical results is also considered a great success for us.

- This study and future studies based on this one will open new doors into infants' posture and will reveal many unknown and uncertain issues regarding the foot growth and development of standing and walking skills.

1.4 The Outline of the Thesis

It is clear that measuring and quantifying the infants foot across early developmental milestones is beneficial. Studies on younger kids who are just learning to walk, however, have provided only a limited amount of information, and there are still questions and gaps in our knowledge about how the foot structure changes in response to the application of pressure during the development of standing and walking skills [16]. Investigating the spatiotemporal evolution of physiological postural control strategies in infants and exploring the developmental changes in active usage of a contact surface by evidence-based clinical practice gives us the opportunity to explore the less known aspects of the infants upright stance. Doing collaborative research in a multidisciplinary study provides extra benefits for filling the blank spots in technology and public health and brings more reliable and applicable services for both healthy communities and patients. We assume this study as a small section of a huge investigation on the very unknown features of the early development phases in infants.

CHAPTER 2

EXPERIMENTS AND METHODS

Experiments and data collection are performed in Posture Laboratory at Gazi University Hospital, Physical Therapy, and Rehabilitation Department.

2.1 Overview of the Subject testing and data acquisition

A longitudinally study on 22 female and 22 male healthy infants (mean age of 12.5 months old, and mean weight of 93.65 ± 9.98 N) (first trimester, T1) was performed and we kept on screening the same subjects at every three months (19 females and 12 males at mean age of 15.5 months old, and mean weight of 98.27 ± 10.82 N (second trimester, T2), 17 females and 7 males at mean age of 18.4 months old, and mean weight of 107.94 ± 12.25 N (third trimester, T3)), during their normal checkup appointments in Gazi University Hospital, Social Pediatrics Department-Ankara/Turkey. The data collection procedure started when an infant and his/her parent came to the lab. First, a short introduction about the test and its purpose was given to each infant's parents. Then the following questions were asked about the infant:

- Child's personal information (name, surname, ID number)
- If he/she can stand without any help
- If they used a baby walker
- The month of standing alone
- The month of walking alone
- Explaining the test for them

- Meanwhile, we had a friendly conversation with the infant and tried to communicate by giving him/her some toys to feel safe and relaxed around.

Before the experiments for each infant, gender, age, used hand (if certain), weight, height, and foot length were recorded. These recorded information were further used in interpreting the results of numerical and statistical analysis.

Next, for starting the test, the parents were asked to put the infant on the setup and let him/her be there standing or sitting playing with toys and books until he/she gets used to the setup (1-5 min). When the infant feels ready, the parents were instructed to put him/her on the center of the square of the Tekscan® Matscan pressure pad, placed on top of a Bertec® force platform, and try to take his/her attention for at least 3 seconds. In this step, the weight (N) of the infant was measured with the force plate (3 sec). Then, the main trial was starting. Each trial was fulfilled by an infant standing on a pressure pad placed on top of a force plate to collect the pressure distribution data beneath the feet for 15 sec at T1, and 25-sec long duration at T2 and T3 and was repeated at least three times. During the data collection, infants' parents were beside them trying to get infants' attention towards themselves preventing them from being distracted and/or moving and walking around. After finishing the data collection, the next appointment was given for 3 months later. Force and moment signals at x-y-z axes were acquired at a sampling rate of 50 Hz by a force-plate (Bertec®, FP4060-10 600×400mm). Center-of-Pressure (CoP) time signals at antero-posterior (AP, CoPx) and medio-lateral (ML, CoPy) directions were then computed. Pressure distribution data under each foot were collected at 50 Hz using Tekscan® Pressure Pad. A picture taken during the experiment is given in Figure 2.1. The data collection setup additionally contained one camera for videotaping the infants' reactions.

2.2 Data Analysis

Postural control can be measured in several ways, but one of the most frequently used methods to evaluate prospective postural control during movement is to quantify the displacement of the center of pressure (CoP) over a relatively short time scale (seconds or minutes). The CoP is the location of the vertical reaction vector on the surface

Figure 2.1: An example subject during the data collection on a pressure pad placed on top of a force plate

on which the individual is positioned and is a weighted average of the forces acting on the surface [40]. Movement of the CoP is the body's neuromuscular response to the position of the body's center of mass [40]. Movement of the CoP over time reflects postural adjustment and creates a time series that can be analyzed for cyclical patterns [41]. Since CoP signal is measured from a plane in force plate, it has two components, CoPx and CoPy. While CoPx is the location of CoP on the antero-posterior direction, CoPy is the location of CoP on the medio-lateral direction.

In the Pressure Pad software, since the video quality is not high enough and specially in infants' feet with low pressure and force, and due to an incomplete shape of the feet, projection of foot shape is not perfect, so by applying the predesigned setup of "Drawing Polygons" facility of the Pressure Pad Matscan® software for dividing foot regions, each foot was divided into two regions as shown in figure 2.2. Selected foot regions were heel region (talus and calcaneus bone), and five metatarsal bones and phalanges; named as hind, and front regions, respectively. Since the arch of the foot in infants is not completed yet, there is no mid-foot region in selected areas. Distributed ground reaction forces were calculated then. The MatScan sensor detects subject's plantar pressure. This sensor is made up of over $2288\ (4452)$ individual pressure-sensing locations, which are referred to as "Sensing Elements" or "Sensels." The sensels are arranged in rows and columns on the sensor. Each sensel is 70.2579

mm^2 and the output of each sensel is divided into 256 increments and displayed as a value ("Raw" sum) in the range of 0 to 255. Thus, pressure distribution data of pre-mentioned regions in the left and right foot were obtained as a function of time.

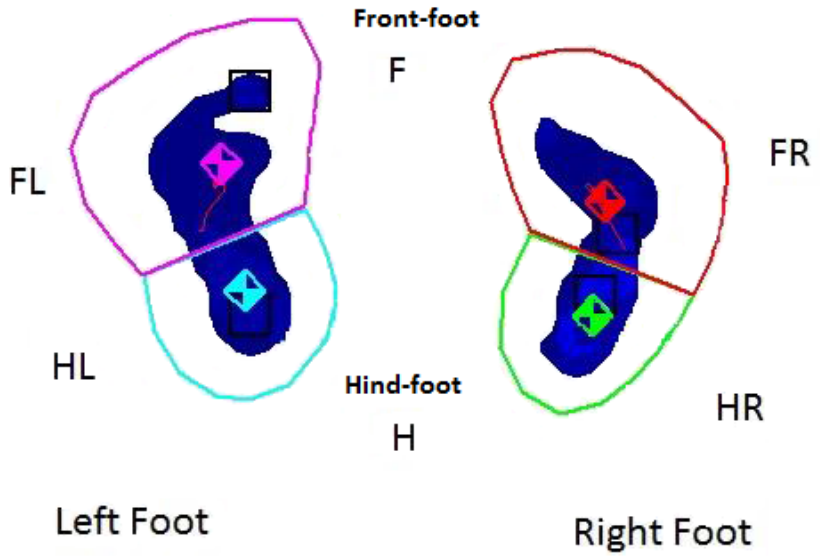

Figure 2.2: Regions of the foot

Since the applied pressure in infants' feet is lower than a healthy adult subject, for getting the optimal results from the plantar pressure beneath infants' feet, we changed the sensitivity level of the MatScan to Mid-1, which is one step more sensitive to the pressure than Default. Based on the method recommended by the MatScan manufacturer (Tekscan), before starting the data collection on each subject, calibration was performed. For calibration, the weight of the subject (in Newton) was separately measured by Bertec force platform through a 3 seconds quiet stand of the subject on the setup, and entered manually into the Matscan software. Then, this weight is applied automatically at an appropriate scaling to the raw outputs of the sensing elements such that the total force of the pressure pad is consistent with the weight of the subject.Next, Force signals of each foot were obtained as a function of time by averaging the pressure distribution data over its related plantar surface. And the four regions of the foot at the first phase of the analysis were named as FL for fore left,FR for fore right,HL for hind left and, HR for hind right (Figure 2.2).

2.3 Time Series Analysis

Center of Pressure (CoP) of time signals from the data collected by the force plate and the pressure pad were computed. In the time domain, mean and the variance at the CoP time signals were estimated in both anterio-posterior (CoPx) and medio-lateral (CoPy) directions. The representative plot of CoPx of a subject in T1 was given in figure 2.3.

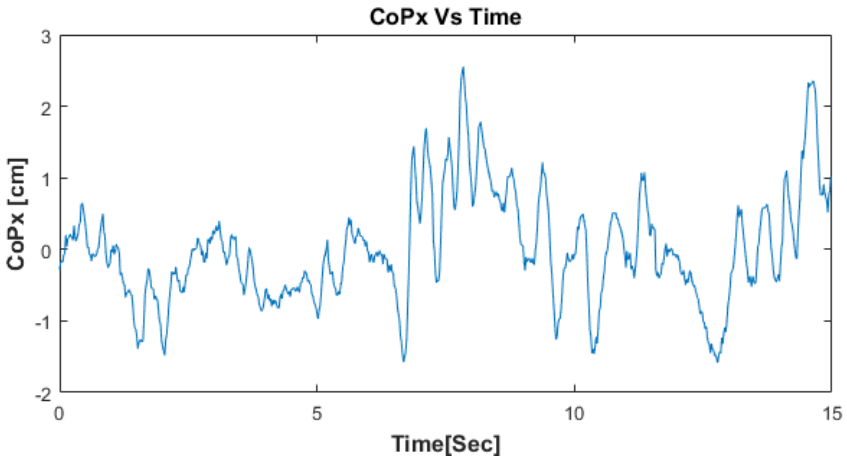

Figure 2.3: A Sample Plot of CoPx vs Time in T1

As shown in equation 2.1 and 2.2, these two components can be calculated using three force plate signals, F_z, M_x, M_y. Since we collected the data through 15 seconds in T1 and 25 seconds in T2, and T3, with 50 Hz, the array size of each trial was 750 and 1250, respectively.

$$\mathbf{CoP_x(i)} = -\frac{M_y(i)}{F_z(i)}, i = 1, ..., 750 \tag{2.1}$$

$$\mathbf{CoP_y(i)} = \frac{M_x(i)}{F_z(i)}, i = 1, ..., 750 \tag{2.2}$$

This time series signals, from which is derived metrics to describe human postural sway, was analyzed in both time and frequency domains. Before the analysis, linear detrend had been applied to the CoP data.

2.4 Frequency Domain Analysis

The frequency domain analysis is a good method to measure the amount of power presented at each frequency. Therefore, understanding the dynamics of the body sway and the strategies used by subjects through the spatiotemporal evolution is important.

2.4.1 Fast Fourier Transform (FFT)

To investigate the frequency characteristics of each foot's Front and Hind regions' signals, their force distributions were analyzed in the frequency domain. And to calculate frequency domain measures, we used MATLAB Fast Fourier Transform (FFT) function. Time series were detrended linearly before Fast Fourier Transformation. In the frequency domain, 50% and 95% power frequency, Centroidal Frequency (CFREQ), and Frequency Dispersion were calculated from methods described in Prieto et al. ([41]).) and ([42]).

2.4.2 Spectral Moments

Spectral moments, μ(k) were calculated through the following equation for $k = 0, 1, 2$:

$$\mu_k = \sum_{i=1}^{m} (i \times \Delta f)^k . G_x(i \times \Delta f) \tag{2.3}$$

Where Δf (1/T; T being the data collection time) is the frequency resolution, m is Nyquist frequency (1/2 of the sampling rate) divided by Δf and $G_x(f)$ is the power spectral density function estimate as a function of frequency, $f$in [Hz], obtained by FFT ([43]):

$$\begin{aligned} R_{xx}(\tau) &= \frac{1}{T} \int_0^T X(t) X(t+\tau) dt \\ G_x(f) &= 2 \int_{-\infty}^{+\infty} R_{xx}(\tau) e^{2\pi f \tau} d\tau \end{aligned} \tag{2.4}$$

Where τ is the delay operator and R_{xx} is the auto-correlation function.

The total power (POWER) is the integrated area of the power spectrum when $k = 0$ in equation (2.3).

$$\mathbf{POWER} = \mu_0 = \sum_{i=1}^{m} G_x(i \times \Delta f) \tag{2.5}$$

The 50% and 95% power frequency are the frequency which is found below 50% and 95% of the total power.

$$\sum_{i=1}^{v} G_x(i \times \Delta f) \geq 0.50 \times \mu_0 \tag{2.6}$$

$$\sum_{i=1}^{v} G_x(i \times \Delta f) \geq 0.95 \times \mu_0 \tag{2.7}$$

Where v is the smallest integer for which the equation holds.

2.4.3 Centroidal frequency (CFREQ)

After calculating the spectral moments and power, centroidal frequency (CFREQ) is defined as the frequency at which the spectral mass is concentrated, which is the square root of the ratio of the second to the zeroth spectral moment (see equation 2.3):

$$CFREQ = \sqrt{\frac{\mu_2}{\mu_0}} \tag{2.8}$$

Where we can also call it as the second moment. Moreover, for postural analysis we need more specific metric that gives us more reliable result in both high and low frequencies, thus we used the modified CFREQ (CFREQM) which is estimated from the equation below:

$$CFREQM = \frac{\mu_1}{\mu_0} \tag{2.9}$$

Which is also called the weighted average or the first moment.

2.4.4 Frequency dispersion (FREQD)

The frequency dispersion (FREQD) is a unitless measure of the variability in the frequency content of the power spectral density:

$$FREQD = \sqrt{1 - \frac{\mu_1^2}{\mu_0 \times \mu_2}} \tag{2.10}$$

The frequency dispersion is zero for a pure sinusoid and increases with spectral bandwidth to a maximum of one [44].

2.5 Pressure pad data analysis

2.5.1 Plantar pressure distribution chart

Plantar pressure measurements can be used to assess the loads to which the human body is subjected in quiet stance or normal walking. Measuring the distribution of force over each foot is useful as it provides detailed information specific to each region of contact. In this study, we investigate on the pressure distribution beneath newly standing infants' feet. Pressure pad distribution chart is an option in the MatScan pressure pad software, in which the matrix of whole movie of the frame data can be obtained. This matrix, which is called the plantar pressure distribution chart, represent all the collected data (whole movie) and it is possible to monitor the plantar pressure distribution changes during the quiet stance of the infant, frame by frame, and pixel by pixel.

2.5.2 Image processing of pressure pad matrices

Image processing analysis is the method we used for analyzing the matrices of pressure pad data frame by frame. In this method, we automized the previous method, the one in which we monitored all the frames of a matrix of every trial by a normal eye, and we took the record of any changes during 15 and 25 seconds of a quiet stance (750 and 1250 frames of a matrix). The automatized method, using MATLAB, make

tracking the changes faster, easier and more reliable, beside making possible to do lots of data process and analyses.

In this method, first we import the pressure pad data to MATLAB software, (each data represents one trial of a quiet stance of a subject), then we do the rest of the analysis by MATLAB codes. The original data which is imported to MATLAB contains both noise and required data, therefore, in the first step we need to eliminate noise from original data. By excluding noise, we have almost pure signal of a quiet stance which in the next step needs to be separated into left and right foot, and then with this code we can divide each foot into three regions of Fore, Mid and Hind which is more accurate with respect to the two regions we divided by the MatScan software tools. For each foot's region separation, we select 2 pixels of each foot one from first metatarsal bone beneath the second finger, and next from the end of the calcaneus to determine the index of the foot, and define the region limits of each foot ([45][46][47][48]).

Figure 2.4 shows the MATLAB figures in which a frame of the related matrix opens, and we should choose the index margins of each foot first by clicking under the second metatarsal region and then clicking on the lower calcaneus region and then press enter key to define the action. This procedure can be repeated as many times as we need and at the end the result of for example left foot index will be the mean of all the indexes we defined. Additionally, the first frame which is opened for one foot is the frame which has the most contact pixels with the mat, however the next frames will be chosen randomly from 750 or 1250 frames of that matrix. The same process will be repeated for the right foot and then we will have three identified regions for each foot, and the required estimations and measurements can be calculated for each region or the whole foot.

By investigation on each foot's three regions (Fore, Mid, Hind) we can evaluate the changes in pressure, force, moment arms (Anteroposterior (AP) and Mediolateral (ML) fluctuations), contact area, stabilogram, and frequency domain (Fast Fourier Transformation (FFT)) in each region (FL, FR, ML, MR, HL, HR) separately, and then each region's information can be compared with each foot's and both feet's data. Moreover, the changes of each region through the time can be followed by comparing each trimester's findings with the previous or next ones. Also, by the help of

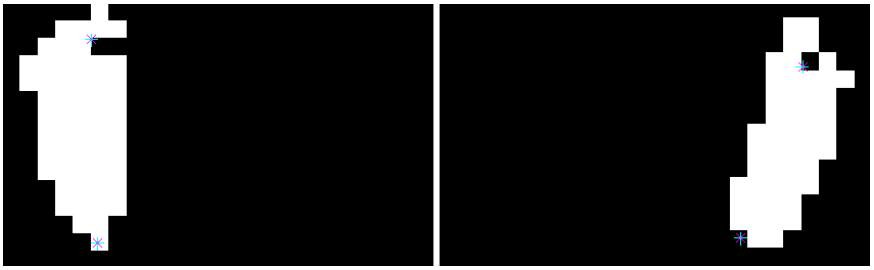

Figure 2.4: Frames of a pressure pad matrix for left and right foot to define the foot index.

this method the foot displacement problem is solved, and we can follow the changes during any foot movements and record the foot displacement frames as well as fluctuations in force and pressure distribution. We named this foot displacement as contact loss frames and the number of frames in which the foot has no contact as Δt.

After dividing each foot into three regions, the most critical evaluation that needed to be assessed during the image processing analysis are:

- **The AP and ML moment arms (cm):**

  Anteroposterior: AP-FL, AP-FR, AP-ML, AP-MR, AP-HL, AP-HR

  Mediolateral: ML-FL, ML-FR, ML-ML, ML-MR, ML-HL, ML-HR

  Pressure pad data is a matrix with 44 rows and 52 columns. And depending on the data collection time, we have 44×750×52 (for 15sec trials), and 44×1250×52 (for 25sec trials) matrices. Figure 2.5. shows the pressure pad matrix and three segments of a foot. All the estimations and calculations of this section will be based on these figures and matrices.

  Based on the figure 2.5, for estimating the weighted average moment arms, the following equations are calculated:

$$d_{FL}(AP) = \frac{\sum_i d_i \sum_j f_{ij}}{\sum_i \sum_j f_{ij}} \tag{2.11}$$

$$d_{FL}(ML) = \frac{\sum_i d_i \sum_j f_{ij}}{\sum_i \sum_j f_{ij}} \tag{2.12}$$

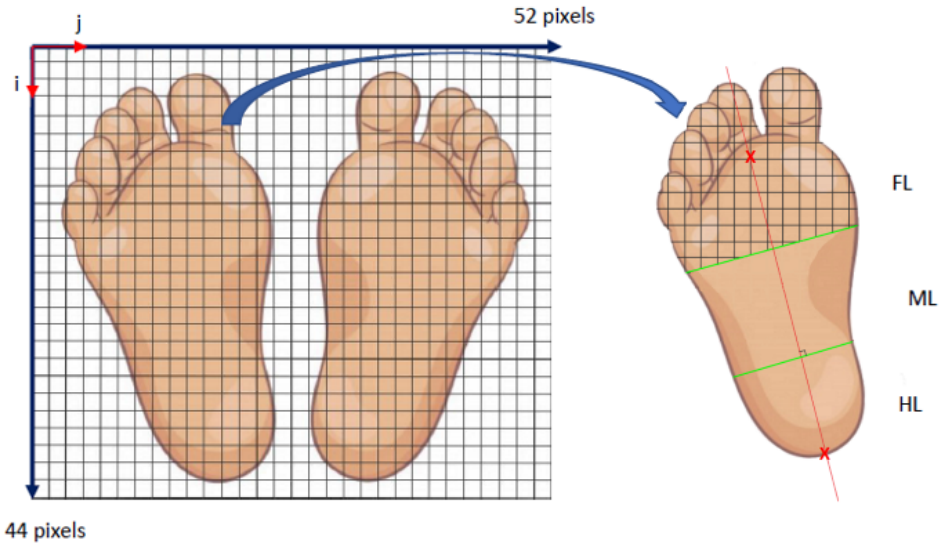

Figure 2.5: pressure pad matrix with 44 rows and 52 columns, three segments of the left foot (FL, ML, HL)

Where, AP is anteroposterior, and ML is mediolateral directions. f_{ij} is random variable, i is the number of rows, and j is the number of columns. For obtaining the weighted average moment arms of ML, and HL, and FR, MR, and HR, equations 2.11, and 2.12 can be repeated for those regions. Since the direction of matrix rows is positive from top to down, while the positive direction of anteroposterior is from down to top, in the MATLAB code we subtract the number of rows from the related number.

- **Pressure of each region (kPa):**

  The physical dimension of the pressure on each pixel of the pressure pad which is obtained from the Matscan software is given as kPa, and in order to change that to N, we need to multiply it with 0.0702579, thus we can write the following equation for the pressure on the Fore region of the left foot:

$$d_{FL}(P) = \frac{(\sum_i d_i \sum_j p_{ij}) \times 0.0702579}{(\sum_i \sum_j p_{ij}) \times 0.0702579} \tag{2.13}$$

  The equation 2.13 can be repeated for all the six regions of the feet for obtaining the related moment arm from the pressure data on each region of the feet.

- **Area of each region (cm^2):**

  The area of each pixel on the pressure pad is equal to 0.702579 cm^2, and for calculating the area for feet's six regions in [cm^2], we multiply the number of pixels in each row and column of each region (n) by the value of $\sqrt{0.702579}$, which is the value to change the result from pixel to cm.

- **Weight of each region and total weight (N):**

  Weight of each region is calculated by multiplying the pressure of that region by 0.0702579, which is the value of changing the pressure results from kPa to N. The total weight is being obtained from adding the six region's weight values.

- **Normalized weights with respect to each foot's weight (ratio):**

  There is also the normalized weight which is being obtained through the following equations for each region with respect to that foot's weight:

$$R_{FL} = \frac{W_{FL}}{W_L} \quad , \quad R_{FR} = \frac{W_{FR}}{W_R} \tag{2.14}$$

$$R_{ML} = \frac{W_{ML}}{W_L} \quad , \quad R_{MR} = \frac{W_{MR}}{W_R} \tag{2.15}$$

$$R_{HL} = \frac{W_{HL}}{W_L} \quad , \quad R_{HR} = \frac{W_{HR}}{W_R} \tag{2.16}$$

  Where $W_L(t)$ is:

$$W_L(t) = \sum_{K=F,M,H} W_{KL}(t) \tag{2.17}$$

  And $W_R(t)$ is:

$$W_R(t) = \sum_{K=F,M,H} W_{KR}(t) \tag{2.18}$$

- **Normalized pressure with respect to area of each region (kPa):**

The pressure signal from the pressure pad, for each pixel of the mat (p_{ij}), is obtained as kPa:

$$\begin{aligned} kPa &= \frac{N}{cm^2} \\ &= \frac{N}{10^{-4}m^2} \\ &= \frac{N}{m^2}10^4 \\ &= \frac{N}{m^2} \cdot 10 \cdot 10^3 \\ &= 10kPa \end{aligned} \tag{2.19}$$

Since the area of each pixel is 0.702579 cm^2, so we multiply each p_{ij} with this area, which gives us a metric in N ($kPa \cdot cm^2 = N$). So, then by summation of f_{ij} [N] on both i and j, we obtain the total Regional Weight (Force):

$$\begin{aligned} W_{Regional} &= \sum_i \sum_j p_{ij} \cdot 0.702579(cm^2) \\ &= 0.702579(cm^2) \sum_i \sum_j p_{ij} \end{aligned} \tag{2.20}$$

Where, for total weight of each region, we repeat the above equation. Next, for estimating the regional mean pressure we divide the total regional weight to the area of that region:

$$\bar{p}_{FL} = \frac{W_{FL}}{A_{FL}} \quad , \quad \bar{p}_{FR} = \frac{W_{FR}}{A_{FR}} \tag{2.21}$$

$$\bar{p}_{ML} = \frac{W_{ML}}{A_{ML}} \quad , \quad \bar{p}_{MR} = \frac{W_{MR}}{A_{MR}} \tag{2.22}$$

$$\bar{p}_{HL} = \frac{W_{HL}}{A_{HL}} \quad , \quad \bar{p}_{HR} = \frac{W_{HR}}{A_{HR}} \tag{2.23}$$

Thus, by substituting one of the above equations, we can rewrite it as follow:

$$\bar{p}_{Regional} = \frac{0.702579(cm^2)\sum_i \sum_j p_{ij}}{n \cdot 0.702579(cm^2)} = \frac{\sum_i \sum_j p_{ij}}{\sum_i \sum_j 1_{ij}} \tag{2.24}$$

Where, n is the total number of pixels in each row and column of each region.

- The frequency domain metrics (μ(k), CFRQ, and FD, (Equations 2.3, 2.8, 2.10))
- Mean and variance of weights and moment arms
- Plots of Weights, Moment arms, Contact area, Stabilogram, FFT, and PSD
- Runs test for randomness which is an algorithm to detect if the values in the data are in a random order or not. The test is based on the number of runs of consecutive values above or below the mean of data vector. The result h is 1 if the test rejects the null hypothesis at the 5% significance level, or 0 otherwise.

2.6 Statistical Analysis

Statistical analysis is the science of collecting, exploring and presenting large amounts of data to discover underlying patterns and trends. In this study we applied different types of the statistical analysis due to the different purposes for data evaluation. Since from all the subjects that were being studied, there were five female subjects that have been come to all the three trimesters and formed a group of common subjects that needed to be analyzed through the repeated measure analysis with a significance level of 0.05. The other type of the statistical analysis was belong to the all subjects that created a larger group with a much higher statistical power than the five subjects. And, since there were several metrics that we needed to investigate, the Multi-Factor, (Univariate) type of the analysis with a significance level of 0.05 was conducted to examine the effects of the Trimester, Foot, Region, and Gender. Moreover, for the first section of the thesis (Overall CoPx and CoPy), we did the One-Way ANOVA to study the general effects of the Trimesters on the frequency metrics.

CHAPTER 3

RESULTS

Results obtained from the experiments are presented in this chapter. First, the time series analysis and frequency domain analysis and then results obtained from statistical analysis are presented.

3.1 Overall CoPx and CoPy Analysis

3.1.1 Time Domain Analysis Results of the CoPx and CoPy signals

The following time domain figures are the graphs of an exemplar female subject, showing the development stages, for three trimester T1, T2, and T3, and comparing them with an adult sample.

3.1.1.1 CoPx and CoPy signals

CoPx plot shows the subject's behavior during the trial in anteroposterior axis. The path of change and develop in the anteroposterior axis can be followed in figure 3.1 This figure shows the CoPx vs time, through eighteen months of an infant, and its comparison with an adult plot. There is a decrease in the amplitude and frequency form T1 to T3, which shows an adaptation of an infant to standing and controlling the posture.

The same pattern of improvement can be observed in the CoPy plot. CoPy plot shows the subject's behavior during the trial in mediolateral axis. The path of change and develop in the mediolateral axis can be followed in figure 3.2.

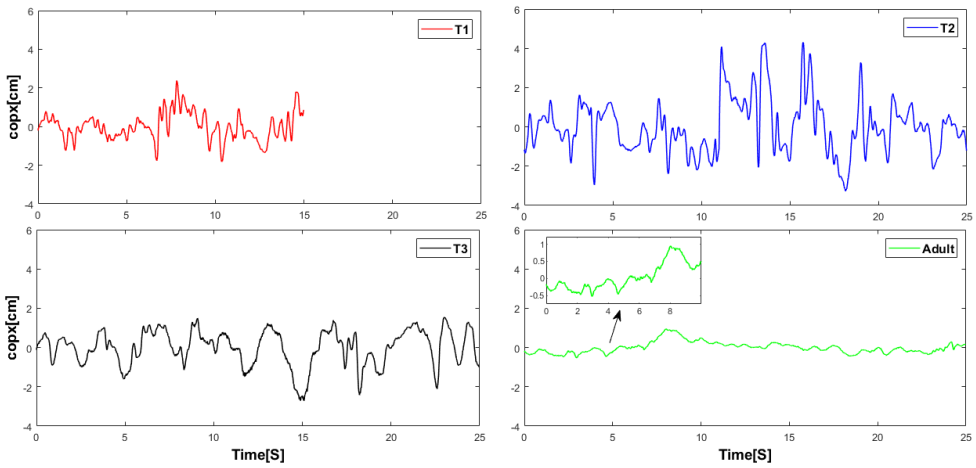

Figure 3.1: CoPx plot vs Time of an exemplar subject in T1, T2, T3 and an Adult

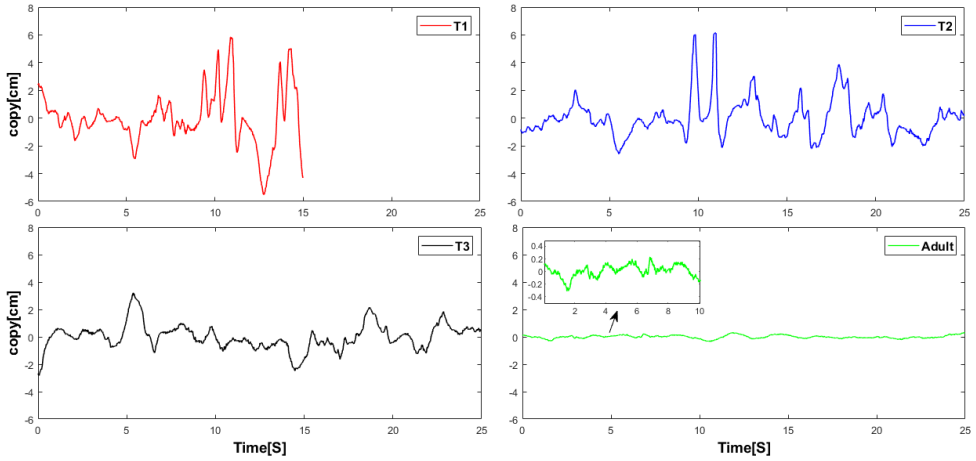

Figure 3.2: CoPy plot vs Time of an exemplar subject in T1, T2, T3 and an Adult

3.1.1.2 Stabilogram

Stabilogram which is a graphical representation of the small movements of a person in a steady stance (CoPy versus CoPx) is also a good way of space evaluation in postural control. The reason for plotting stabilogram is to eliminate time from the graph, meaning that the points in the stabilogram (for example two points near each other) are not related by the time, which means if two points are near each other they are not necessarily happened at the same time, this is a space neighborhood, not the time. The other important result from the stabilogram graph is the final pattern in space. The pattern of an adult stabilogram is a mature signature, while the infant's

graph is a random scattered immature pattern. Figure 3.3 reveals how this pattern changes and shrinks during infant's growth from 12 to 18 months. And gradually it becomes more like an adult pattern.

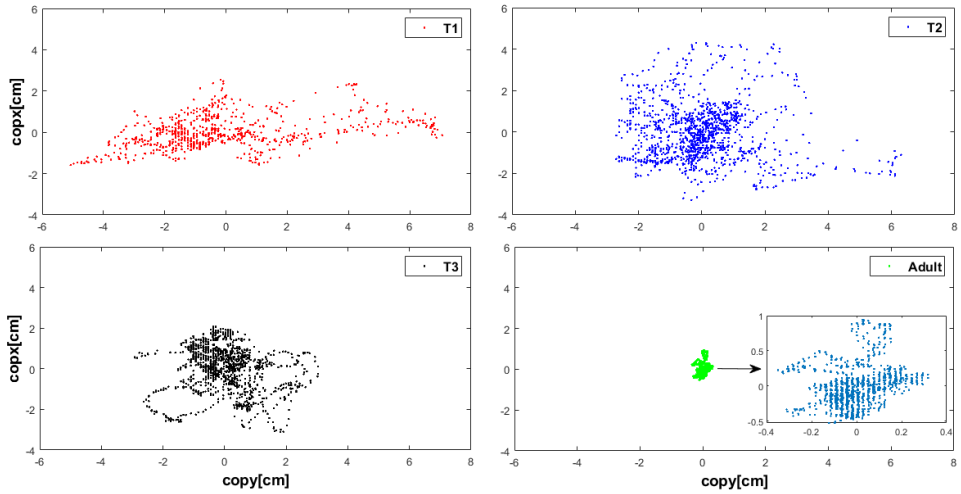

Figure 3.3: Stabilogram plot of an exemplar subject in T1, T2, T3 and an Adult

3.1.1.3 Phase plane

Phase plane is the graphical representation of the position (CoP) versus its velocity. It illustrates with how much velocity the infant has visited the corresponding position. For example, if the infant has visited a position with too high (positive or negative) velocities, it means that he/she has been spent the minimum time in that position, while in low velocities, the position has been visited more frequently and much more time has been spent there. Figure 3.4, clearly reveals this in the characteristic pattern observed through the following epochs information and tells the differences in velocity and positions from 12 months to 18 months, as well as its comparison with adult in both CoPx and CoPy signals.

3.1.2 Frequency Domain Analysis Results of the CoPx and CoPy signals

The following frequency domain figures are the graphs of an exemplar female subject, showing the developmental stages, for three trimester T1, T2, and T3. In the Magnitude of CoPx and CoPy plots of frequency, we can see how the frequency

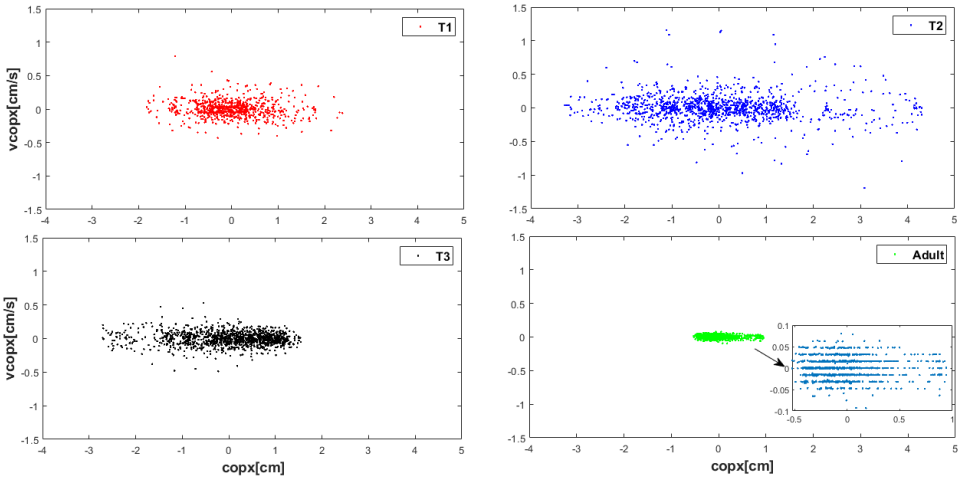

(a) Phase Plane of CoPx

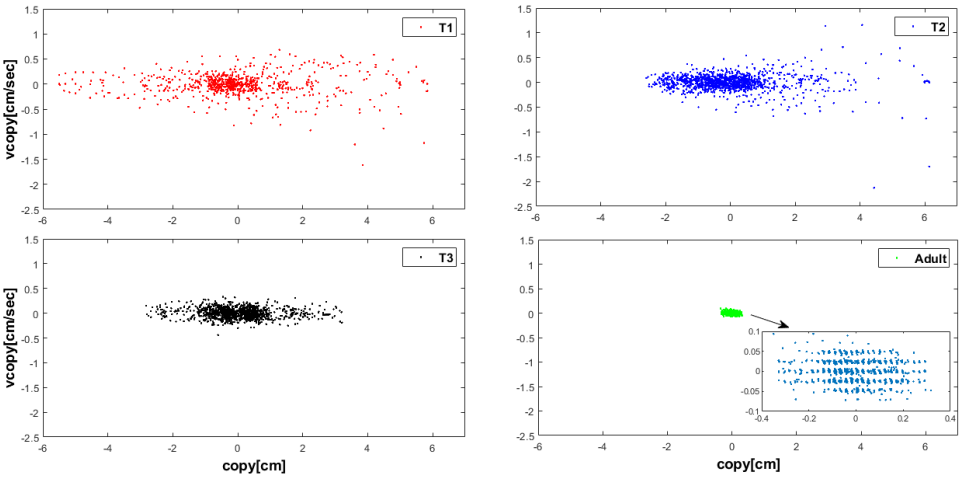

(b) Phase Plane of CoPy

Figure 3.4: Phase plane of a) CoPx b) CoPy of an exemplar subject in T1, T2, T3 and an Adult

shifts towards the left of the plot (lower frequencies), as the infant passes from T1 to T3.See figure 3.5

3.1.3 Statistical Analysis

In this study, One-Way ANOVA with a significance level of 0.05 was conducted to compare independent variables, which are the trimesters (T1, T2, T3). Metrics included in statistical analysis are Mean, Variance, $\%50$ and $\%95$ Power Frequency, CFREQ, and FD. The detailed table of metrics that have been significantly different are the following:

Table 3.1: Mean and Standard deviations of all the significantly different metrics for overall CoPx and CoPy

DV / IV		CFREQ	$50\%PF$	$90\%PF$
CoPx				
Trimester	T1	$2.39 \pm 0.36^{a,b}$	$0.64 \pm 0.40^{a,b}$	$2.26 \pm 0.54^{a,b}$
	T2	1.65 ± 0.15	0.34 ± 0.15	1.54 ± 0.48
	T3	1.55 ± 0.14	0.33 ± 0.16	1.35 ± 0.32
CoPy				
Trimester	T1	$2.86 \pm 0.41^{a,b}$	$0.58 \pm 0.45^{a,b}$	$2.34 \pm 1.06^{a,b}$
	T2	1.70 ± 0.27	0.33 ± 0.20	1.57 ± 0.69
	T3	1.60 ± 0.139	0.24 ± 0.14	1.16 ± 0.40
a. T1>T2, *b*. T1>T3, *c*. T2>T3				

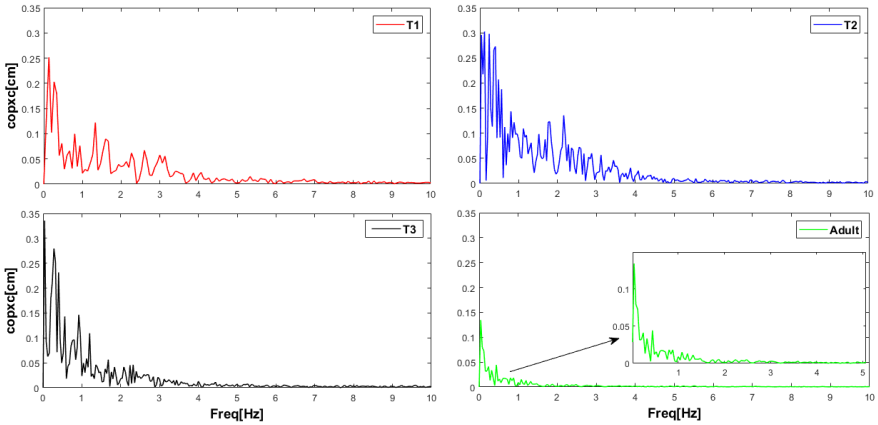

(a) Frequency plot of CoPx

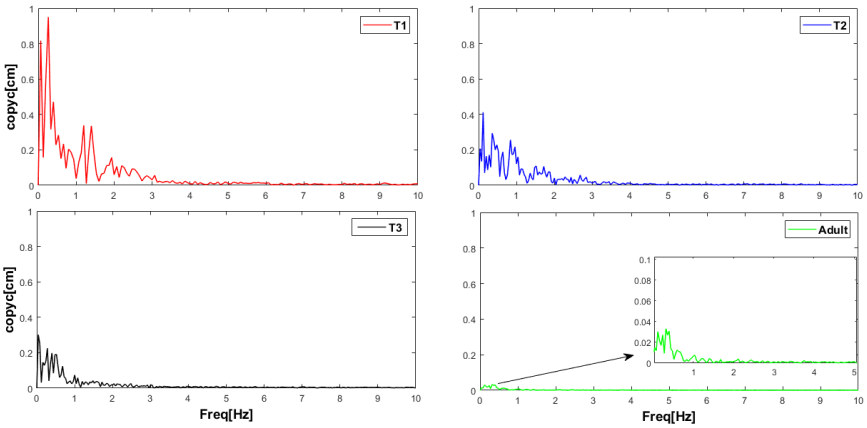

(b) Frequency plot of CoPy

Figure 3.5: Magnitude of a) CoPx b) CoPy plot vs Freq. of an exemplar subject in T1, T2, T3, and an Adult

3.2 Pressure pad data analysis

3.2.1 Plantar pressure distribution chart

For analysis of the pressure distribution chart, a "MATLAB" code is needed for getting the required information for each infant and trial, to observe the pressure changes in both feet and in each trial. It also helps to monitor the path of changes of pressure distribution through the study from 12 months to 24 months. To see how the spatiotemporal evolution effect the changes in the plantar pressure distribution during infants second year of life, we need to observe each foot section closely (frame by frame and pixel by pixel). Before writing a code for this purpose, we needed to realize in which aspects we are interested to follow the pressure changes, and after making this goal clear, we can write the related code. Thus, first there was a need to explore some subject's trimester trials manually, which is scanning each matrix by a human eye, frame by frame and pixel by pixel. After this process, the interested regions and aspects that are needed to be investigated by detail become clear and the code can be written based on the required information and metrics.

Therefore, the analysis started by a manual exploring with human eye: Figure 3.6 shows a random frame of an infant matrix, in which a quiet stance is taking place. For this investigation, a group of five common subjects from three trimester have been chosen, to see the differences of each trimester and comparing them with previous ones, as well as comparing infants' stance behavior with each other. For all five subjects, the first trimester trials' matrix includes 750 frames (since they stand for 15 seconds), and the second and third trimester trials' matrix includes 1250 frames (since they stand for 25 seconds). In all the matrices, we defined three ranges of forces to color the foot regions based on these ranges. For the forces between 1-15 (N), the pixels become yellow (Y), for the forces between 15-30 (N), the pixels become blue (B), and for the forces larger than 30 (N), the pixels become red (R), (Figure 3.6).

Based on the exemplar matrix shown in Figure (3.6), each infant's three trimester trials had been investigated frame by frame and the important observations were noted. The most critical aspects that needed to be noticed during the matrix analysis are:

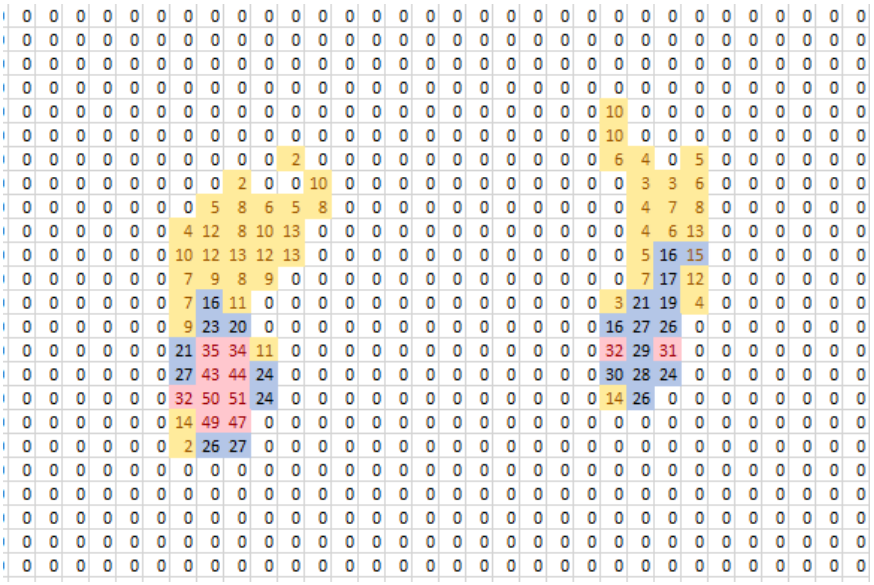

Figure 3.6: Plantar Pressure distribution based on Force categories

- The position of both feet with respect to the X and Y axis and each other
- Foot shape (is it a complete foot shape or not)
- If the feet have fully contact with the pad
- If there is any foot displacement during the trial
- The positions of force distribution
- The AP sways and number of contact loss of the six foot regions (FL, FR, ML, MR, HL, HR) during the sways, if there is any
- If any force on toes is noticed
- Which foot is more stable
- If any projection of arches has been noticed

Then, the next step is to convert this information collected through the human eye observation into a code, in which we can be able to analyze these changes and behavior in a more reliable and trusted way and evaluate the required metrics.

3.2.2 Image processing of pressure pad matrices

In the previous section, the analysis started by a manual exploring with human eye, and there was a close observation on the path of changes of pressure distribution through the study from 12 to 20 months. In this section of study, as we mentioned earlier, the investigation continued by enhancing a "MATLAB" code for the purpose of the image processing of the pressure pad matrices.

The analysis on each foot's three regions which are: FL, FR, ML, MR, HL, and HR presented the changes in pressure, force, moment arms (AP and ML fluctuations), contact area, stabilogram, and frequency domain (FFT, and PSD) in each region separately, and then each region's information can be compared with each foot's and both feet's data. Moreover, the track of changes of each region through the time followed by comparing each trimester's findings with the previous or next ones. Also, by the help of this method the foot displacement problem solved, and we can follow the changes during any foot movements and record the foot displacement frames as well as fluctuations in force and pressure distribution.

From all the subjects, there were 5 common subjects (all Female) for three trimesters. For each trimester of each subject, we did the image processing analyses and from total of 5 subjects and within their 15 trials there were total 4 trials in which the subjects have displaced one of their foot, which was their left foot. Two of these 4 displacements belong to subject one's T1 and T2, and one of them belongs to subject four's T2, and the other one is for subject five's T3. The number of Δt (foot contact loss frames) from all the subjects in which the foot had contact loss was between 4 and 10 frames ($4<\Delta t<10$).

Table (3.2) shows the contact loss frames of each foot and their length for 5 subject in three trimesters. It also shows how many times the foot has lost its contact, which is the number of Δt repeat. For example, subject 1, T1, has two Δt (4 and 7) repeats, which indicate that this subject has two foot displacements, first for 4 frames (from 445 to 551), and then had another for 7 frames long (form 710 to 717).

Table 3.2: Contact loss frames of each foot and their Δt for 5 common subjects in three trimesters.

Subject	Trimester	Contact Loss Frames		Δt	
		L	R	L	R
Subject 1	T1	[545-551,710-717]	-	4,7	-
	T2	[489-493,545-551]	-	5,7	-
	T3	-	-	-	-
Subject 2	T1	-	-	-	-
	T2	-	-	-	-
	T3	-	-	-	-
Subject 3	T1	-	-	-	-
	T2	-	-	-	-
	T3	-	-	-	-
Subject 4	T1	-	-	-	-
	T2	[414-417]	-	4	-
	T3	-	-	-	-
Subject 5	T1	-	-	-	-
	T2	-	-	-	-
	T3	[759-768]	-	10	-

3.2.3 Statistical Analysis

In the statistical analysis of this section we want to know if our independent variable which is the three trimester groups and is a categorical variable, has a significant influence on the dependent variable that's all the numeric measurements including the frequency and time metrics.

So, the null hypothesis is that there's not a significant difference in the parametric values of the infants during their first 6 month of post standing (T1, T2, T3), and the alternative hypotheses, which is also known as the research hypothesis or scientific hypothesis, is that there is a shift from right to left spectral band in the parametric

values of frequency domain metrics of the infants during their first 6 month of post standing (T1, T2, T3), and we can follow the spatiotemporal evolution from this analysis. The parametric values that we analyzed in the SPPS are: Centroidal frequency (CRFQ), frequency dispersion (FD), 50% and 90% power Frequency and mean and variance of the anteroposterior moment arms and pressure.

There were two groups of analysis based on the subjects. First, we had repeated measure analysis for our 5 common female subjects, and second, we did General Linear Model Univariate (Multi-factor ANOVA) for 31 subjects.

3.2.3.1 Repeated Measure ANOVA

In this method, we compare the results of the 5 common female subjects that have come to all the three trimesters' data collection. Therefore, the analysis need to be repeated measure ANOVA.

In the repeated measure ANOVA, there are two factors to do the analysis on the within subjects variables (Trimester and region) for each metric (CFREQ, FD, 50% and 90% PF, Mean, and Variance). The results of the analysis are divided in to two main sections of AP moment arms (CoPx), and pressure signals.

- **SPSS result of Repeated Measure ANOVA of 5 Common Subjects for Time Domain in Pressure Distribution and CoPx signals::**
  - **Pressure CFREQ, and CFREQM(Modified):** The results of CFREQ and CFREQM of pressure signal showed significantly decreased values in Fore region,for both left and right foot, and Mid region for right foot. These results showed the Major frequency shifts in pressure signal happens on the fore feet, while the hind feet are almost stable.(Figure 3.7, and Table 3.3)
  - **CoPx CFREQ, and CFREQM(Modified):** The results of CFREQ showed significantly different values for Mid and Hind regions, in both left and right foot, while for the CFREQM, beside the Mid and Hind feet, fore regions (FL&FR) were also significantly different (Table 3.4) due to the

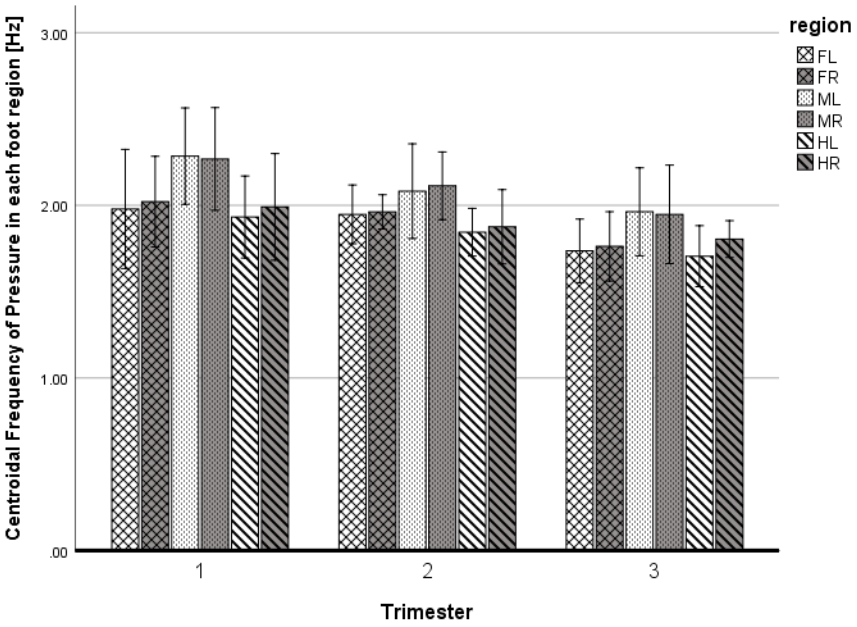

(a) $CFREQ$

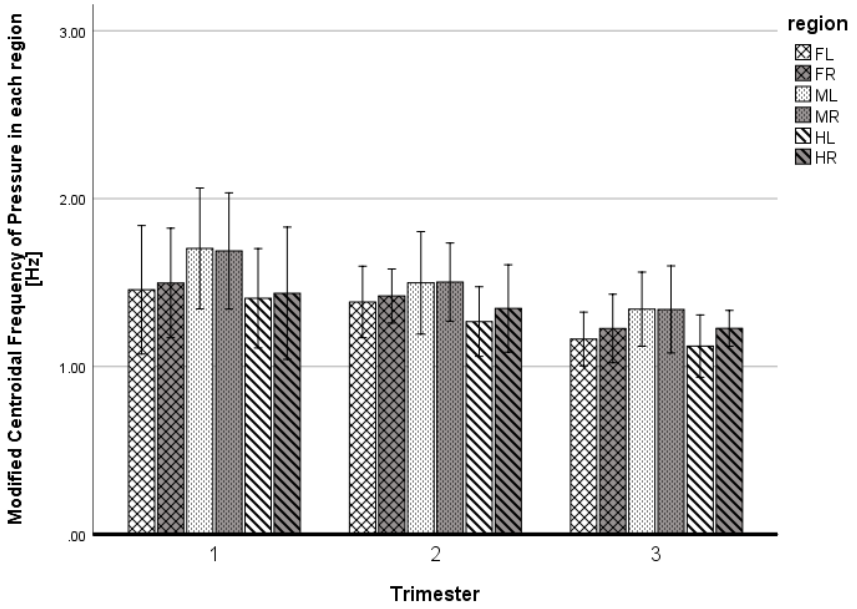

(b) $CFREQM$

Figure 3.7: Five common subjects' a) CFREQ and b) CFREQM of Pressure signal in each foot region, from T1 to T3

difference in CFREQ, and CFREQM equations.

Based on these two equations (2.8 & 2.9), we can say that equation 2.8 causes the effect of small frequencies (0<f<1) getting smaller and large frequencies getting larger, as a result of the second moment; i.e., while punishing the frequencies smaller than 1, rewarding the larger frequencies. Thus, when passing from T1 to T2 and T3, the power shifts towards the lower frequency band, and while CFREQ is recognizing this shift only in Mid and Hind regions, the CFREQM metric is more sensitive and can follow this shift in Fore region as well. On the other hand, these results are related to the comparison of foot regions with trimester, and from the previous observations during the data collection, we know that at first the most variations and noise were noticed on the Hind and Mid regions, since the infants were mostly stand on these regions, and the role of the Fore foot was almost negligible because at first fore foot and specially fingers didn't contain noticeable force, they were mostly folded and it was like the infant wants to grasp the ground with the fingers and lean to the posterior parts of the foot to prevent falling, and a large amount of the force was shifting between two hind regions, while gradually in T2, and then T3, fore foot also got some variation of the force transmission and its role gets more noticeable in time (from T1 to T3).See figure (3.8)

– **Pressure FD:** The results of FD of pressure signal showed increase in complexity of signal in both Fore feet, and Mid-right regions. (Figure 3.9, and Table 3.3)

– **CoPx FD:** The FD results showed a significant increase in complexity from T1 to T2 and T3 in all three regions of the left foot, while for the right foot there was only a significant increase in the hind-foot from T2 to T3, (Figure 3.9). There were significantly higher complexity in FL ($T2 > T1 \& T3 > T1$), ML ($T2 > T1 \& T3 > T1$), HL($T2 > T1 \& T3 > T1$), and HR ($T3 > T2$).See table (3.4)

We know that pure sine signal has FD=0, and the more complexity in signal causes an increase in FD from 0 up to maximum=1 ([41]). And here, we can follow the fact that the infants CoPx signals get more complex in

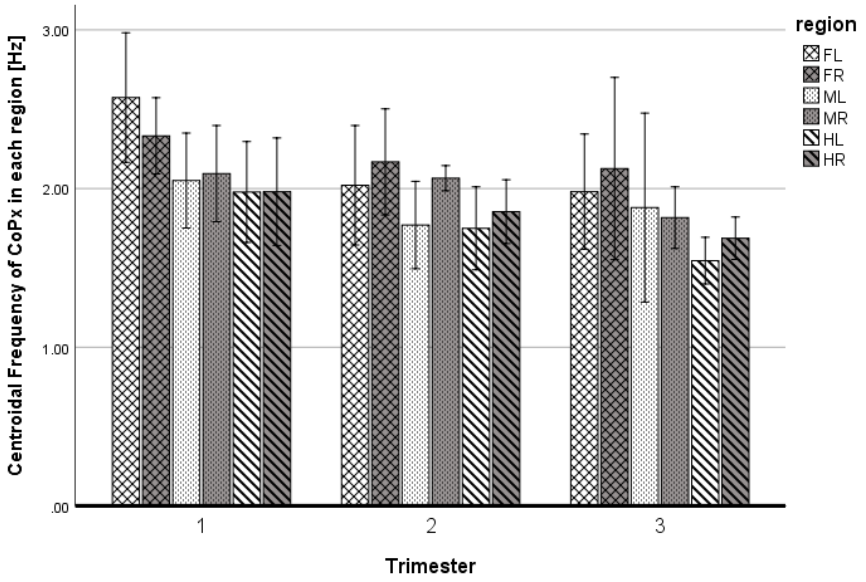

(a) $CFREQ$

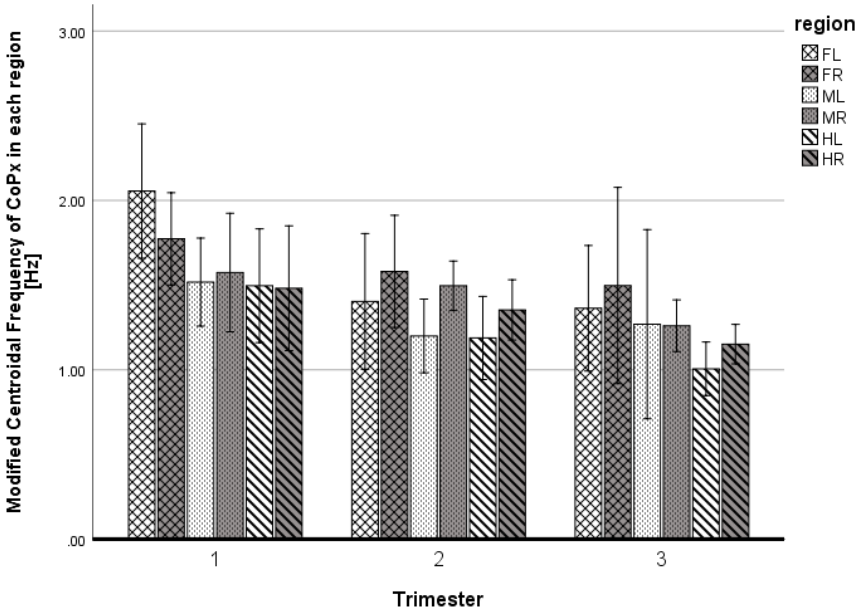

(b) $CFREQM$

Figure 3.8: Five common subjects' a) CFREQ and b) CFREQM of CoPx in each foot region, from T1 to T3

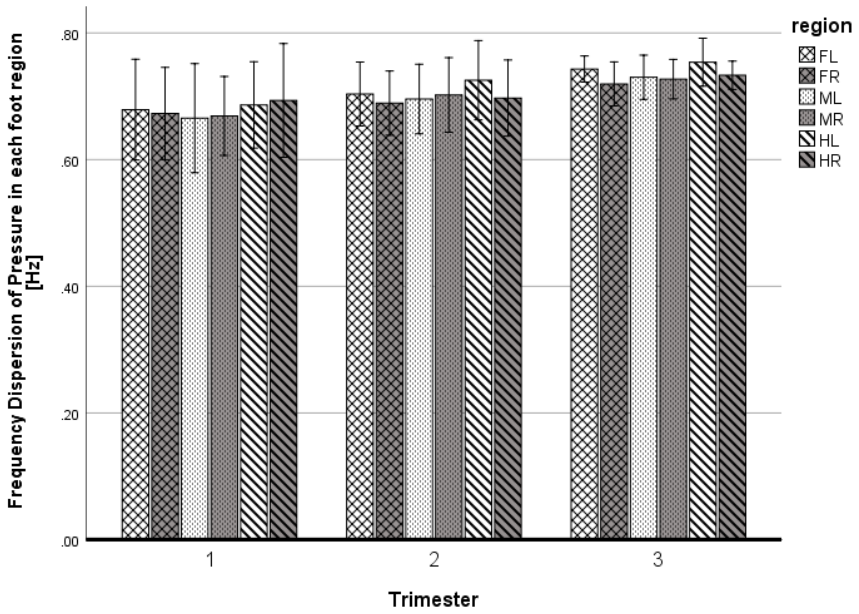

(a) FD of Pressure

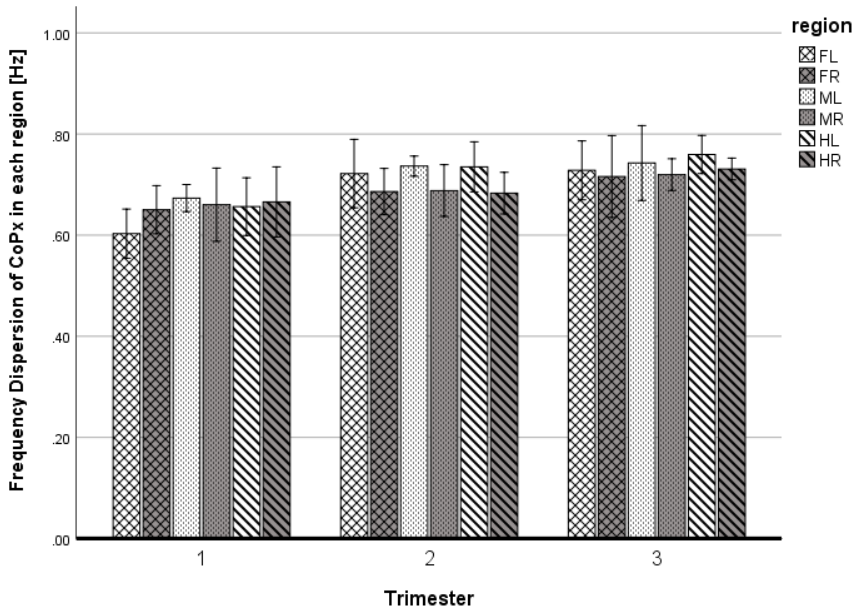

(b) FD of CoPx

Figure 3.9: Five common subjects' a) FD of Pressure and b) FD of CoPx in each foot region, from T1 to T3

time from T1 to T3.

– **Pressure 50% and 90% Power Frequency:** The 50% power frequency results showed a significant decrease in MR from T1 to T2, and the 90% power frequency results revealed a significant decrease in FL, ML, and MR regions of the foot from T1 to T3 (Figure 3.10, and Table 3.3)

– **CoPx 50% and 90% Power Frequency:** There was a shift to the lower frequencies (left) and a significant decrease in the 50% and 90% PF (Figure 3.11), when trimesters progressed from T1 to T3.See table (3.4)

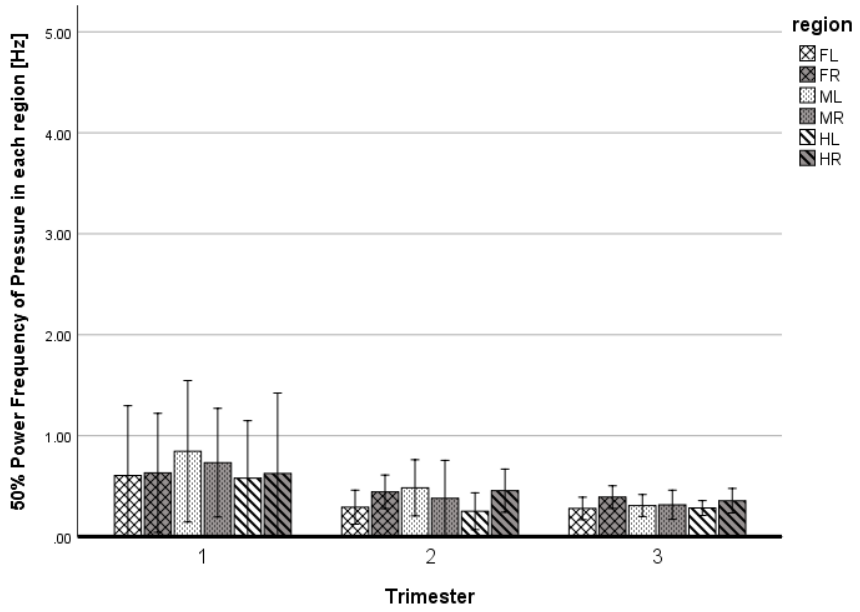

(a) $50\%PF$

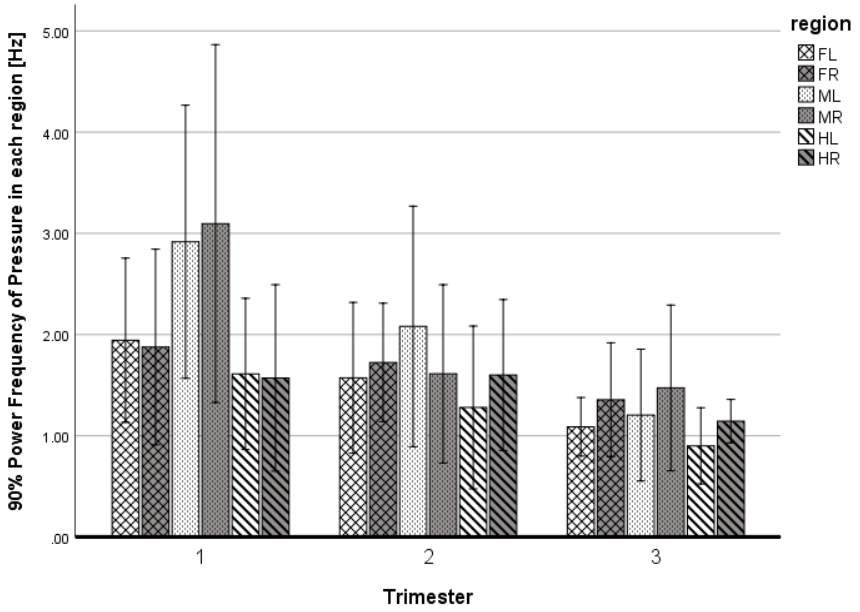

(b) $90\%PF$

Figure 3.10: Five common subjects' a) 50% PF and b) 90% PF of Pressure signal in each foot region, from T1 to T3

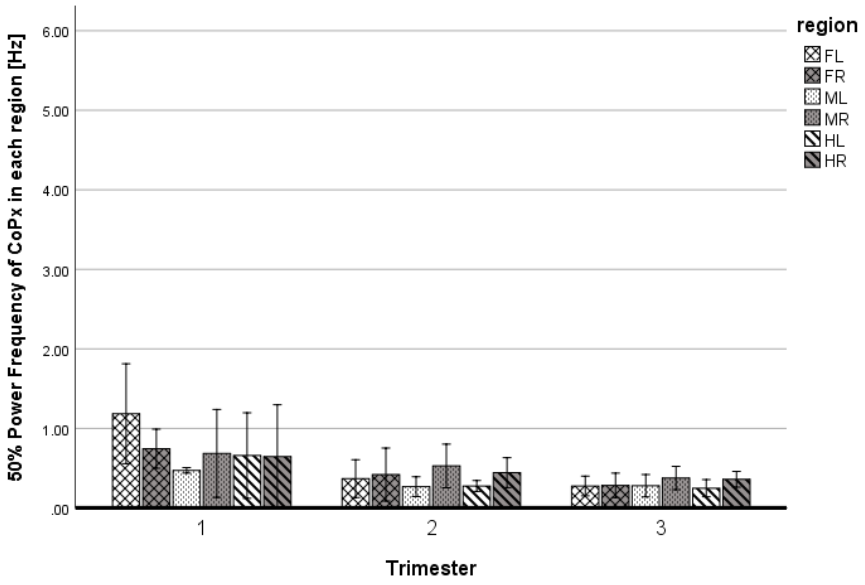

(a) $50\%PF$

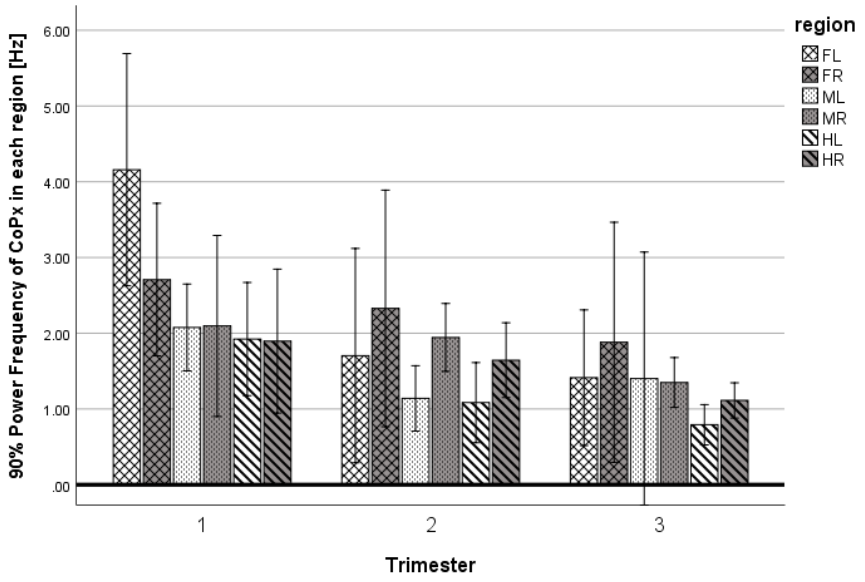

(b) $90\%PF$

Figure 3.11: Five common subjects' a) 50% PF and b) 90% PF of CoPx in each foot region, from T1 to T3

Table 3.3: Mean and Standard deviations of all the significantly different Pressure metrics of five common subjects

Pressure		FL	FR	ML	MR	HL	HR
CFREQ	T1		2.02 ± 0.21^{b}		2.07 ± 0.06^{b}		
	T2	1.95 ± 0.14^{c}	1.96 ± 0.08^{c}				
	T3	1.74 ± 0.15	1.76 ± 0.16		1.95 ± 0.23		
CFREQM	T1		1.50 ± 0.26^{b}		1.69 ± 0.28^{b}		
	T2	1.38 ± 0.17^{c}	1.42 ± 0.13^{c}				
	T3	1.16 ± 0.13	1.23 ± 0.16		1.34 ± 0.21		
FD	T1				0.67 ± 0.05		
	T2	0.70 ± 0.04	0.69 ± 0.04				
	T3	0.74 ± 0.02^{f}	0.72 ± 0.03^{f}		0.73 ± 0.03^{e}		
$50\%PF$	T1				0.73 ± 0.43^{a}		
	T2				0.38 ± 0.30		
	T3						
$90\%PF$	T1	1.94 ± 0.65^{b}		2.92 ± 1.09^{b}	3.10 ± 1.42^{b}		
	T2						
	T3	1.09 ± 0.23		1.20 ± 0.52	1.47 ± 0.66		
a. T1>T2, *b*. T1>T3, *c*. T2>T3, *d*. T2>T1, *e*. T3>T1, *f*. T3>T2							

Table 3.4: Mean and Standard deviations of all the significantly different CoPx metrics of five common subjects

CoPx		FL	FR	ML	MR	HL	HR
CFREQ	T1			2.05 ± 0.24^{a}		1.98 ± 0.26^{b}	
	T2			1.77 ± 0.22	2.07 ± 0.06^{c}		1.90 ± 0.16^{c}
	T3				1.82 ± 0.16	1.55 ± 0.12	1.70 ± 0.11
CFREQM	T1	$2.06 \pm 0.32^{a,b}$	1.77 ± 0.22^{a}	1.52 ± 0.21^{a}		1.50 ± 0.27^{b}	
	T2	1.40 ± 0.32	1.60 ± 0.27	1.20 ± 0.20	1.50 ± 0.12^{c}		1.35 ± 0.14^{c}
	T3	1.36 ± 0.30			1.30 ± 0.12	1.00 ± 0.13	1.15 ± 0.10
FD	T1	0.60 ± 0.04		0.67 ± 0.02		0.66 ± 0.05	
	T2	0.72 ± 0.05^{d}		0.74 ± 0.02^{d}		0.74 ± 0.04^{d}	0.68 ± 0.03
	T3	0.73 ± 0.05^{e}		0.74 ± 0.06^{e}		0.76 ± 0.03^{e}	0.73 ± 0.02^{f}
$50\%PF$	T1	$1.18 \pm 0.51^{a,b}$	0.75 ± 0.20^{b}	$0.47 \pm 0.03^{a,b}$			
	T2	0.37 ± 0.20		0.27 ± 0.10			
	T3	0.28 ± 0.10	0.28 ± 0.12	0.28 ± 0.11			
$90\%PF$	T1	$4.16 \pm 1.23^{a,b}$		2.08 ± 0.46^{a}		$1.92 \pm 0.60^{a,b}$	
	T2	1.70 ± 1.14		1.14 ± 0.35	1.94 ± 0.36^{c}	1.08 ± 0.43	
	T3	1.41 ± 0.72			1.35 ± 0.26	0.79 ± 0.21	
a. T1>T2, *b*. T1>T3, *c*. T2>T3, *d*. T2>T1, *e*. T3>T1, *f*. T3>T2							

3.2.3.2 Multi-factor ANOVA

The results of the multi-factor ANOVA cover two main sections of the analysis: CoPx, and Pressure results, and each of these main sections have been analyzed in time domain, including Mean and Variance metrics, and frequency domain including CFREQ, FD, 50% and 90% PF metrics. So, a factorial ANOVA (Univariate) was conducted to compare the main effects of Trimester, Foot, Region and Gender (M:Male, F: Female) which are the Independent Variables as well as their interaction effects on the CFREQ,CFREQM, FD, 50% and 90% PF, and Mean and Variance metrics (Dependent Variables).

- **SPSS result of Multi-factor ANOVA for Time Domain in Pressure Distribution and CoPx signals:**
  - **Pressure Mean:** In the Mean metric of the time domain in pressure distribution, the Levine's test showed that the variances of the groups were not equal (F(35, 294)=3.381, p=.000). The significantly different results were observed in **Region** at p<.001, and **Gender** at p=.005.See Figure (3.12)

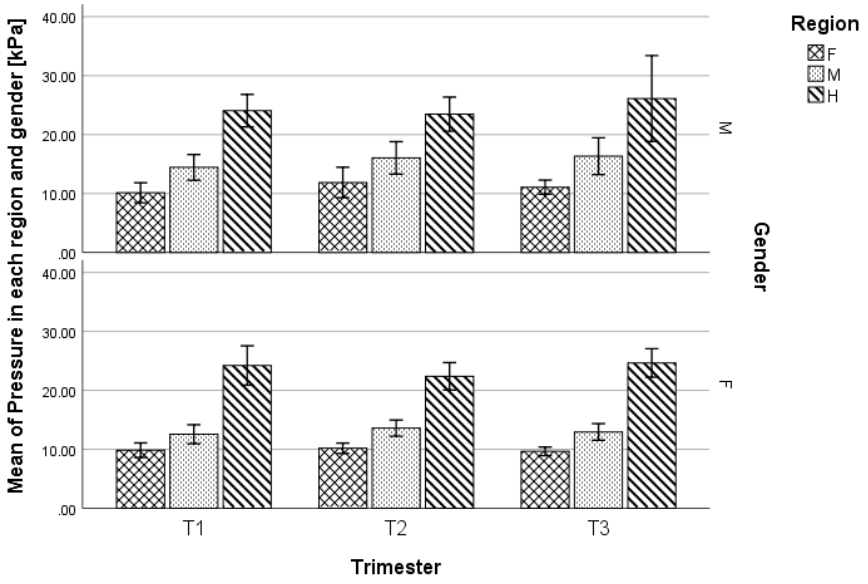

Figure 3.12: Mean of Pressure in each region and gender

Region: The overall mean of regions is $16 \pm 7.37kPa$, however, Hind foot region is $23.89 \pm 6.47kPa$, while Mid- $13.87 \pm 3.91kPa$, and Front foot region

is $10.26 \pm 2.51kPa$. The above information may point to the fact that Hind region is acting as a support while front region has the least pressure. All of the regions are significantly mutually different with respect to each other. The main effect of Region yielded an effect size of 0.619 indicating that 61.9% of the variance in the Mean metric was explained by Region (F(2, 323)=262.833, p=.000).

Moreover, based on the observations during the manual image processing procedure, the pressure distribution on T1 was mostly focused on the Hind and Mid regions, while there was scattered low pressures on Fore region (Figure 3.13.a). This pattern changed in time, and by passing through T1 to T2 and T3, the path of pressure beside Hind and Mid, followed toward Fore region as well. Such that in T2 and then T3, the amount of pressure applied on Fore region increased respectively (Figure 3.13.b,c). The pressure under the toe was also got noticeable by moving from T1 toward T3. Figure (3.13) shows the changes in the pressure distribution during the pass from 12 months to 20 months in infants.

Further more, the pattern of the pressure on the Mid region was also notable. This pattern, especially during the first trimester, was a bean shape overall higher pressure, concentrated on the Hind and Mid regions, such that while the pressure on the Hind foot was mostly the same, there was a change in the pressure distribution under the Mid foot. Two type of pressure distribution was noticed on Mid foot, the first one was a higher pressure distribution on the outer mid feet (Ipsilateral), while the second was mostly on the inner side of the one Mid foot and the outer side of the other Mid foot (Contralateral). These two pattern were randomly repeated, and since arch projection hasn't started yet, the medial side of the foot was carrying pressure as much as the lateral side.

Gender: Male subjects have significantly larger pressure than females. The main effect of Gender yielded an effect size of 0.024 indicating that 2.4% of the variance in the Mean metric was explained by Gender (F(1, 323)=7.947, p=.005).

- **CoPx Mean:** The Mean analysis in the CoPx metric gives us the information about the position of each foot region on the pressure pad in [cm]

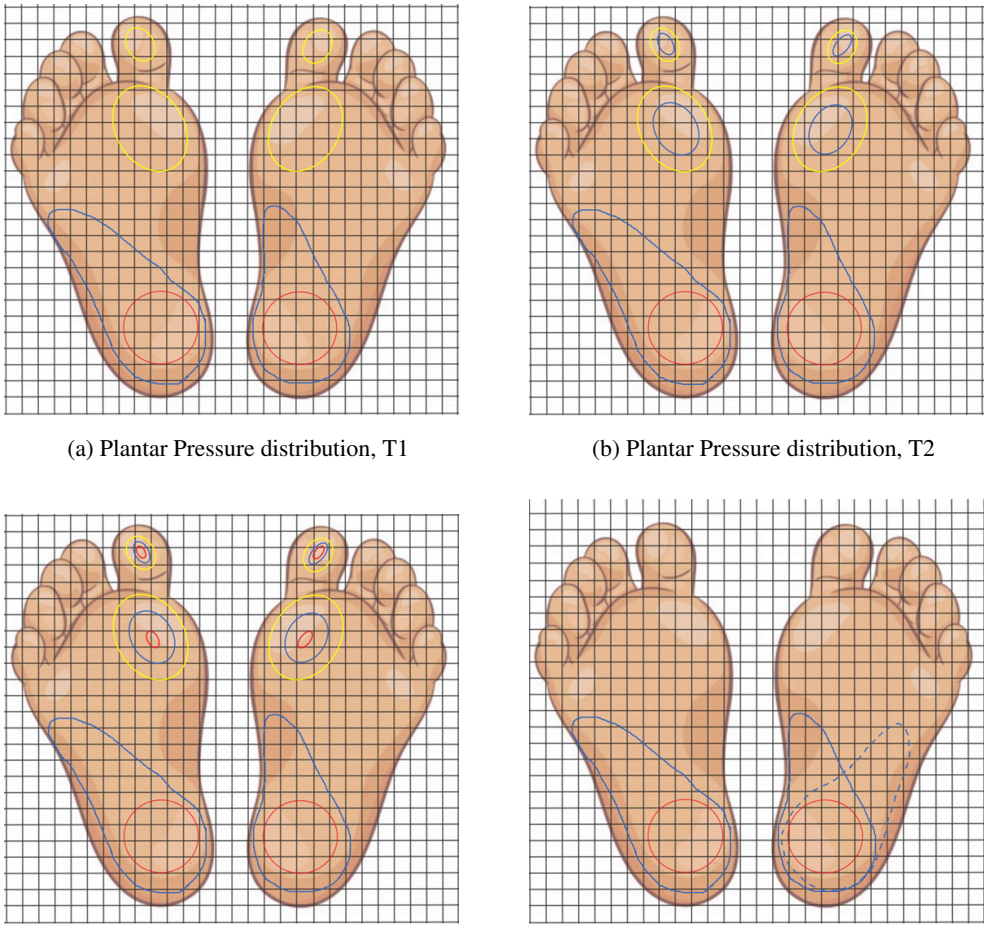

(a) Plantar Pressure distribution, T1

(b) Plantar Pressure distribution, T2

(c) Plantar Pressure distribution, T3

(d) Plantar Pressure distribution on M and H

Figure 3.13: Plantar Pressure distribution from T1 to T3. a) forces between 1-15 (N), shown in yellow, b) forces between 15-30 (N), shown in blue, c) forces larger than 30 (N), are shown in red, d) Pressure on the Mid and Hind regions (Continuous blue path is contralateral, dotted path is Ipsilateral)

with respect to the i,j axis. Since infants are more mobile regarding adults, it is more probable that the position of both feet may not be in line, and this plot gives us the mean related coordination for each foot region in three trimesters. Also, the high variance of the mean metric is due to the foot displacements that have been accrued in some of the subjects during the data collection period (3.14).

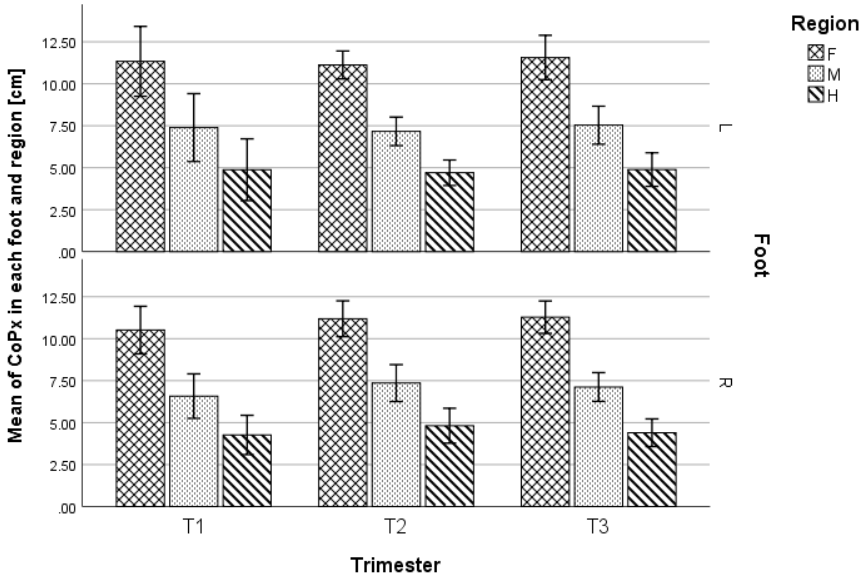

Figure 3.14: Mean of CoPx in each foot and region

– **Pressure Variance:** In the Variance metric of the time domain in pressure distribution, the Levine's test showed that the variances of the groups were not equal (F(35, 294)=5.371, p=.000). The significantly different results were observed in **Region** at p<.001.See Figure (3.15)

Region: the variance of the Hind region is significantly larger than Fore and Mid regions. The main effect of Region yielded an effect size of 0.467 indicating that 46.7% of the variance in the Mean metric was explained by Region (F(2, 323)=141.313, p=.000).

– **CoPx Variance:** Although there is no significant difference in the trimester variance, it is valuable to estimate the area under the PSD. This estimate is about the overall walk at all frequencies of CoP at Anteroposterior direction in all foot regions and Gender from T1 to T3.(Figure3.16)

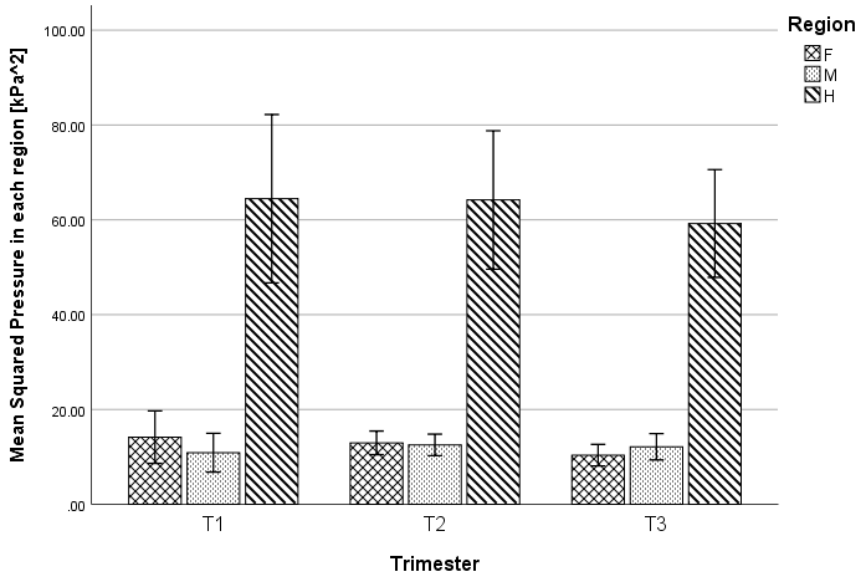

Figure 3.15: Variance of Pressure in each region

- **SPSS result of Multi-factor ANOVA for Frequency Domain in Pressure Distribution and CoPx signals:**

  - **Pressure CFREQ:** In CFREQ of the frequency domain metrics, the Levine's test showed that the variances of the groups were not equal (F(35, 294)=1.876, p=.003). The significantly different results were observed in **Trimester**, and **Region**, both at p<.001.See Figure (3.17)

Trimester: In trimesters, there was a shift from right to left (lower frequencies) when T1 proceeds towards T3. The main effect of Trimester yielded an effect size of 0.120 indicating that 12.0% of the variance in the CFREQ metric was explained by Trimester (F(2, 323)=21.989, p=.000).

Region: Mid region has a significantly larger frequency band of power (about 2Hz, which is resonance frequency of walking) compared to Fore and Hind regions. The main effect of Region yielded an effect size of 0.100 indicating that 10.0% of the variance in the Mean metric was explained by Region (F(2, 323)=17.997, p=.000).

  - **CoPx CFREQ:** Starting with CFREQ of the frequency domain metrics, the Levine's test showed that the variances of the groups were not equal

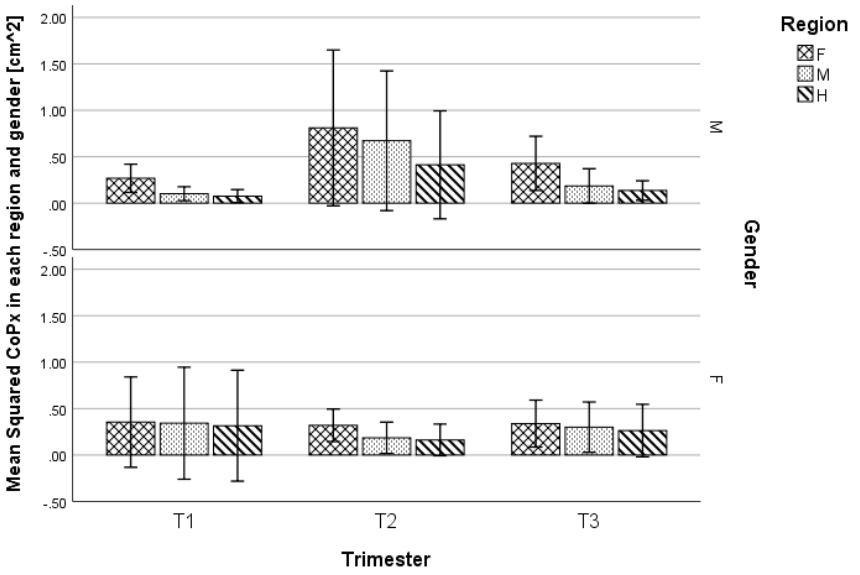

Figure 3.16: Variance of CoPx in each region and gender

(F(35, 294)=1.843, p=.004). The significantly different results were observed in **Trimester**, **Region**, and **Gender** at p<.001, p<.001, and p=.013, respectively, Figure(3.18).

Trimester: In trimesters, there was a shift from right to left (lower frequencies) when T1 proceeds towards T3. The main effect of Trimester yielded an effect size of 0.119 indicating that 11.9% of the variance in the CFREQ metric was explained by Trimester (F(2, 323)=21.855, p=.000).

Region: There was larger CFREQ value in Fore region with respect to Mid and Hind. The main effect of Region yielded an effect size of 0.124 indicating that 12.4% of the variance in the CFREQ metric was explained by Region (F(2, 323)=22.897, p=.000).

Gender: Females had larger CFREQ than males. The main effect of Gender yielded an effect size of 0.019 indicating that 1.9% of the variance in the CFREQ metric was explained by Gender (F(1, 323)=6.247, p=.013).

– **Pressure FD:** In the frequency dispersion metric, the Levine's test showed that the variances of the groups were not equal (F(35, 294)=1.497, p=.040). The significantly different results were observed in **Trimester**, and **Gender** at p<.001, and p=.002, respectively.See Figure (3.19)

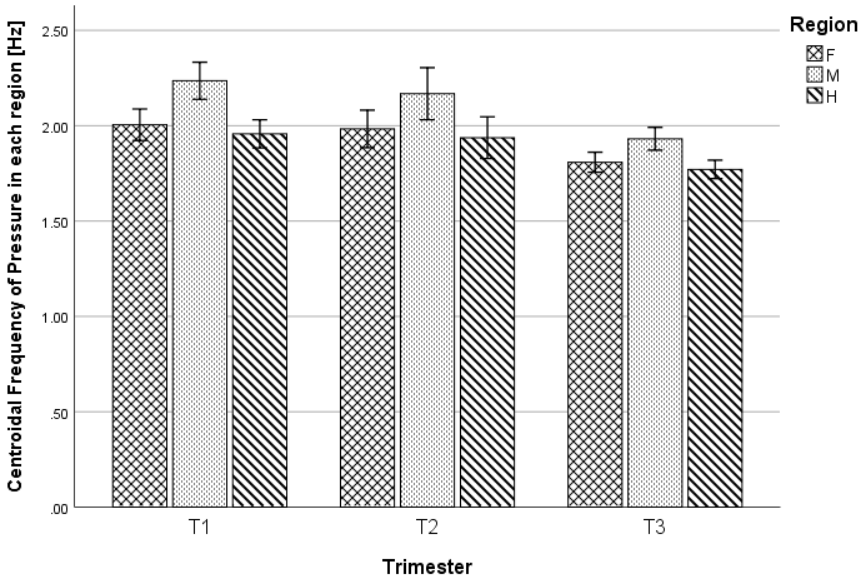

Figure 3.17: CFREQ of Pressure in each region from T1 to T3

Trimester: By moving from T1 to T3, Complexity increases in all trimesters, respectively.The main effect of Trimester yielded an effect size of 0.284 indicating that 28.4% of the variance in the FD metric was explained by Trimester (F(2, 323)=64.102, p=.000).

Gender: Female has a higher complexity compared to male in pressure distribution. The main effect of Gender yielded an effect size of 0.030 indicating that 3.0% of the variance in the FD metric was explained by Gender (F(1, 323)=10.042, p=.002).

Region: Although multi comparison post-hoc analysis dose not point to a significant value, (P=.079), there exist a significant trend between front compared to hind region, presenting a higher FD in Hind foot.

– **CoPx FD:** In the frequency dispersion metric, the Levine's test showed that the variances of the groups were equal (F(35, 294)=1.168, p=.245). The significantly different results were observed in **Trimester**, and **Region** at p<.001, and p=.042, respectively. See Figure (3.20)

Trimester: By moving from T1 to T3, Complexity increases in all trimesters, respectively.The main effect of Trimester yielded an effect size of 0.311 indicating that 31.1% of the variance in the FD metric was explained by Trimester

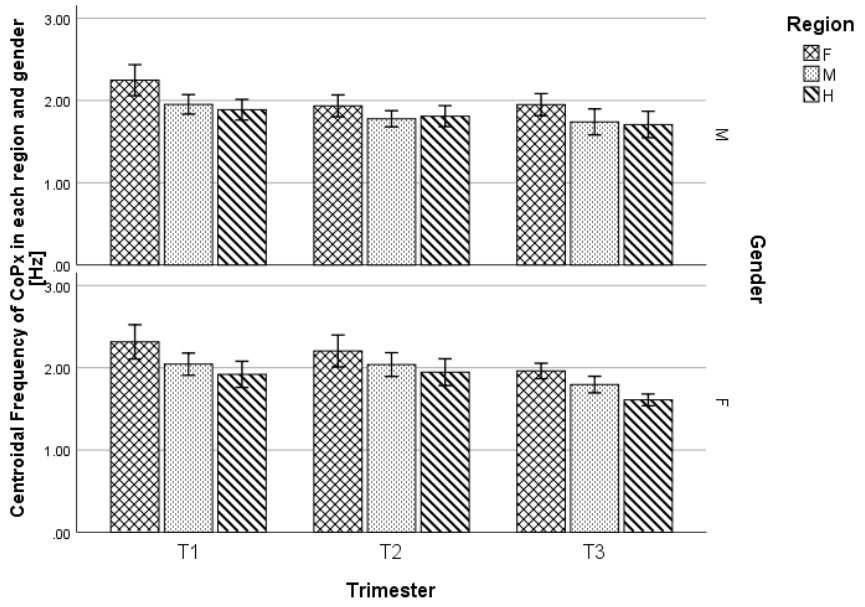

Figure 3.18: CFREQ of CoPx in each region and gender from T1 to T3

(F(2, 323)=72.813, p=.000).

Region: The Hind region presents much more complex signal patterns compared to fore region. The main effect of Region yielded an effect size of 0.019 indicating that 1.9% of the variance in the FD metric was explained by Region (F(2, 323)=3.190, p=.042).

– **Pressure** 50% **and** 90% **Power Frequency:** In the 50% and 90% Power Frequency metric the Levine's test showed that the variances of the groups were not equal, with (F(35, 294)= 3.289, p=.000) for 50% PF and (F(35, 294)= 2.271, p=.000) for 90% PF. The analysis showed significantly different results in **Trimester** for 50% PF at p<.001, and **Trimester** and **Region** for 90% PF, both at p<.001.See Figure (3.21)

Trimester: The cut off frequencies of 50% power are 0.638, 0.360, and 0.333 with respect to three trimesters, respectively. On the other hand, the cut off frequencies of 90% power are 2.072, 1.475, and 1.206 with respect to three trimesters, respectively. When the cut off frequency of 50% power is compared against adult spectrum, we observe that 50% power frequency bands of pressure distribution are within the adult spectrum. However, cut off frequency of 90% power of CoPx in infants has still 10 times higher (faster) frequency bands

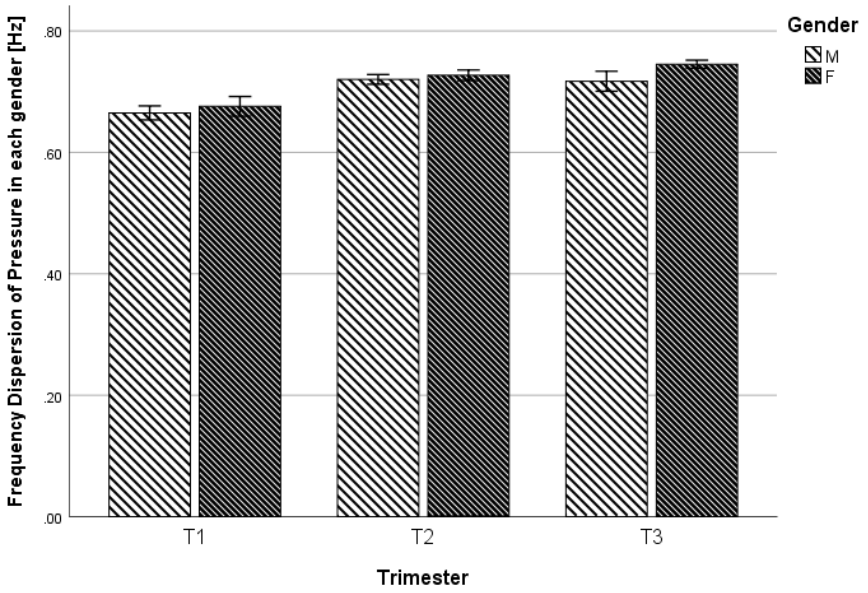

Figure 3.19: FD of Pressure in each gender from T1 to T3

compared to adults. The main effect of Trimester yielded an effect size of 0.224 indicating that 22.4% of the variance in the 50% PF metric was explained by Trimester (F(2, 323)=46.645, p=.000). While, The main effect of Trimester yielded an effect size of 0.232 indicating that 23.2% of the variance in the 90% PF metric was explained by Trimester (F(2, 323)=48.914, p=.000).

Region: Mid region showed significantly larger cut off frequency for 90% power compared against Fore and Hind regions. The main effect of Region yielded an effect size of 0.063 indicating that 6.3% of the variance in the 90% PF metric was explained by Region (F(2, 323)=10.792, p=.000).

- **CoPx** 50% **and** 90% **Power Frequency:** In the 50% Power Frequency metric the Levine's test showed that the variances of the groups were not equal with (F(35, 294)= 3.382, p=.000) for 50% PF and (F(35, 294)= 2.916, p=.000) for 90% PF. The analysis showed significantly different results in **Trimester** for 50% PF at p<.001, and **Trimester** and **Region** for 90% PF, both at p<.001.See Figure (3.22)

Trimester: There was a shift to the lower frequencies (left) in the 50% and 90% PF, when trimesters progressed from T1 to T3. The main effect of Trimester yielded an effect size of 0.245 indicating that 24.5% of the variance in the 50%

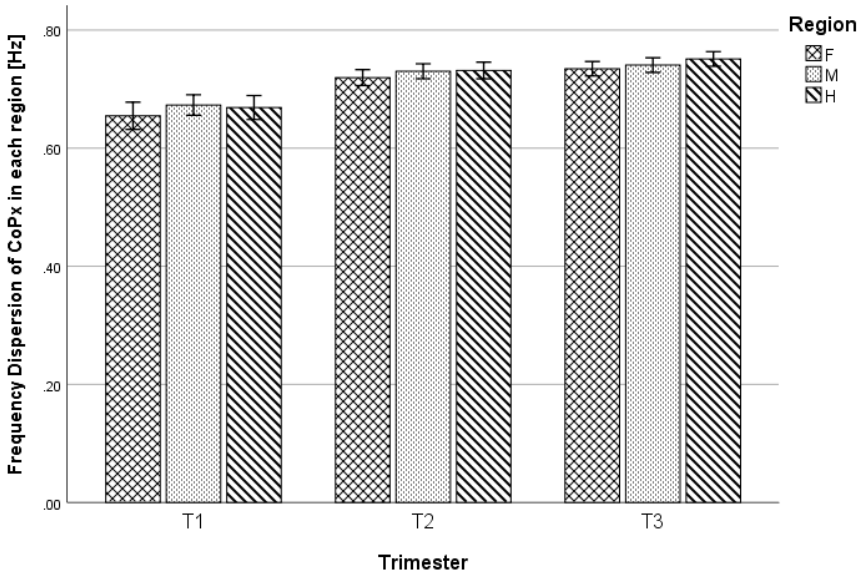

Figure 3.20: FD of CoPx in each region from T1 to T3

PF metric was explained by Trimester (F(2, 323)=52.378, p=.000). While, the main effect of Trimester yielded an effect size of 0.187 indicating that 18.7% of the variance in the 90% PF metric was explained by Trimester (F(2, 323)=37.270, p=.000).

Region: Front region showed significantly larger cut off frequency for 90% power compared against Mid and Hind regions. The main effect of Region yielded an effect size of 0.076 indicating that 7.6 % of the variance in the 90% PF metric was explained by Region (F(2, 323)=13.307, p=.000).

Table 3.5 shows the Mean and Standard deviations of all the significantly different pressure metrics, for all three trimesters.

Table3.6 shows the mean and standard deviation values of the CoPx analysis in time and frequency domain metrics.

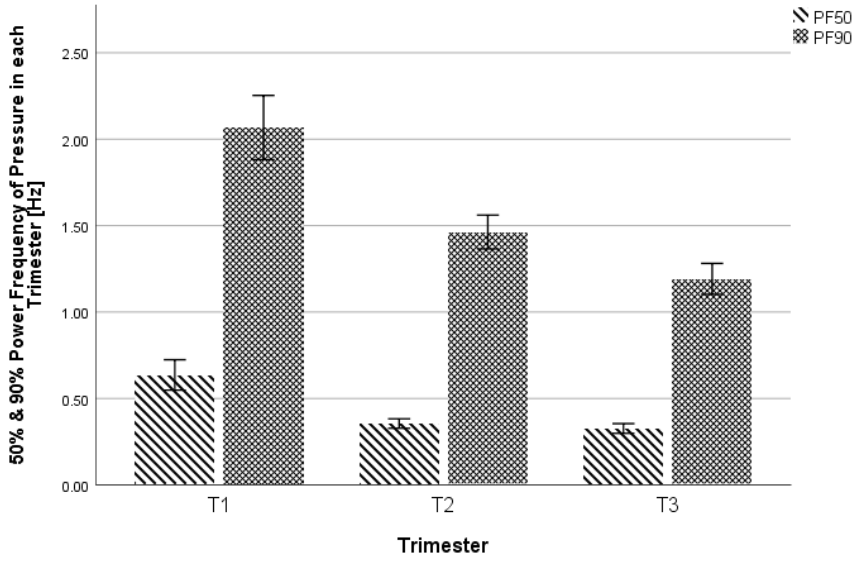

(a) $50\%\&90\%PF$

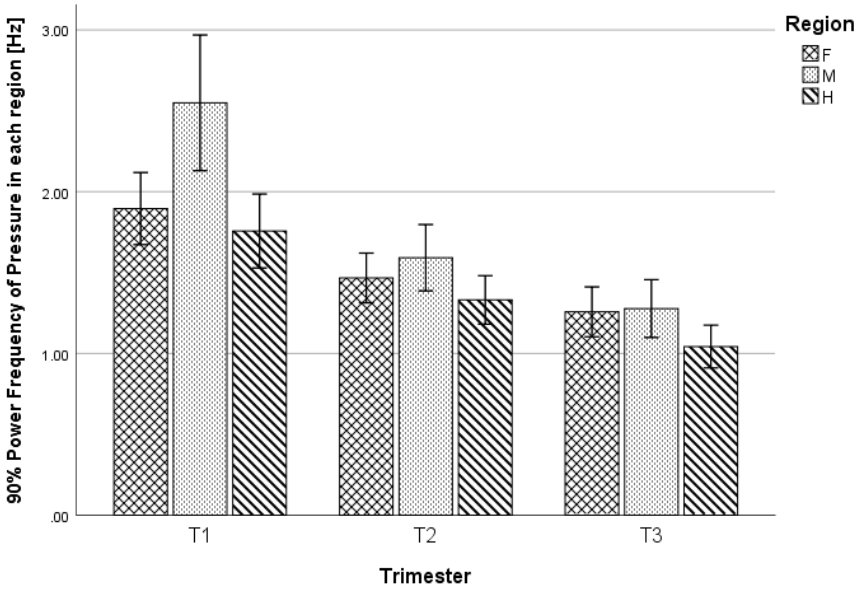

(b) $90\%PF$

Figure 3.21: a) 50% and 90% PF of Pressure signal in each trimester and b) 90% PF of Pressure signal in each region, from T1 to T3

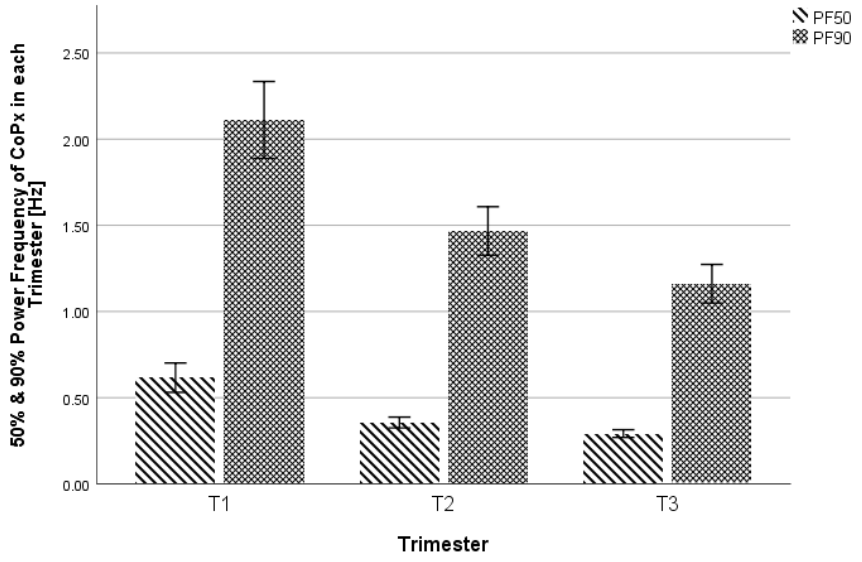

(a) $50\%\&90\%PF$

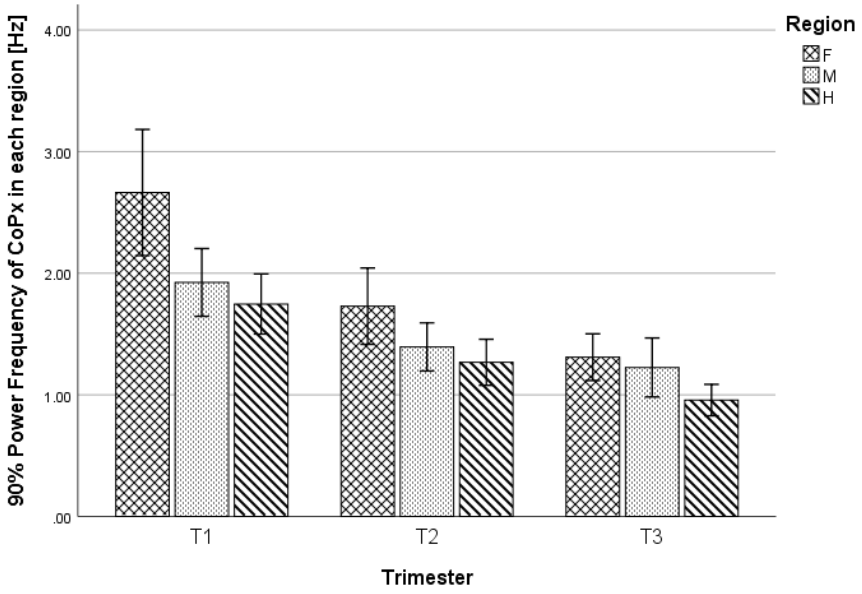

(b) $90\%PF$

Figure 3.22: a) 50% and 90% PF of CoPx signal in each trimester and b) 90% PF of CoPx signal in each region from T1 to T3

Table 3.5: Mean and Standard deviations of all the significantly different pressure metrics

Pressure							
IV \ DV		CFREQ	FD	$50\%PF$	$90\%PF$	Mean	Variance
Trimester	T1	2.07 ± 0.23^{b}	0.67 ± 0.05	$0.64 \pm 0.38^{a,b}$	$2.07 \pm 0.80^{a,b}$		
	T2	2.03 ± 0.40^{c}	0.73 ± 0.04^{d}	0.35 ± 0.16^{c}	1.50 ± 0.60^{c}		
	T3	1.84 ± 0.18	$0.74 \pm 0.04^{e,f}$	0.33 ± 0.16	1.20 ± 0.51		
Region	F	1.92 ± 0.26^{b}			1.48 ± 0.56^{b}	10.26 ± 2.51	12.25 ± 9.22
	M	$2.09 \pm 0.35^{c,d}$			$1.68 \pm 0.86^{c,d}$	13.87 ± 3.91^{d}	12.02 ± 8.49
	H	1.88 ± 0.27			1.31 ± 0.55	$23.89 \pm 6.47^{e,f}$	$62.35 \pm 42.30^{e,f}$
Gender	M		0.70 ± 0.04			17.07 ± 7.30^{a}	
	F		0.73 ± 0.05^{b}			15.60 ± 7.37	
a. T1>T2, *b*. T1>T3, *c*. T2>T3, *d*. T2>T1, *e*. T3>T1, *f*. T3>T2							
a. F>M, *b*. F>H, *c*. M>H, *d*. M>F, *e*. H>F, *f*. H>M							
a. M>F, *b*. F>M							

Table 3.6: Mean and Standard deviations of all the significantly different CoPx metrics

CoPx					
IV \ DV		CFREQ	FD	$50\%PF$	$90\%PF$
Trimester	T1	2.07 ± 0.30^{b}	0.67 ± 0.05	$0.62 \pm 0.36^{a,b}$	$2.11 \pm 0.95^{a,b}$
	T2	2.00 ± 0.44^{c}	0.73 ± 0.45^{d}	0.36 ± 0.18^{c}	1.47 ± 0.82^{c}
	T3	1.80 ± 0.27	$0.74 \pm 0.04^{e,f}$	0.29 ± 0.13	1.16 ± 0.63
Region	F	$2.10 \pm 0.40^{a,b}$	0.71 ± 0.05		$1.78 \pm 1.08^{a,b}$
	M	1.90 ± 0.31^{c}	0.72 ± 0.05^{d}		1.45 ± 0.75^{c}
	H	1.80 ± 0.33	$0.73 \pm 0.05^{e,f}$		1.25 ± 0.61
Gender	M	1.90 ± 0.25			
	F	1.96 ± 0.41^{b}			
a. T1>T2, *b*. T1>T3, *c*. T2>T3, *d*. T2>T1, *e*. T3>T1, *f*. T3>T2					
a. F>M, *b*. F>H, *c*. M>H, *d*. M>F, *e*. H>F, *f*. H>M					
a. M>F, *b*. F>M					

3.2.3.3 Adult data comparison

In this section we specifically compare and discuss the Multi-factor ANOVA results and plots of infants with an exemplar adult data in both pressure and CoPx signals for each of the metrics.

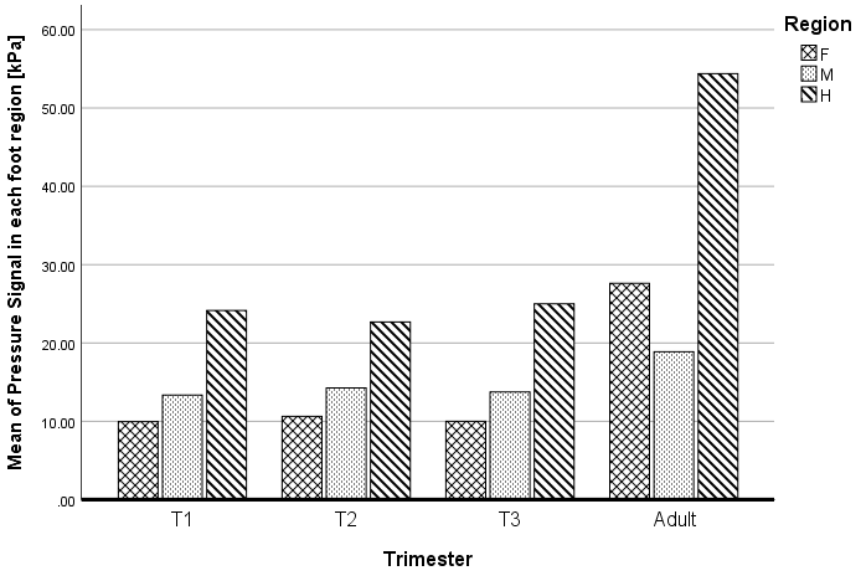

Figure 3.23: Mean of pressure of infants Vs Adults in each region of the foot

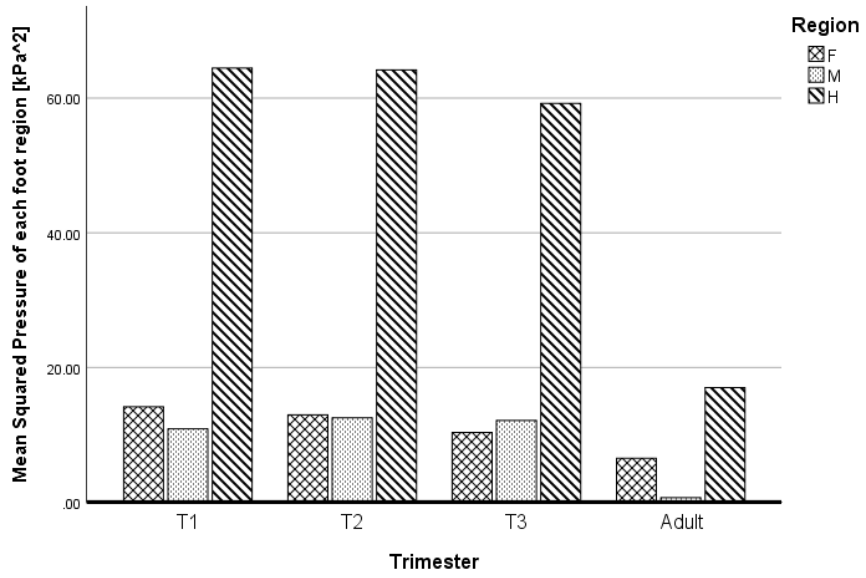

Figure 3.24: Variance of Pressure of infants Vs Adults in each region of the foot

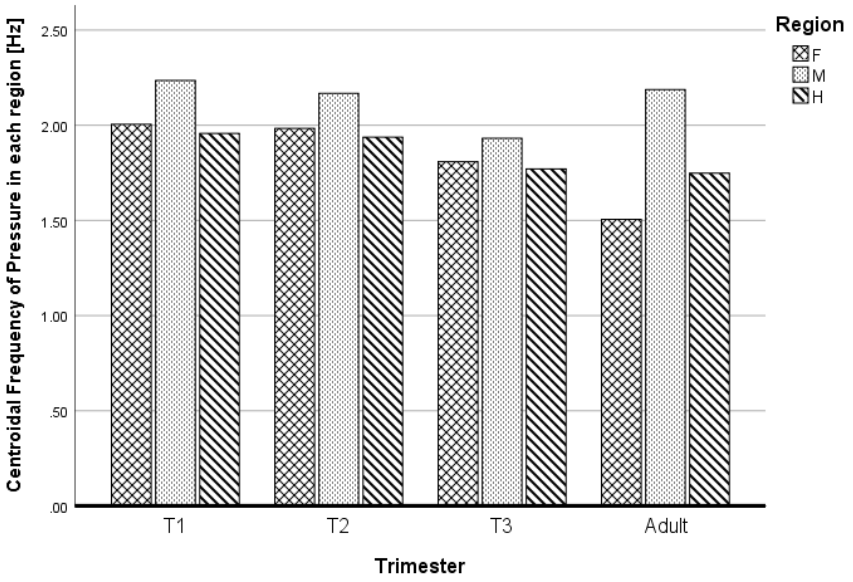

Figure 3.25: CFREQ of Pressure of infants Vs Adults in each region of the foot

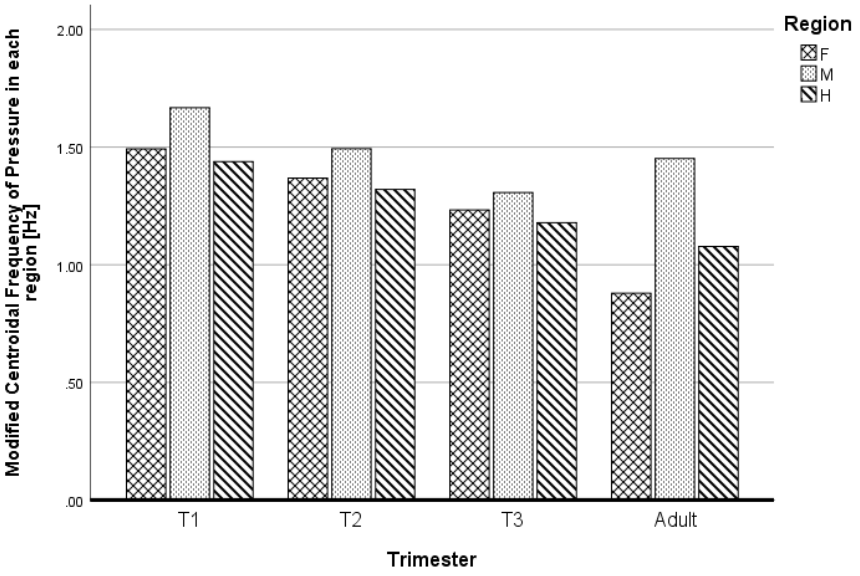

Figure 3.26: CFREQM of Pressure of infants Vs Adults in each region of the foot

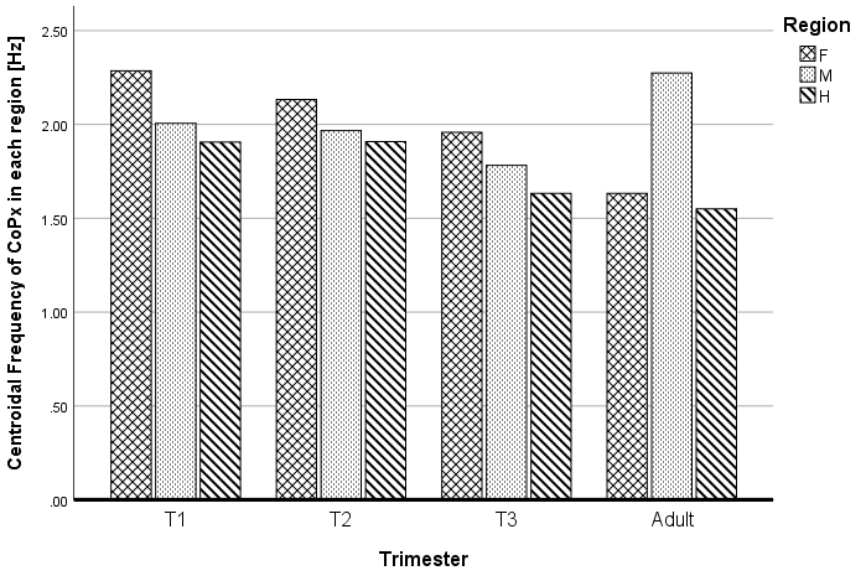

Figure 3.27: CFREQ of CoPx of infants Vs Adults in each region of the foot

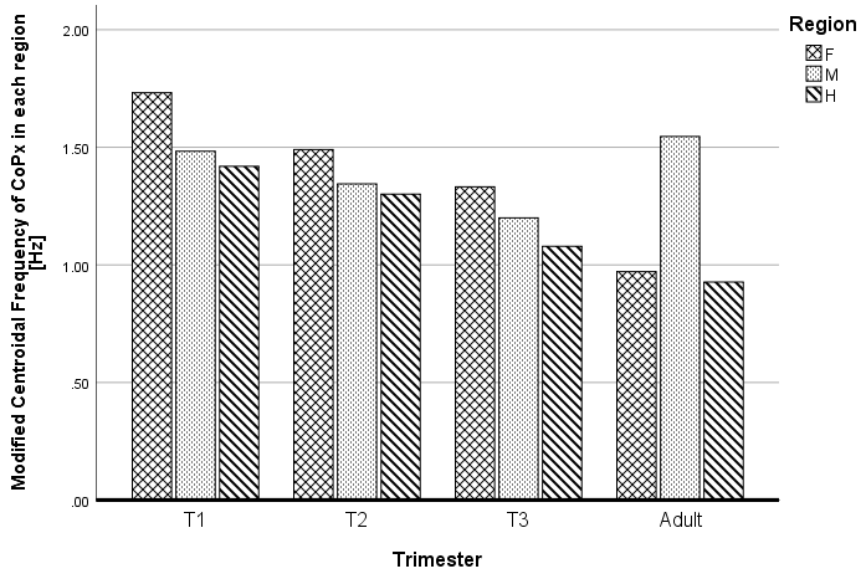

Figure 3.28: CFREQM of CoPx of infants Vs Adults in each region of the foot

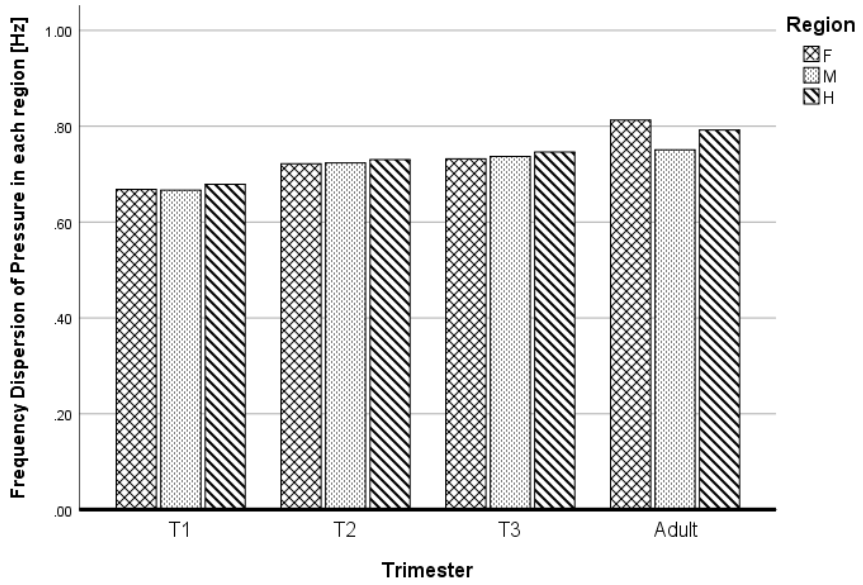

Figure 3.29: FD of Pressure of infants Vs Adults in each region of the foot

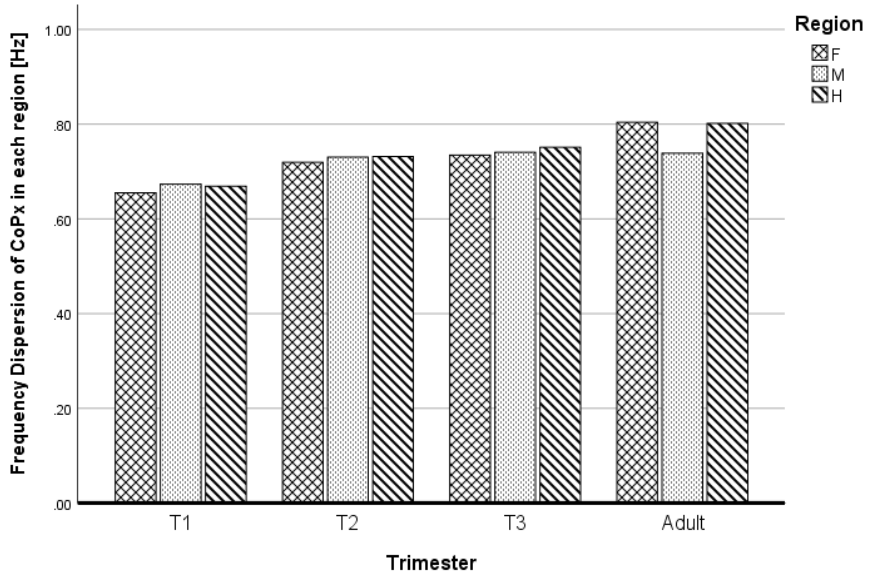

Figure 3.30: FD of CoPx of infants Vs Adults in each region of the foot

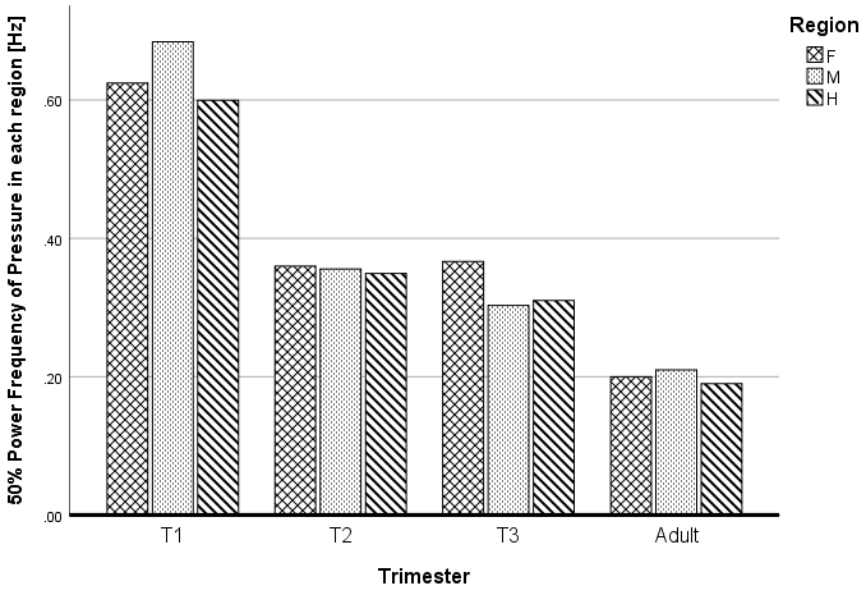

Figure 3.31: 50% PF of Pressure of infants Vs Adults in each region of the foot

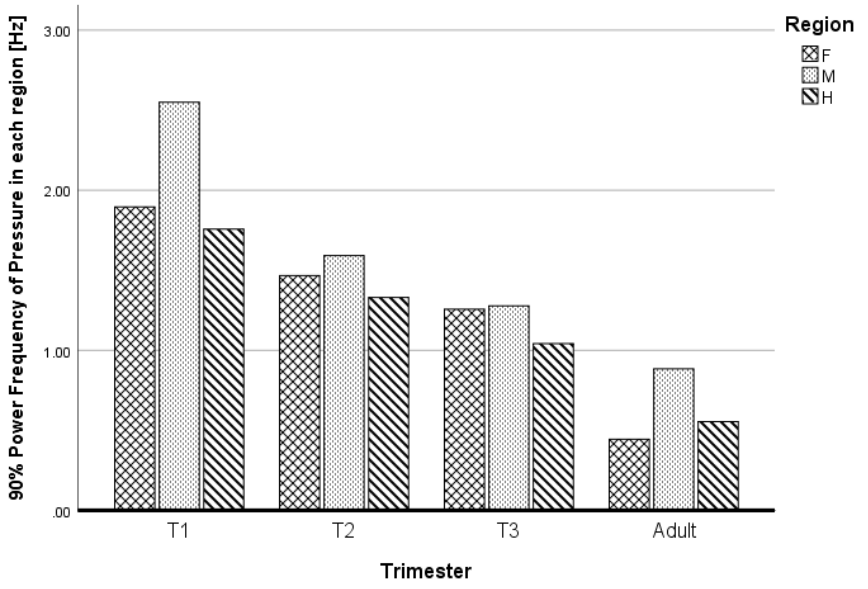

Figure 3.32: 90% PF of Pressure of infants Vs Adults in each region of the foot

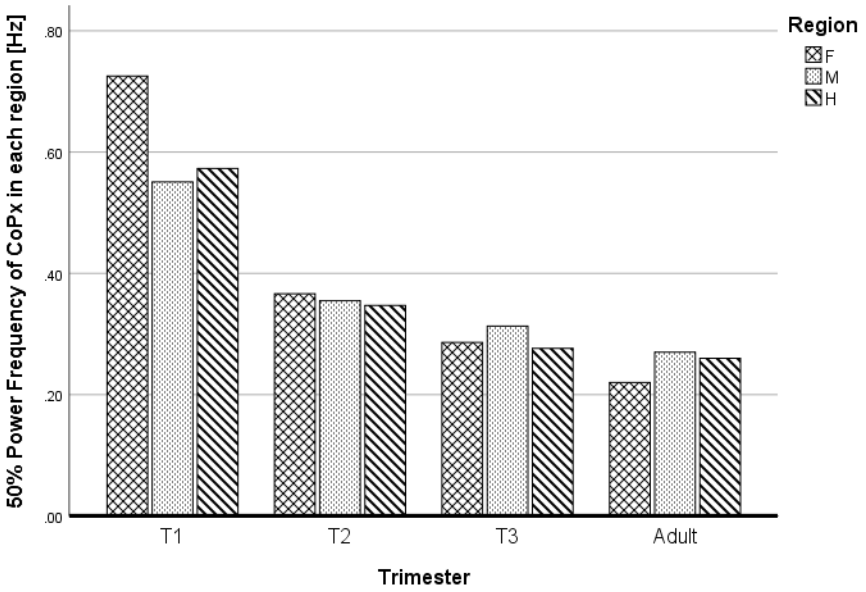

Figure 3.33: 50% PF of CoPx of infants Vs Adults in each region of the foot

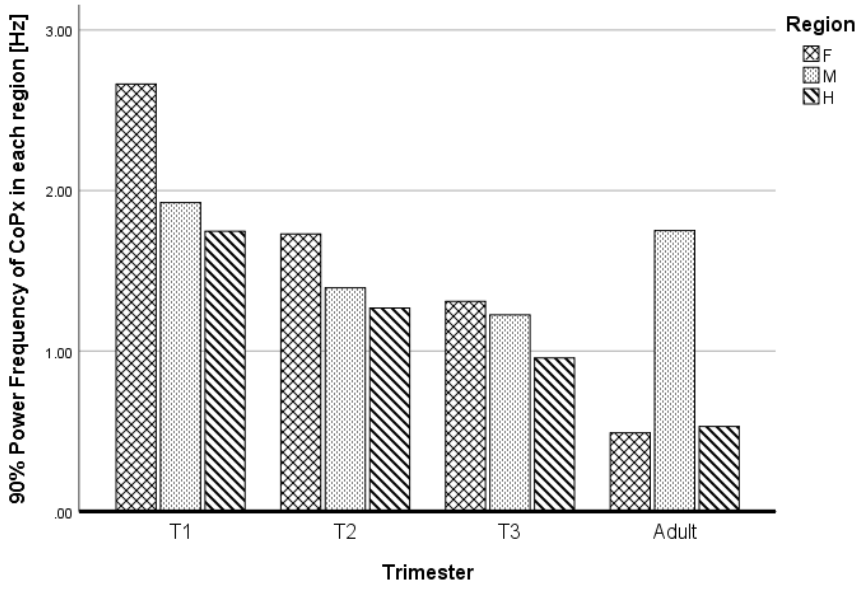

Figure 3.34: 90% PF of CoPx of infants Vs Adults in each region of the foot

CHAPTER 4

NONLINEAR DYNAMICS

4.1 Introduction to nonlinear dynamics

4.1.1 Types of Systems:

There are three types of systems:

- **Deterministic system:** Deterministic system is a system that is not random. The cause and effect are linked in this type of the system and the current state determines the future state.
- **Dynamic System:** Is a system that evolves by time.
- **Nonlinear system:** Is a system where the relationships between the variables that matter, are not linear.

4.1.2 Types of Time Systems:

4.1.2.1 Discrete time system:

In this system time proceeds in clicks. "Map" is a discrete time system and time makes no sense in between iterates. Modeling tool for this time system is difference equation.

$$\mathbf{X}_{n+1} = \mathbf{f}(\mathbf{x_n}) \tag{4.1}$$

where n is time, x is the state of the system, and f is the map, which takes the current state (x_n), and moves it one time click forward and gives (x_{n+1}).

In the notation $\mathbf{X}_{n+1} = \mathbf{f}(\mathbf{x_n})$, is a polynomial mapping, example of how complex, chaotic behaviour can arise from very simple nonlinear dynamical equations [49].

The reason to study maps is that their dynamics are representative, which is a good example of what can happen in nonlinear dynamical systems, but the math is a lot easier. A good way to understand the nonlinear dynamics better, is to start the ideas and examples in the context of maps and then circling back around through those ideas in the context of flows.

4.1.2.2 Continuous time system:

In this type of system, time proceeds smoothly, and the space and time are continuous. "Flow" is a continuous time system. Modeling tool for this system is differential equation.

A flow is something like pendulum, dynamics that operate continuously in time and space.

State Space and State Variables: The state space of a dynamical system is the set of all possible states of the system. Each coordinate is a state variable, and the values of all the state variables completely describe the dynamics of the system. In other words, each point in the state space corresponds to a different state of the dynamical system. A state variable is one of the variables used to describe the state of a dynamical system. Each state variable corresponds to one of the coordinates of the underlying state space.

4.1.3 Nonlinear Time Series Analysis :

When we have time series data from a dynamical system, the measurement may be a point of the state variables, but that's not always possible. In a complicated dynamical system, we may not know what all the state variables are, and even if we did know

what they were, it might be hard to measure them. And even if we can measure them, we may not be able to do that without affecting the dynamics of the system that we are studying. The theory and algorithms that is mostly used is based on an assumption that we know all the state variables, what they are, and what their values are. But reality is very different. We generally have a measurement of one quantity that is acquired from some function of some number of the state variables.However the act of doing that single measurement projects the state space down onto a single axis. If we want to study the full version of those dynamics we have to undo that projection, in other words we need to expand that squashed flat data back into its original form [50], (Figure 4.1). One way of doing this is by computing derivatives from the data, however there are two major problems with that approach first it magnifies noise, another major problem is that it's not often possible to know what all the state variables of the system are and it's extremely rare that we can measure all of them and the act of doing all those measurements might actually change the system dynamics. Often we don't even know how many dimensions the system has. Therefore, we need to estimate the dynamical order of the system in order to expand it sufficiently enough for a real appearance in the space; e.g., with a technique called delay coordinate embedding.

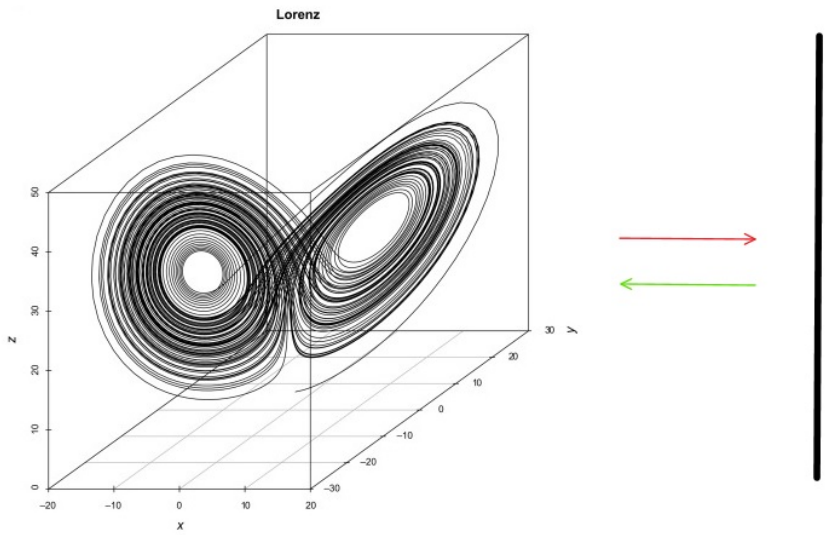

Figure 4.1: Expanding the squashed flat data of a Lorenz system back into its original form [1]

4.1.3.1 Delay-Coordinate Embedding:

The basic idea of this method is that we plot the data against delayed versions of itself and this new space is called reconstruction space and it has as many axes as we choose. The so called phase points in that reconstructed space from the data form a vector of delayed coordinates. The number of axes represents the number of dimensions that we are embedding the data in. In order to do the reconstruction correctly, we need to choose m, the dimension and τ, the time delay, properly.

So, for choosing a proper τ and m we need a τ greater than zero in theory, and an m which is big enough so that the crossings are gone from the standpoint of the data and the computations that we are using. We also need to avoid choosing a delay that's a multiple of a period for the reason that all the points in reconstruction space will be on the main diagonal (redundancy).

4.2 Nonlinear Noise and Dynamics in Human Posture

Human posture has two major branches that can be investigated individually:

1. Physiological

2. Mathematical Modeling (Dynamics and Control)

For the physiological part, there are several guidelines such as: Neuromuscular skeletal system, Metabolic system (energy), Neuro-endocrine system, etc.

We use the neuromuscular skeletal section to investigate the mathematical modeling branch of the posture and assume the rest of the physiological sections as given. However, for creating a space in the given instant (for establishing a spatiotemporal evolution for a given signal), we need a space variable which may be a random variable, x_t, or a deterministic one, $x(t)$ that does not contain the history of the particle. The mathematical modeling branch of the investigation is actually the theoretical and methodological part of the study. Therefore, for explaining the developmental aspects of the posture and dynamics, we use the information from the physiological guidelines. As a whole, we assume that there is a randomness, and we want to in-

vestigate on the dynamics including linear and nonlinear characteristics. On the other hand there is noise in the signal which needs to be investigated along with the dynamics.Since, motor learning may be affected by existence of the noise, the main question here is how much of a signal is containing noise and how much of it is dynamics. For this purpose, we suggest to divide the signal analysis into two main sections of noise and dynamics studies.

Moreover, we already assume that the collected postural signal has been assessed by considering all the anthropometric measurements that is needed and effective in the results.

4.3 Reconstruction of Dynamic at Phase Space by Introducing Time Delay Vectors:

4.3.1 Statistical Mechanics and Information of Human Postural Dynamics

To investigate the dynamics of human posture in a more detailed and reliable way, we need to expand postural dynamics at m-dimensional phase space [51]. If we have a CoPx signal of a quiet stance, in order to estimate the proper time delay (τ) and dimension (m), we use the reconstruction method, which is called the time delay method [6]. In this method the dimension of the phase space is not known, so we need to reconstruct the dynamics from the observable state in m-dimensional state space by selecting a fixed time delay, τ [52]. We assume that CoPx(N) is an observable dynamical-state of the complex postural control system, where N is the total number of data collected.

$$\mathbf{CoPx(i)} = X(1), X(2), ..., X(N) \tag{4.2}$$

Where $i = 1, 2, ...N$, and N is the total number of data collected.

In this method, the new independent variables will be $x(t)$, $x(t + \tau)$, $x(t + 2\tau)$,..., being obtained from a single time series, $x(t)$. (X_i) is the the amplitudes of the data samples in the original time series of measurements, and have been collected by using

a fixed time interval (Δt). Equation (4.3),

$$\mathbf{X(i)} = X_1, X_2, ..., X_N \tag{4.3}$$

where N is the total number of the data points in the time signal. Then we select a fixed time delay τ and write from the previous eq. (4.3) the sequence of base functions of vectors which is called phase space in the m-dimensional state space.(4.4):

$$\begin{aligned}
\mathbf{X_1} &= x_1, x_2, ..., x_{N-(m-1)\tau} \\
\mathbf{X_2} &= x_{1+\tau}, x_{2+\tau}, ..., x_{N-(m-1)\tau+\tau} \\
&\vdots \\
\mathbf{X_m} &= x_{1+(m-1)\tau}, x_{2+(m-1)\tau}, ..., x_N
\end{aligned} \tag{4.4}$$

The coordinates of the phase space, ξ_i where $i = 1, 2, \ldots, m$, are defined as phase points or delay vector, with a length of k, (equation 4.5); based on the parsimony principle $k = N - (m-1)\tau$.

$$\begin{aligned}
\xi_{\mathbf{1}} &= x_1, x_{1+\tau}, ..., \ x_{1+(m-1)\tau} \\
\xi_{\mathbf{2}} &= x_2, x_{2+\tau}, ..., x_{2+(m-1)\tau} \\
&\vdots \\
\xi_{\mathbf{k}} &= x_{N-(m-1)\tau}, x_{N-(m-1)\tau+\tau}, ..., x_N
\end{aligned} \tag{4.5}$$

For being sure that the trajectories have no intersect within, we need to find the proper dimension which is high enough for the reconstruction. based on the dimension m and the time delay τ, different coordinate transformation and structures in the reconstruction embedding spaces will be obtained. As an example we take a time series of numbers from 1 to 10, and we want to apply some rules ,with a given N=10, for estimating the dimension m and time delay τ. And since $k = N - (m-1)\tau$, then we will have:

$$\mathbf{X = 1\ \ 2\ \ 3\ \ 4\ \ 5\ \ 6\ \ 7\ \ 8\ \ 9\ \ 10} \tag{4.6}$$

If we assume $m = 2$, for $N = 10$ we will have:

$$\mathbf{k = 10 - (2 - 1)\tau} \tag{4.7}$$

And therefore, we will have:

$$\mathbf{k + \tau = 10} \tag{4.8}$$

The possible answers for k and τ from the above equation, will be:

Table 4.1: Solutions of τ and k, for $m = 2$,

τ	X_1	X_2	k
1	[1,9]	[2,10]	9
2	[1,8]	[3,10]	8
3	[1,7]	[4,10]	7
4	[1,6]	[5,10]	6
5	[1,5]	[6,10]	5

Therefore if we want to divide the previous signal into two ($m = 2$), and since all the data points should be included in the estimation, maximum τ needs to be 5, but the solution is not unique and every $\tau \leq 5$ can be the answer, while minimum k is also 5, and every $5 \leq k \leq 9$ can be the answer.

Based on the method we used to estimate the maximum τ and minimum k, we reached to three rules:

1. All data should be used in the phase space (parsimony principle)

2. All signals must have the same length (because each element of these signals will be the coordinates of the phase space)

3. The general rule for the given N will lead us to estimate m and τ (eq.4.9,4.10), such

that for non-overlap signals,for each estimation, we will have k many phase points:

$$\mathbf{k_{min}}(\mathbf{m}, \tau_{\mathbf{max}}) = \frac{N}{m} \tag{4.9}$$

And since $N = k_{min} + \tau_{max}$:

$$\tau_{\mathbf{max}} = \frac{N}{m} \tag{4.10}$$

Where k_{min} and τ_{max} are dependent to m, and will be satisfied as long as the the signals are not overlapping with each other, and $\frac{N}{m}$ is a real number to satisfy the parsimony principle. Moreover, if $\tau \geq \tau_{max}$, there will be a gap between signals, in another words, whenever $m \times \tau > N$, gap appears between signals.

On the other hand, if there is an overlap on the signals, although it can increase the phase points, it will affect the result of $\tau_{critical}$.Therefore by increasing τ, we need to check the Independence, otherwise it causes redundancy (Figure 4.2). Moreover, $\tau_{critical}$ is not necessarily equal to τ_{max}, and it depends on the number of data points and overlap signals.

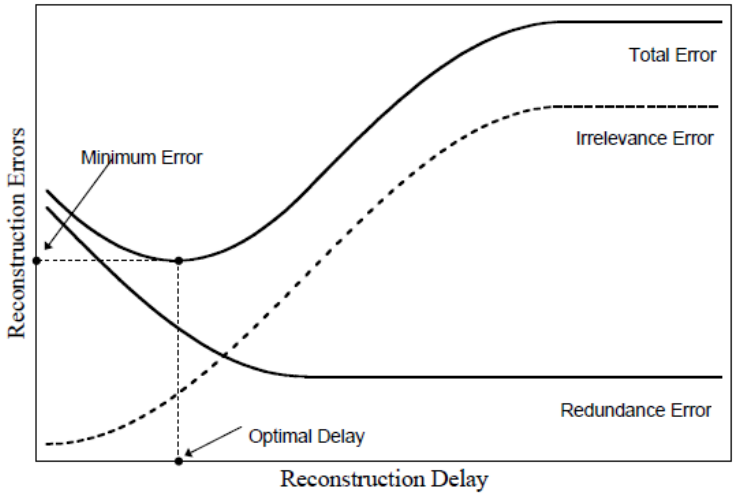

Figure 4.2: Reconstruction error is minimum at the optimum time-delay ($\tau_{critical}$) [2]

On the other hand, $\tau_{critical}$ catches the periodicity and saturates if there is any periodicity, and if not, we don't have any $\tau_{critical}$. Hence, based on figure 4.2, since we don't

know the value of $\tau_{critical}$, we need a method and a metric that help us finding that, and this method is known as average displacement method [2].As we know figure 4.2 is a graphic for a given m, in the left side of the figure, for $\tau = 0$, (when we plot the whole signal with respect to itself and it gives us a line),there is a redundancy in the system and as we move to the right side of the figure and increase the value of τ, at first maximum overlapping occurs between for example two signals for $m = 2$, then by increasing the value of τ overlapping decrease and at some point it reaches to the non-overlap point and somewhere between the maximum overlap and non-overlap, we can find the $\tau_{critical}$. And at the right side of the figure, we reach to the irrelevancy. An important side note here is that, if a signal is periodic, it never goes to irrelevancy. It either becomes independent or redundant.

4.3.2 Average Displacement Method

The method of average displacement which can also be called as m-dimensional embedded phase space, is a function of τ and it is a way to estimate whether the coordinates of phase space (ξ) are far enough with respect to each other. It helps to find out how much delay and how much independency we have, in another words,we will estimate the optimum independency regarding the distance between the phase points (is the attractor expanded enough?).

Based on the coordinates of the phase space of the reconstructed attractor at m-dim phase space, average displacement $S(_\tau)$ is defined as:

$$\mathbf{S}_\tau = \frac{1}{N-(m-1)\tau} \sum_{k=1}^{N-(m-1)\tau} \sqrt{\sum_{i=1}^{m-1} (x_{k+i\tau} - x_k)^2} \tag{4.11}$$

Where, $x_{k+i\tau}$; $i = 0, \ldots, (m-1)\tau$ are the coordinates of the k^{th} phase point (ξ_k) of the reconstructed attractor at the m-dim phase space [2]. In another words, we have k-many phase points in m-dim phase space, and the physical dimension of $S(_\tau)$ is meter [m].

If we have a sin function and plot the graph of $S(\tau)$ with respect to τ, we will have

the following:

$$\mathbf{X(t)} = Asin(\omega t) \tag{4.12}$$

Where, $T = 100sec, fs = 50Hz, fper = 0.1Hz$, and variances of the two-signals match. By embedding the dynamics in m-dimensional phase space, our plot will be like figure 4.3, for m=5:

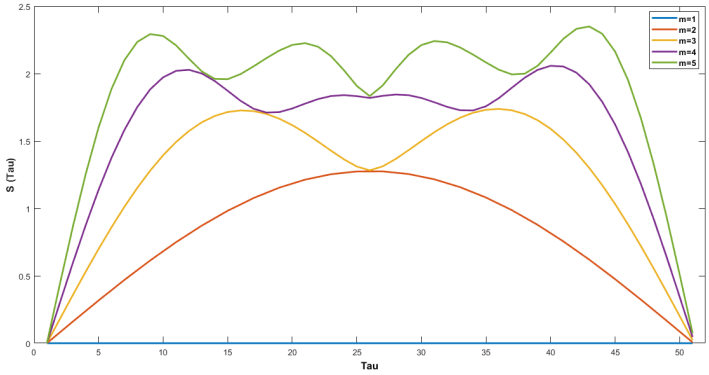

Figure 4.3: S average displacement of a sine function with respect to its delay in m=5 dimensions

In figure 4.3, by looking at the speed of the error,(points when the slope of $S(\tau)$ is zero), we can see that by increasing the m, the zero crossing points change. This means that every time the curve reaches its max point (the zero crossing point for speed), the coordinates separate from each other. And if the pattern gets repeated after passing the max point, this means that our signal is periodic. In this example, for sine signal, the max point in $m = 2$, is the half cycle of the unit circle, and after that it repeats the pattern because it is a periodic signal. Moreover, by increasing the m, the slope of the figures of $S(\tau)$ increases. Because, based on equation (4.11), since it is a dimension metric, the increase of the dimension brings more coordinates to the plot and it causes an increase in the slope of the plot. This happen for smaller τ values, while as τ increases as well, the converging regions increase in bigger τ values,too.

The method of Average displacement is being used for error estimation, and for controlling the error, we use three terms to describe the error and estimate it, which are:

redundancy (dependency), independency, and irrelevancy while it is not easy to differentiate in-between irrelevancy versus independency. We use these terms to estimate a minimum error.

On the other hand, we can also call these m-dim embedding reconstruction as m-many velocity equations if the independency of the coordinate axes is guaranteed (equation 4.13):

$$\dot{\mathbf{X}}_{\mathbf{m}\times\mathbf{1}} = f_{m\times 1}(x_{m\times 1}) \tag{4.13}$$

Such that in the above equation we are estimating the $f(x)$, which is a flow and since this function is unknown, we try to estimate it for different τ values.

Another question may come up is that, why all the $S(\tau)$ curves in figure 4.3 start from zero?

Because for any given m, at the beginning of the signal, τ is equal to zero, which means that the signal is comparing to itself and redundancy is maximum and error is zero because all the coordinates overlap. Therefore the inner summation in equation (4.11) goes to zero. Therefore, if the coordinates overlap, it creates a line and $S(\tau)$ curves cross the zero point. Then, the second the coordinate start to separate from each other and expand, the curve reaches its maximum value when it repeated its pattern, and it goes to zero again when $\tau = 2\pi$.

Now if we want to show the behaviour of a white noise in the plot of $S(\tau)$ with respect to τ, we will have (figure 4.4):

On the other hand, from a statistical point of view, the inner summation (i_m) in the equation 4.11 is calculating the x vectors with respect to a reference. For example, the first vector is the result of the difference between x_1 and $x_{1+\tau}$. The next vector is the result of the difference between x_1 and $x_{1+2\tau}$, and so on, until $m-1$, such that:

$$\mathbf{i_m} = \sqrt{(x_{1+\tau} - x_1)^2 + (x_{1+2\tau} - x_1)^2 + ... + (x_{1+(m-1)\tau} - x_1)^2} \tag{4.14}$$

Then the above equation will calculated for X_2, X_3, until the k^{th} phase point which

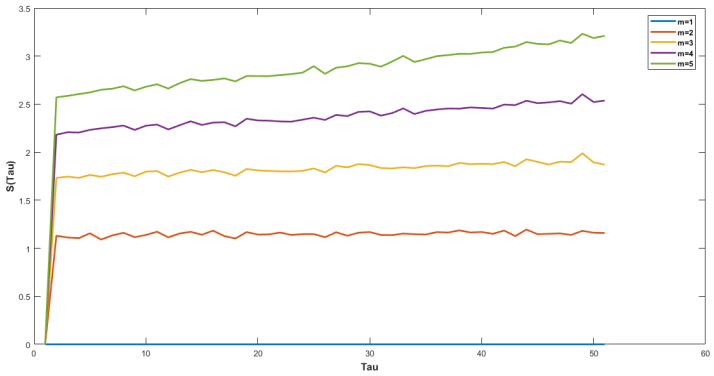

Figure 4.4: S average displacement of a white noise with respect to its delay in m=5 dimensions

will be $X_{N-(m-1)\tau}$. And we know that i_m is not a vector space; rather is an error optimisation, like a regression analysis. Now if we continue this method and estimate the trajectories and phase points, it will lead us to the stabilogram diffusion method [3] and not the average displacement method. In another words we will calculate the stabilogram diffusion in an established attractor which is not the point of this section of the study. And actually, in this section, there isn't any established attractor and the main question here is how to establish an attractor in a correct embedding dynamics.

However, by following the goal of the this section,if we find the $\tau_{critical}$ and find the attractor from the average displacement method, for a given m, then we can continue with stabilogram diffusion method and do the noise analysis. The important note here is that, saturation in a specific dimension and finding the related results doesn't give us any information about it noise level, and to investigate the noise of a signal, we need to do the next section "Stochastic Process of Nonlinear Analysis" for stabilogram diffusion analysis.

Therefore, the general definition of the average displacement method can be followed through figure 4.6, for m=2, where we choose one vector as reference and investigate its difference from the next vectors, which is somehow similar to the linear regression method that looks into the differences from the expected values.

As a first step, our supposition is that if $\tau = \tau_{critical}$, all the vectors' differences are happen to be on the reference line or the main diagonal (the angle between the x axis

and diagonal is 45 degrees) and it means that the vectors are fully time correlated or linearly dependent. In another words, we can interpret this supposition in two ways:

1. Signal function: If we slide on a signal up to τ, and the signal doesn't change, it will remain on the reference line and this will happen if and only if the signal is periodic,(figure 4.5).

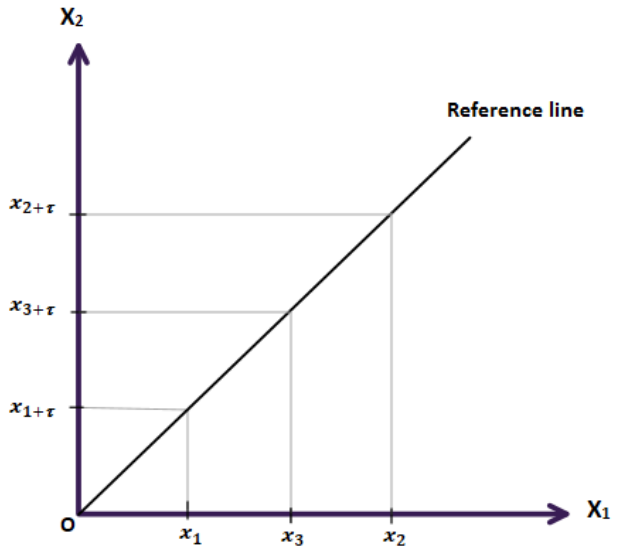

Figure 4.5: if $\tau = 0$ or $\tau = T$ in m=2 dimensions, where T is the period of the periodic function. Note: the order of the vectors on X_1 and X_2 are shuffled and sorted from smallest to largest values.

2. Algebraically speaking: If we write each vector component as a matrix, we will have the following matrices:

$$v_1 = \begin{bmatrix} x_1 \\ x_1 + \tau \end{bmatrix} \quad v_2 = \begin{bmatrix} x_3 \\ x_3 + \tau \end{bmatrix} \quad ... \quad v_{N-(m-1)\tau} = \begin{bmatrix} x_{N-(m-1)\tau} \\ x_{N-(m-2)\tau} \end{bmatrix} \tag{4.15}$$

Now if:

$$c_1 v_1 + c_2 v_2 + ... + c_{N-(m-1)\tau} v_{N-(m-1)\tau} = 0 \tag{4.16}$$

Where, $v_1, v_2, ..., v_{N-(m-1)\tau}$ are the delay vectors and are linearly dependent unless c_i values are zero for all i.

Thus, from these two point of views, if we have a periodic time function $f(t)$, we will have a relation between linear dependency (Algebra) and time correlation (Signal).

However, the first step was only a supposition, and for finding the error in reality, we will continue with step two: Here we look into the amount of expansion from the main diagonal .

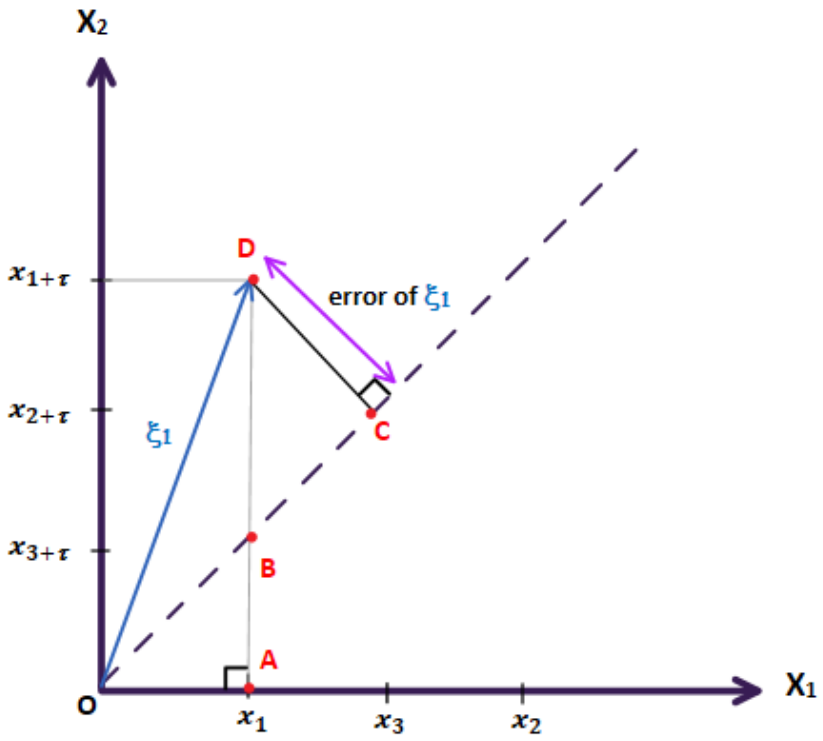

Figure 4.6: phase points error estimation in m=2 dimensions. Note: the order of the vectors on X_1 are shuffled and sorted from smallest to largest values, and on X_2 is sorted based on the τ values.

Figure 4.6 shows the estimation of error at each phase points (here ξ_1) by calculating the difference between the coordinates of the vectors (here $(x_{1+\tau} - x_1)$). Based on the figure 4.6, and from the similarity between $\triangle OAB$ and $\triangle BCD$, we can write

the following equations:

$$
\begin{aligned}
\frac{\mathbf{OA}}{\mathbf{OB}} &= \frac{\mathbf{DC}}{\mathbf{DB}} \\
\frac{\mathbf{x_1}}{\sqrt{\mathbf{2x_1}^{\mathbf{2}}}} &= \frac{\mathbf{DC}}{\mathbf{x_{1+\tau}} - \mathbf{x_1}} \\
\frac{\mathbf{x_1}}{\sqrt{\mathbf{2}}\mathbf{x_1}} &= \frac{\mathbf{DC}}{\mathbf{x_{1+\tau}} - \mathbf{x_1}} \\
\mathbf{x_{1+\tau}} - \mathbf{x_1} &= \sqrt{\mathbf{2}}\mathbf{DC} \\
(\mathbf{x_{1+\tau}} - \mathbf{x_1})^{\mathbf{2}} &= \mathbf{2}(\mathbf{DC})^{\mathbf{2}}
\end{aligned}
\tag{4.17}
$$

Thus, by assuming given τ, and m, from equation 4.17, we can say that this expression is an statistical measure, and $\overline{DC}$ is not a vector space and is an error, which by expanding the equation to the main equation 4.11, it is equal to twice the average of how much the attractor is expanded from the main diagonal in m-dim space. In another words, S-Average Displacement is the average of K-many distances from the main diagonal at m-dim phase space.

Now, in this definition if the vectors happen to overlap (redundant), it means that during the estimation of m, we have not used the correct base vectors which has been created by using τ. As we know, for estimating the m, we need base vectors, and the base vectors are being created by each jump equal to τ, so that these base vectors introduce the m dimension through the given τ, which leads us to place k-many phase points correctly without any overlapping. And this is the result that S_τ gives us and help us to estimate the best amount of expansion from the main diagonal. So, our purpose here is to search for m many independent base vectors, to be extracted from observations spanning through redundancy to irrelevancy. Moreover, the angles between these vectors are also important for interpretation of the postural behaviour point of view and need to be calculated.

4.3.3 Stochastic Process of Nonlinear Analysis

The second section of studying a nonlinear system is investigating the characteristics of the noise embedded in the dynamical system. Based on the previous study on noise structure [3], we can calculate how much delay and how much quadratic variations (variance) have been changed with respect to Δt (figure 4.7). This figure shows the COP trajectories in a two dimensional random walks for given vector space (x, y) . The displacement analysis was carried out by computing the square of the displacements between all pairs of points separated in time by a specified time interval Δt [3]. Variance is linearly related to t, which is also related to the previous section, such that by increasing the τ, variance will be increased. Here,based on figure 4.7 and equation 4.18, we will be looking for the structure of the noise in the system.

Therefore,the previous section (Average Displacement Method) was the study of the determinism in the system and was investigating the expansion of the coordinates and attractor, while this section is the study of the noise in the same system and it follows how the variance increases in time.

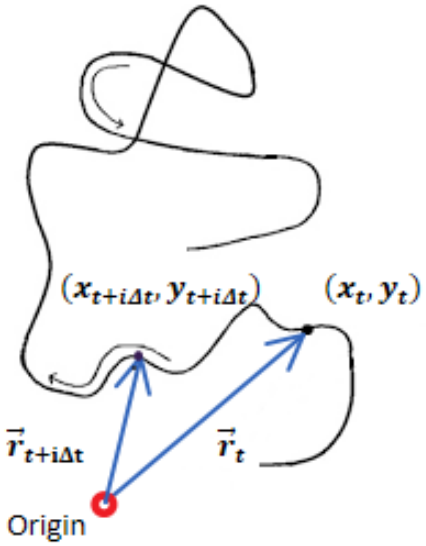

Figure 4.7: stabilogram diffusion [3]

$$\Delta\vec{r}_i = \vec{r}_{t+i\Delta t} - \vec{r}_t \tag{4.18}$$

Where, $i\Delta t = \tau$; $i = 1, ...N$ and is also equal to one over the sampling frequency ($\frac{1}{f}$).

Thus, for a given m, quadratic variation is a function of τ [3].

As an example for CoP, we can write the square of the magnitude of Δr, ($(\Delta r)^2$) as following:

$$\vec{r_1}(t) = (x_1(t), y_1(t)) = x_1(t)\hat{i} + y_1(t)\hat{j} \tag{4.19}$$

$$\vec{r_2}(t+\tau) = (x_2(t+\tau), y_2(t+\tau)) = x_2(t+\tau)\hat{i} + y_2(t+\tau)\hat{j} \tag{4.20}$$

$$\Delta\vec{r} = (x_2 - x_1)\hat{i} + (y_2 - y_1)\hat{j} \tag{4.21}$$

$$\sqrt{(\Delta r)^2} = \sqrt{(x_2 - x_1)^2 + (y_2 - y_1)^2} \tag{4.22}$$

Where $\sqrt{(\Delta r)^2}$ is euclidean, given that these two vectors are independent. Moreover, $\sqrt{(\Delta r)^2}$ is equivalent to $\sqrt{(\Delta \xi)^2}$, with this difference that Δr is given since we know the m, while we need to find the $\Delta\xi$ through the estimated m.

Stochastic process is a study of ensemble signals, and it actually creates a particle's random walk (figure 4.8).

As we mentioned before, this method is a 2-D random walk, but it is not necessarily needed to be a 2-D curve, it can be an m-D curve as well. another important note here is that this curve is time explicit.

Since stabilogram diffusion is not a limit problem,and its more like rolling a dice in each decision making, it is not a function of time and it can be expressed like the following stochastic equation which is the equation of noise for 1-D random walk [53]:

$$\mathbf{\Delta x} = \sqrt{2D}(\Delta t)^{\frac{1}{2}} N(0,1) \tag{4.23}$$

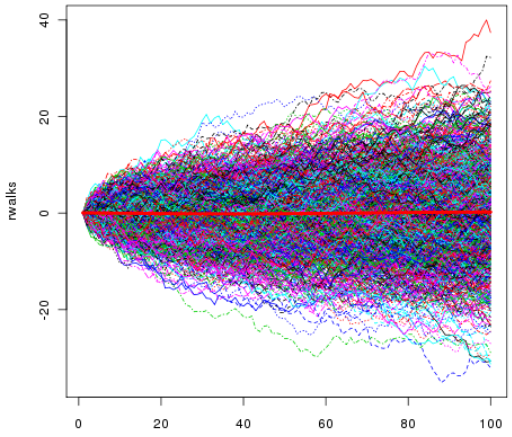

Figure 4.8: Random Walks [4]

Where D is the diffusion coefficient and the physical dimension of it will be the following:

Since physical dimension of $2Dt$ is $[\frac{m^2}{sec} \times sec = m^2]$, we can write the first segments as:

$$\frac{\mathbf{m^2}}{\mathbf{sec}} = \frac{m}{sec} \times \frac{1}{\frac{1}{m}} \tag{4.24}$$

Where $\frac{m}{sec}$ is velocity.Also, the right side of the equation can be written as:

$$\frac{\mathbf{1}}{\mathbf{sec}} \times \mathbf{m} \times \frac{\mathbf{1}}{\frac{\mathbf{1}}{\mathbf{m}}} \tag{4.25}$$

Where $\frac{1}{sec}$ is frequency.

The second statistical moment will be:

$$< \mathbf{\Delta x}.\mathbf{\Delta x} > = \ 2D\Delta t < N(0,1)N(0,1) > \tag{4.26}$$

Where $< \Delta x.\Delta x >$ with physical dimension of $[m^2]$ is a function of Δt. When it is summed over $i\Delta t$, it creates statistical power and it turns out to be the variance as

function of t.

Equation 4.23 shows that by passing t amount of time, the value of the variance will be $2Dt$ with physical dimension of $[\frac{m^2}{sec} \times sec = m^2]$, so by passing Δt amount of time, there will be $2D\Delta t$ variance, and from expression <N(0,1)> in equation 4.23 we know that, the mean is 0 and variance is 1, therefore, $2D\Delta t$ is the variance.

The expression $< N(0,1)N(0,1) >$ in equation (4.26) means that we take the result of rolling a dice once, and multiple it by itself.

Moreover, to estimate the next x, based from the previous equation (4.18), we can write the iteration rule of the noise equation as equation of motion of the spatiotemporal evolution of a random variable as follow:

$$\mathbf{x_{t+\Delta t}} - \mathbf{x_t} = \Delta x \tag{4.27}$$

Thus, we will have:

$$\mathbf{x_{t+\Delta t}} = x_t + \Delta x \tag{4.28}$$

Where, both x_t and Δx are random variables and thus this is an statistical addition of previous step in order to find the next step.

Since this section is based on rolling a dice, next we will come to the statistical moments, and we know that for <N(0,1)>, mean is zero $(\mu = 0)$ and variance is one, $(\sigma^2 = 1)$, and the problem is both spatial and temporal. The first statistical moment is $< x >$ for given t, and the second statistical moment will be $< \Delta x.\Delta x >$.

From figure 4.8, which is a graphical expression of ensemble signals, we can show their Gaussian properties. We know that x_t is a random variable and since this method is not Newtonian, it is actually fate of a single particle, and since here we have ensemble of x_t (time series), so quadratic variation is defined for ensemble of particles. From equation (4.26) we know that expression $< \Delta x.\Delta x >$ is variance or the second moment (σ^2), which may also be multivariate; e.g., 2-D random walk, however in the expression Δx from equation (4.23) is univariate.

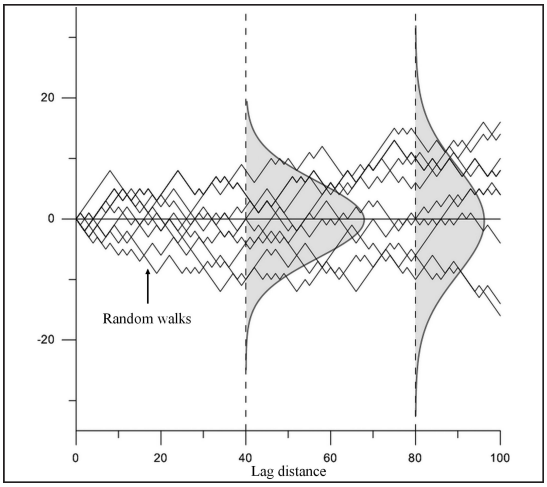

Figure 4.9: Illustration of multiple random walk paths and their Gaussian properties, in which the variance of the histogram formed by the multiple path values increases [5]

Now, based on equation 4.23, which is the basic equation of the stochastic dynamics that means rolling a dice each time to go from i to $i + \Delta t$, for X_N we can write:

$$\mathbf{X_N} = \sum_{i=1}^{N} (\Delta x)_i \tag{4.29}$$

Where x_N is the x in the Nth step, since all the Δx are i.i.d (independent identical distribution) and independent form each other. From figure 4.8, we have one random variable (Δx), N many step for each walker(signal), and also we have n many walker and if we want to keep the pattern of ensemble signals bounded, meaning that while they expand towards positive and negative direction of the y axis, we need to call them back to maintain in a bounded standard deviation region, which is the case for human postural sway dynamics as we never fall while swaying! Now, we can rewrite the equation 4.23 as follow:

$$\mathbf{\Delta x} = \ x_{i+1} - x_i = \ \sqrt{2D}(\Delta t)^{\frac{1}{2}} N(0,1) \tag{4.30}$$

And, if we have two random variables x_1 and x_2, such that:

$$\mathbf{x_1} \triangleq N(\mu_1, {\sigma_1}^2), \quad \mathbf{x_2} \triangleq N(\mu_2, {\sigma_2}^2) \tag{4.31}$$

Where, μ is the mean and σ is the variance. So, we can write:

$$\mathbf{x_1} + \mathbf{x_2} = N(\mu_1 + \mu_2, {\sigma_1}^2 + {\sigma_2}^2) \tag{4.32}$$

where, means and variances of x_1 and x_2 are added which is the characteristic of the normal distribution.Now, since with this method we cant call back the signal, we need to create a velocity by which it is proportional to the current position of the signal. So, the physical dimension of the velocity is m/s, and we know that physical dimension of the $\sqrt{2D}$ in the equation 4.30 is $\sqrt{\frac{m^2}{s}}$ and the physical dimension of the $(\Delta t)^{\frac{1}{2}}$ is $\sqrt{s}$, therefore, the physical dimension of the Δx will be [m]. Thus, in order to add a velocity to equation 4.30, we need to write as following:

$$\mathbf{\Delta x} = x_{i+1} - x_i = \sqrt{2D}(\Delta t)^{\frac{1}{2}} N(0,1) + V(x_i)\Delta t \tag{4.33}$$

Where, $V(x_i)$ can be written as λx_i, and $\lambda = f(frequency)$, the physical dimension of λ is $\frac{1}{s}$, and the physical dimension of x_i is m, then by multiplying the $V(x_i)$ by Δt, it will be $\frac{1}{s}.m.s = m$. So, the equation will be like:

$$\mathbf{\Delta x} = x_{i+1} - x_i = \sqrt{2D}(\Delta t)^{\frac{1}{2}} N(0,1) + \lambda x_i \Delta t \tag{4.34}$$

Here, we take a limit of Δt to zero ($\Delta t \to 0$), thus we will have dx_i:

$$\mathbf{dx_i} = \sqrt{2D} dB_t + \lambda x_i dt \tag{4.35}$$

Where, dB_t, which is also known as the Wiener process (dW_t) is obtained from $(\Delta t)^{\frac{1}{2}}$ expression multiplied by $N(0,1)$. We also know that cumulative sum of equation 4.35 will gives us the Brownian motion (see equation 4.29). Furthermore, time derivative of equation 4.35 is the velocity equation where $\frac{dB_t}{dt} = w_t$, which is known as the white noise. Therefore, the equation 4.35 will be like:

$$\mathbf{\dot{x}_i} = \sqrt{2D} w_t + \lambda x_i \tag{4.36}$$

Moreover, if we want to write the equation(4.29) for the X after $N\Delta t$ amount of time, we can write as follow:

$$\begin{aligned}
\mathbf{X_{N\Delta t}} &\overset{\mathrm{d}}{=} \sum_{i=1}^{N} (\Delta x)_i \\
&= \sum_{i=1}^{N} \sqrt{2D}(\Delta t)^{\frac{1}{2}} < N(0,1) > \\
&= \sqrt{2D}(\Delta t)^{\frac{1}{2}} \sum_{i=1}^{N} < N(0,1) > \\
&= \sqrt{2D}(\Delta t)^{\frac{1}{2}} N(0,N) \\
&= N(0, 2DN\Delta t)
\end{aligned} \tag{4.37}$$

Where, d on the equal sign of the first row means distribution (fate of many particles). The summation of the mean and variance will leads us to $X_{N\Delta t}$, because means are zero, so their summation will also be zero, and the summation of N many variance will be N. Then, in the next step base on the rule of the normal distribution, which is:

$$\mathbf{C}.\mathbf{N}(\mu_{\mathbf{1}}, {\sigma_{\mathbf{1}}}^{\mathbf{2}}) = N(\mu_1.C, {\sigma_1}^2.C^2) \tag{4.38}$$

the constant section of the equation which is $(\sqrt{2D}(\Delta t)^{\frac{1}{2}})^2$ will multiplied with the variance and we will have $2DN\Delta t$.

Next, for $t = N.\Delta t$, we can write:

$$\begin{aligned} \mathbf{X_t} &= X_{N\Delta t} \\ &= N(0, 2Dt) \\ &= \sqrt{2D}N(0, t) \\ &= \sigma N(0, t) \\ &\triangleq \sigma.B_t \end{aligned} \tag{4.39}$$

Now, by taking derivative of two sides of the above equation with respect to t, we can write:

$$\begin{aligned} dx_t &= \sigma.dB_t - \lambda x_t dt \\ \dot{x_t} &= -\lambda x_t + \sigma\frac{dB_t}{dt} \\ \dot{x_t} + \lambda x_t &= \sigma w_t \\ &= F_t \end{aligned} \tag{4.40}$$

Where F_t is the forcing term which is equal to white noise.

In a comparison between the two methods; i.e., dynamics versus noise, we can tell that in the method to reveal the noise characteristics from an observation, for a given m, we can find an answer for the equation (4.18) by subtracting the coordinates of the corresponding points. While in the reconstruction dynamics method, we estimate the dimension of the dynamics, m in order to embed it (the phase points described through time delay method, see equation 4.5) into the vector (phase) space constructed from independent (orthogonal) estimated signals (see equation 4.4). In summary, in the noise characteristic method, given the vector space, we estimate for the quadratic variation in the observation(s) $(\Delta r)^2$. But, if vector (phase) space is unknown, these two methods will be the identical. Thus, the one and important difference between these two methods is whether there exists a given vector (phase) space or not. And based on the equation (4.4) each X_m is the base functions of the vector

space and must be independent. Please note that equation (4.18) is a special case of more general difference equation (4.11) where deterministic part of the dynamics is searched for, if ever exists.

4.3.4 Information Theory and Dimension Analysis

4.3.4.1 Information Theory

- **Binary Events**

  The definition of information can be written as [6]:

$$I \triangleq K \ln R \tag{4.41}$$

  Where, $K = \log_2 e$. So:

$$\begin{aligned} I &= \log_2 e \ln R \\ &= \log_2 R \\ 2^I &= R \end{aligned} \tag{4.42}$$

  Where, $2^I = R$ is a random walk since this is a binary event with logarithmic base of 2 (points (phase) at the event). "I" is the number of decision making which is known as the information. R is the realization factor (at the reservoir, possible combinations of the points) and can be written as:

$$R(N, n) = \frac{N!}{n!(N-n)!} \tag{4.43}$$

  Where, N is the number of decision makings (freedom), and n is the number of outcomes (phase points).

As an example, for a fair binary process we can write the pascal triangle, N=4:

$$\begin{aligned} n_L + n_R &= N \\ 2^N &= R \\ 2^4 &= 16 \\ &= c(\begin{smallmatrix} 4 \\ 0 \end{smallmatrix}) + c(\begin{smallmatrix} 4 \\ 1 \end{smallmatrix}) + c(\begin{smallmatrix} 4 \\ 2 \end{smallmatrix}) + c(\begin{smallmatrix} 4 \\ 3 \end{smallmatrix}) + c(\begin{smallmatrix} 4 \\ 4 \end{smallmatrix}) \\ 2^N &= \sum_{n=0}^{N} \frac{N!}{n!(N-n)!)} \end{aligned} \tag{4.44}$$

- **Probable Events**

  As an example of probable events, lets assume the pascal triangle and do the calculations:

$$P(N,n) = \frac{N!}{n!(N-n)!)} p^n p^{N-n} \tag{4.45}$$

  Where, $\sum_{i=1}^{2} p_i = 1$. Expression p_i is the probability of a binary event symbols p and q, ($p_1 = p$, and $p_2 = q$), and express the fairness and missing information, while P is the outcome measurement. For the pascal triangle probability event we can write the equation 4.45, as follow:

$$\begin{aligned} P(4,0) &= \frac{4!}{0!(4-0)!)} (\frac{1}{2})^0 (\frac{1}{2})^{4-0} \\ &= \frac{1}{16} \end{aligned} \tag{4.46}$$

  Based on the figure (4.10), p and q are the probabilities of a binary event, where $p + q = 1$. For $p = q = \frac{1}{2}$, nothing is known, and there is a maximum exploration $per\ ipsum$, and in an other word, entropy (the missing information) is maximum. While for $p = 1$ and $q = 0$, or $p = 0$ and $q = 1$ everything is known, and there is a maximum exploitation and minimum entropy. Thus, the more the missing in information, the more the entropy is.

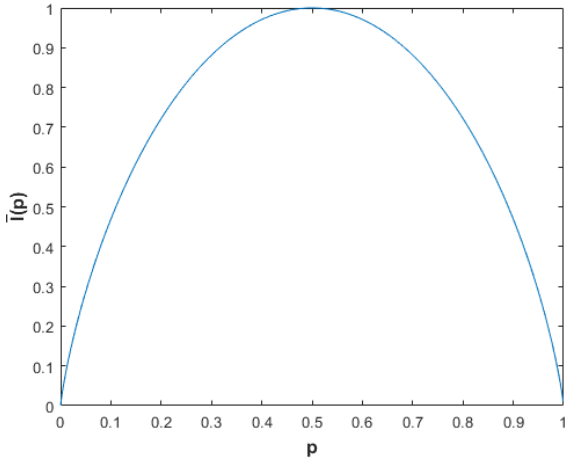

Figure 4.10: Normalized information versus missing information (Shannon Entropy) plot

- **Shannon Information Theory**

  For a binary process via the Stirling's approximation we can rewrite the equation 4.41, by substituting R, as the following:

$$I \triangleq K \ln \frac{N!}{n!(N-n)!} \tag{4.47}$$

  Since the information increases with the number N of the realisations and thus with the number of decisions, the mean value is of interest. Therefore, the information per decision is [6]:

$$\bar{I}(p) = \frac{I}{N} \tag{4.48}$$

  Using the Stirling approximation, leads us to the following result (See Appendix B):

$$\bar{I}(p) = -K \sum_{i=1}^{k} p_i \ln p_i \tag{4.49}$$

  Where K is the constant for logarithmic base conversion, and $\bar{I}(p)$ is positive definite.

Now, for the probability of a binary event $\bar{I}(p)$ can be written as:

$$\bar{I}(p) = -K \sum_{i=1}^{2} p_i \ln p_i \tag{4.50}$$

Lets assume that $p_i = \frac{1}{2}$, (uniform):

$$\begin{aligned} \bar{I}(p) &= -\log_2 e(2 \cdot \frac{1}{2} \ln \frac{1}{2}) \\ &= -\log_2 e(\ln 1 - \ln 2) \\ &= -\log_2 e(-\log_e 2) \\ \bar{I}(p) &= 1 \end{aligned} \tag{4.51}$$

Remark that the p_i in equation 4.49 is no longer has to be equal to $\frac{1}{2}$, and it can be both fair an unfair event. So, missing information is actually measure of the unfairness. Moreover, this equation (4.49) can be used for any logarithmic base (see figure 4.10).

4.3.4.2 Dimension Analysis

In this section the q-dim dimension analysis will be applied. So, the information equation here, is a function of q [54, 6].

$$\bar{I}_q(\varepsilon) \triangleq \frac{1}{1-q} \ln \sum_{k=1}^{W(\varepsilon)} {p_k}^q \tag{4.52}$$

Where $\bar{I}(q)$ is the mean information, and q is not the same dimension that we investigated in the average displacement method (m-dim). We know that in the average displacement method, for embedding the attractor, we used m-dim for estimating the dimension. while in this method, q is the order of relation in between the phase points. Note that the relation between the phase points can be pseudo neighborhood relationships, if the obtained phase points and previous steps of estimating the m and τ are not correct.

Based on the definition of generalized dimension [55, 56, 54] (Rényi dimension). To determine the dimension of the attractor, we consider a uniform subdivision of the phase space into hyper cubes of edge length ε. Let $W(\varepsilon)$ be the number of boxes which contain measuring points and assume that, of N measurements, n_k measuring points lie in the k-th hypercube. The relative frequency of finding a point in the k-th box depends on the measuring accuracy ε, i.e. on the partitioning of the phase space, and is expressed by $p_k = \frac{n_k}{N}$ [6]. The definition of the dimension is given in the following equation:

$$D_q = \lim_{\varepsilon \to 0} \frac{I_q(\varepsilon)}{\ln \frac{1}{\varepsilon}} \tag{4.53}$$

Where, ε is the measuring accuracy or spatial tolerance metric.[6]
In this method, for estimating the dimensions, we scan a hyper-spherical (m-dim) space with m-many radii (r), around each phase point, and count the number of phase points within the sphere, which will be the probability around that phase point ($p_k(r)$) which is the function of r, and we repeat this method k-many times (for each phase point). Moreover, we can say that ($p_k(r)$) is proportional with r, and we can solve it to find the proportionality constant, D.

$$\begin{aligned} p_k(r) &\propto r^{(D)} \\ \ln p_k(r) &\propto D \ln r \\ \frac{\ln p_k(r)}{\ln r} &\propto D \end{aligned} \tag{4.54}$$

So, for any r, we estimate the probability of the phase points to be in the vicinity of a particular phase point (neighborhood relationships around each phase point) in the embedded dynamics to m-dim phase space, and we expect an increase in the number of neighborhood relationships as the radius r increases.

Now lets assume that q=0,1,2 and run the equation 4.52 for q=0:

$$\begin{aligned} \bar{I}_0(\varepsilon) &= \ln \sum_{k=1}^{W(\varepsilon)} 1 \\ \bar{I}_0(\varepsilon) &= 1 \ln W(\varepsilon) \end{aligned} \tag{4.55}$$

$$\begin{aligned} D_0 &= \lim_{\varepsilon \to 0} \frac{\bar{I}_0(\varepsilon)}{\ln \frac{1}{\varepsilon}} \\ &= \lim_{\varepsilon \to 0} \frac{\ln W(\varepsilon)}{\ln \frac{1}{\varepsilon}} \end{aligned} \tag{4.56}$$

Which is known as the box counting. Next we run the equation 4.52 for q=1:

$$\bar{I}_1(\varepsilon) = \frac{1}{1-q} \ln \sum_{k=1}^{W(\varepsilon)} {p_k}^{q=1} \tag{4.57}$$

Which results in the Shannon augmented entropy measure, and needs to be solved through the L'Hospital's rule:

$$\begin{aligned} \bar{I}_q(\varepsilon) &= \frac{\frac{d}{dq} \ln \sum_{k=1}^{W(\varepsilon)} {p_k}^q}{\frac{d}{dq}(1-q)} \\ &= -\frac{d}{dq}(\ln \sum_{k=1}^{W(\varepsilon)} {p_k}^q) \\ &= -\frac{d}{dq} \ln({p_1}^q + {p_2}^q + ... + {p_k}^q) \end{aligned} \tag{4.58}$$

Where here, k is the logarithmic base and is unknown, and the values of q determines the probability of the number of neighbors falling next to each other. We can assume the $({p_1}^q + {p_2}^q + ... + {p_k}^q)$ section as $f(q)$, where for q=1, $p_1, p_2, ..., p_k$ are constant.

So, the right side of the above equation can be written as:

$$\begin{aligned} \frac{d}{dq}\ln(f(q)) &= f'(q)\frac{1}{f(q)} \\ &= f'(q)\frac{1}{\sum_{k=1}^{W(\varepsilon)} {p_k}^{q=1}} \end{aligned} \tag{4.59}$$

So, for q=1, the total $p_k = 1$ over k. Now we solve the $f'(q)$ part:

$$f'(q) = \frac{d}{dq}({p_1}^q + {p_2}^q + ... + {p_k}^q) \tag{4.60}$$

Since the derivative operator is linear, solving $\frac{d}{dq}({p_1}^q)$ is enough. Lets assume that ${p_1}^q = u(q)$, by taking logarithms of the both sides:

$$\ln {p_1}^q = \ln u(q) \tag{4.61}$$

Next, we take the derivatives of both sides:

$$\begin{aligned} \frac{d}{dq}\ln {p_1}^q &= \frac{d}{dq}\ln u(q) \\ \ln p_1 &= \frac{d}{dq}u(q)\cdot\frac{1}{u(q)} \end{aligned} \tag{4.62}$$

First, lets substitute ${p_1}^q = u(q)$:

$$\begin{aligned} \ln p_1 &= \frac{d}{dq}{p_1}^q.\frac{1}{{p_1}^q} \\ {p_1}^q\cdot\ln p_1 &= \frac{d}{dq}{p_1}^q \end{aligned} \tag{4.63}$$

Thus, from equations 4.58 and 4.59, $\bar{I}(q)$ when q=1, can be written as [6]:

$$\begin{aligned} \bar{I}_1(\varepsilon) &= -\frac{\sum_{k=1}^{W(\varepsilon)} p_k \ln p_k}{(\sum_{k=1}^{W(\varepsilon)} p_k) = 1} \\ \bar{I}_1(\varepsilon) &= -\sum_{k=1}^{W(\varepsilon)} p_k \ln p_k \end{aligned} \tag{4.64}$$

And D_1 will be:

$$D_1(\varepsilon) = \lim_{\varepsilon \to 0} \frac{-\sum_{k=1}^{W(\varepsilon)} p_k \ln p_k}{\ln \frac{1}{\varepsilon}} \tag{4.65}$$

Next we run the equation 4.52 for q=2:

$$\bar{I}_2(\varepsilon) = -\ln \sum_{k=1}^{W(\varepsilon)} {p_k}^2 \tag{4.66}$$

And D_2 will be:

$$D_2(\varepsilon) = \lim_{\varepsilon \to 0} \frac{-\ln \sum_{k=1}^{W(\varepsilon)} {p_k}^2}{\ln \frac{1}{\varepsilon}} \tag{4.67}$$

For estimating entropy and all of the above metrics (logarithmic base, I, and R; where only two of the variables are independent, see equation 4.41), first we do the calculation for m=2, $\tau = 1$. In this step we have the phase points and their coordinates, and number of decision makings/observations (N). Thus we start with maximum missing information, and move on toward the known information. A distance matrix needs to be estimated first [57], from the phase points' coordinates to get the information about the distance between each phase points and the others (d) and compare it with the tolerance metric; i.e., ε (see equation 4.54). For any d smaller than tolerance metric, it gives us 1, and for any d larger than tolerance metric, it gives us 0, the result will be an $N \times N$ matrix containing zeros and ones.

4.3.4.3 Dimension Analysis of CoP signal

For dimension analysis of the CoPx signal, each signal can be assumed as one member (batch) of the ensemble with N-many observations/decision makings. So, for this problem, we assume that we know the number of decision makings, but we don't know the logarithmic base, and for the estimation of it, we can only say that it is bounded from the lower values (minimum) which is the resolution of the force plate measurements (see Appendix A). Thus, for estimating the grid-size (lattice-model,[58]) between the maximum and minimum values of CoPx and CoPy (in another words the number of boxes in the matrix of the phase points), we can define a new parameter (c), as a function of ε which is also related to the number of decision making (N) and define it as bellow:

$$\begin{aligned} c_x &= \frac{X_{max} - X_{min}}{\varepsilon} \\ c_y &= \frac{Y_{max} - Y_{min}}{\varepsilon} \end{aligned} \tag{4.68}$$

Now, if the distribution is uniform (4.11), and we know the value of c, we can estimate the logarithmic base.

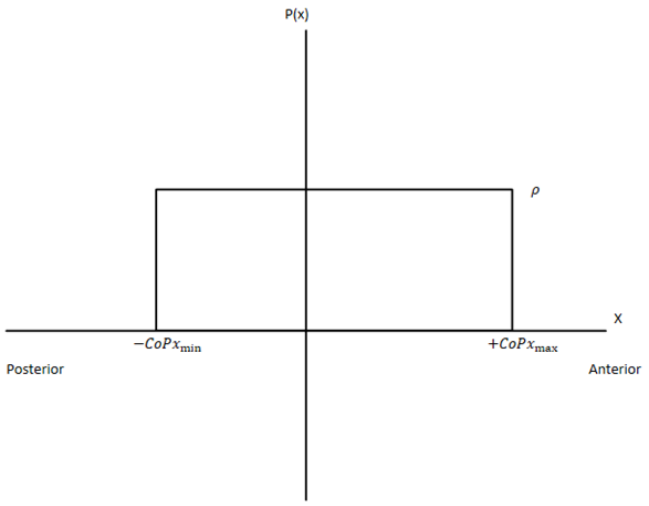

Figure 4.11: Uniform probability density (distribution) function (pdf) of CoPx on Anterior-Posterior axis

From uniformity of the pdf we know that:

$$\begin{aligned} \rho \cdot (CoPx_{max} - CoPx_{min}) &= 1 \\ \rho &= \frac{1}{(CoPx_{max} - CoPx_{min})} \end{aligned} \tag{4.69}$$

Where 1 is the underneath area. So, for figure 4.11 we can write:

$$\begin{aligned} CoPx_{max} - CoPx_{min} &= \Delta CoPx \\ \rho \cdot \Delta CoPx &= 1 \\ \rho &= \frac{1}{\Delta CoPx} \end{aligned} \tag{4.70}$$

We need to find the probable visited positions (the grid-size as a function of, ε) inside this uniform distribution. Since we have c:

$$c = \frac{\Delta CoPx}{\varepsilon} \tag{4.71}$$

Then probability will be $p = \frac{1}{c}$. Please note that the parameter (c), as a function of ε is also related to the number of decision making, N. Now, we can write the maximum entropy (described in the equation, 4.64) as the following [58],(Ch.6, Boltzman

Distribution):

$$\begin{aligned}
\rho = p_k &= \frac{1}{c} \\
\bar{I}(p) &= -\sum_{k=1}^{W(\varepsilon)} p_k \ln p_k \\
&= -\sum_{k=1}^{c} (\frac{1}{c} \ln \frac{1}{c}) \\
&= -c\frac{1}{c} \ln \frac{1}{c} \\
\bar{I}(p)_{max} &= S_{max} = -(\ln 1 - \ln c) \\
S_{max} &= \ln c
\end{aligned} \tag{4.72}$$

From the above equation we can say that entropy is related to the $\Delta CoPx$ and the number of decision making (N). So, we may assume the logarithmic base as c, but it needs to be tested by the real data.

On the other hand, we can implement the ideas of the previous steps (Shannon Information Theory and Missing Information) for the CoPx signal; such as, if p_k in equation 4.72 comes out to be,

$$p_k \triangleq \frac{n_k}{N} \tag{4.73}$$

Then, the condition of the phase points' fair distribution (N-many events) has been deteriorated, unless the probability of each phase point is $\frac{1}{N}$, where N is the number of boxes (total freedom). As an example of the idea for maximization of the free-energy or minimization of the missing information see the problem studied in Appendix C.

Thus, based on chapter 3, [57], for the CoPx signal, we can estimate the distance matrix, and calculate the entropy measure (APproximate ENtropy) and dimension through the following steps:

The original data (CoPx signal) is $x(n) = x(1), x(2), ..., x(N)$, where N is the total number of data points. the embedding dimension m and time delay τ have been estimated from the average displacement method. Also, the tolerance metric (r or

ε), has been estimated through the standard deviation measure [59, 57], see equation 4.80.

- First we form m-vectors $X(1), ..., X(N-(m-1)\tau)$ defined by:

$$X(i) = [x(i), x(i+1), ..., x(i+m-1)] \qquad ; i = 1, ..., N-(m-1)\tau \quad (4.74)$$

  where τ has been taken as 1 (see figure 4.2 against the idea at chapter 3, [57]. This expression needs to be compared to and against to equations 4.4 and 4.5.

- Next we define the distance between $X(i)$ and $X(j)$, $d[X(i), X(j)]$, as the maximum absolute difference between their corresponding scalar elements, which is the n^{th} order distance for m-dim between two phase points. Based on the m-dim generalized euclidean distance definition:

$$\lim_{n\to\infty} \sum_{i=1}^{N} |X(i+1) - X(i)|^n = X_{max} - X_{min} \quad (4.75)$$

  We can write the following equation:

$$d[X(i), X(j)]_{k=0,m-1} = max[|x(i+k) - x(j+k)|] \quad (4.76)$$

- Then, for a given $X(i)$, find the number of $d[X(i), X(j)]$, $j = 1, N-m+1)$ that is $\leq r$ (or ε, the tolerance metric) and the ratio of this number to the total number of m-vectors $(N-m+1)$:

  Lets assume $N^m(i)$ is the number of $d[X(i), X(j)] \leq r$.

  Then $C_r^m(i) = N^m(i)/(N-m+1)$ is estimated for $i = 1, N-m+1$.

- Next we take the natural logarithm of each $C_r^m(i)$, and average it over i:

$$\phi^m m(r) = \frac{1}{N-m+1} \sum_{i}^{N-m+1} \ln C_r^m(i) \quad (4.77)$$

- In the next step we increase the dimension to $m+1$, and repeat the previous steps for estimating $C_r^{m+1}(i)$, and $\phi^{m+1}(r)$.

- Theoretically, the approximate entropy is defined as[57]:

$$ApEn(m, r) = \lim_{N\to\infty} [\phi^m(r) - \phi^{m+1}(r)] \quad (4.78)$$

In practice, the number of data points N is finite and the result obtained through the preceding steps is an estimate of ApEn when the data length is N. This is denoted by:

$$ApEn(m, r, N) = \phi^m(r) - \phi^{m+1}(r) \tag{4.79}$$

The value of the estimate depends on m, r (or, the tolerance metric, ε), and τ . As suggested by Pincus [59], m can be taken as 2 and r be taken as $(0.1, 0.25)SD_x$, where SD_x, is the standard deviation of the original data $x(n)$:

$$SD_x = \sqrt{\frac{1}{N-1}\sum_{n=1}^{N}[x(n) - \frac{1}{N}\sum_{n=1}^{N}x(n)]^2} \tag{4.80}$$

So, by applying all the above steps and conditions into the code, we can analyze the CoPx signal for entropy approximation.

CHAPTER 5

SIMULATION RESULTS

5.1 Sinusoidal and White Noise Signals Simulations:

Lets assume a sinusoidal signal $x(t) = Asin(\omega t + \phi)$ where A is the amplitude, ω is the angular frequency (rad/sec), and ϕ is phase angle (rad). Figure 5.1 shows four different shapes of a Sine wave regarding the changes in amplitude, angular frequency, and phase angle of a sine signal, respectively.

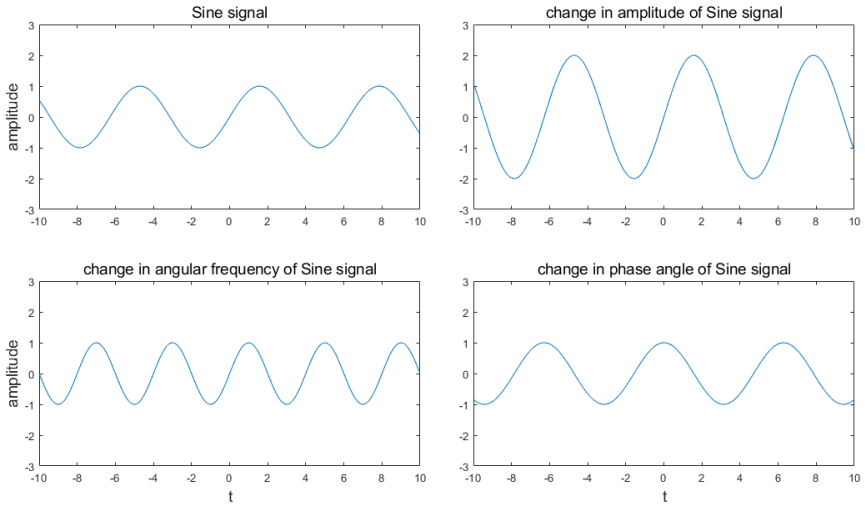

Figure 5.1: Four different shapes of a Sine Wave

Now, lets assume a simple sinusoidal signal with $A = 1$ [cm], $\omega = 1$ [rad/sec], $\phi = 1$ [rad], sampling frequency (fs) of 50Hz and period (T) of 100 seconds.(Figure5.2)

Next, lets create a white noise signal (WN=wgn(1000,1,0);) (Figure5.3).

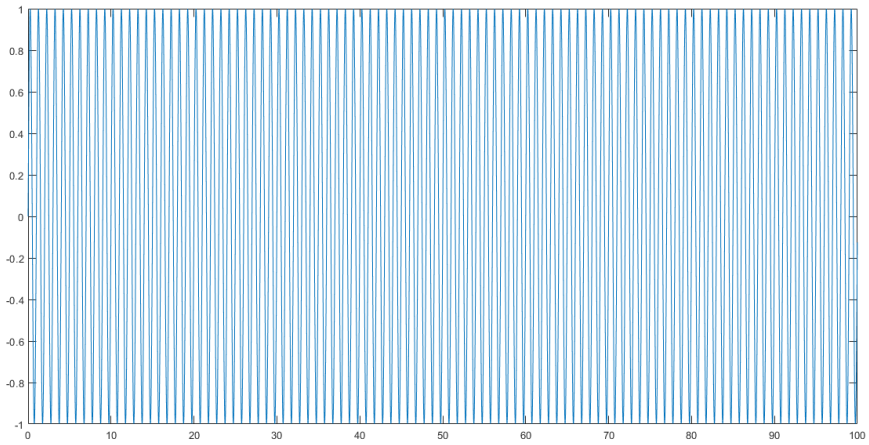

Figure 5.2: A sample Sine Wave

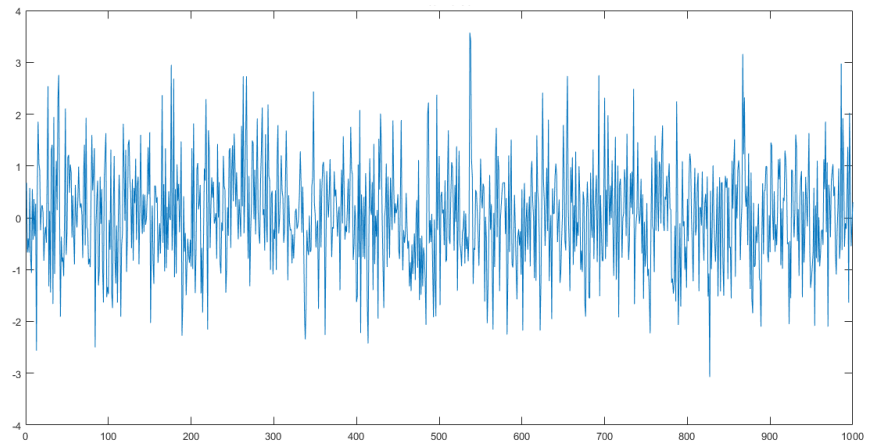

Figure 5.3: A sample White Noise signal

5.2 Nonlinear Analysis Results of the Sinusoidal and White Noise Signals:

By applying the s-displacement method, we can estimate the τ_c for both sine and white noise signals Table 5.1. Figure5.4 shows the $S(\tau)$ plots of sine wave and white noise, respectively.

5.3 Nonlinear Analysis Results of the CoPx signal:

The nonlinear analysis on the CoPx signals, results in finding the τ_c for different dimensions. Moreover the related $S(\tau)$ plots for each CoPx signal provide more

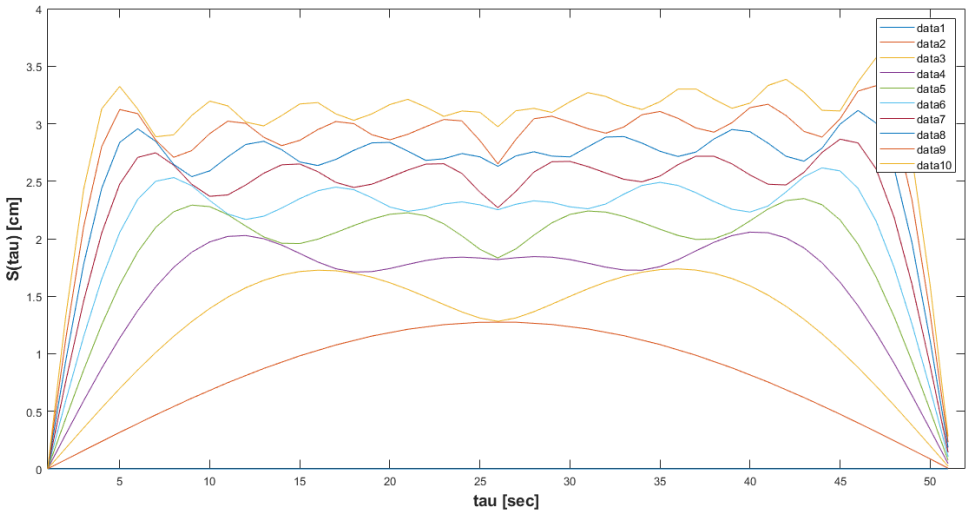

(a) $S(\tau)$ of sine wave

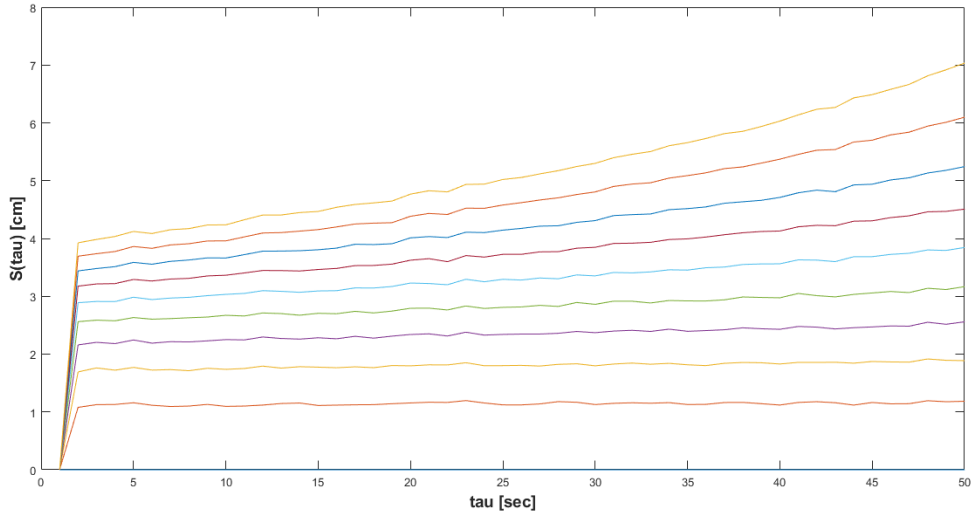

(b) $S(\tau)$ of White Noise

Figure 5.4: $S(\tau)$ plots of a) sine wave and b) White Noise signals

Table 5.1: Time delay (τ_c) values for sine and white noise (WN) signals

m	τ_c (Sine)	τ_c (WN)
2	19	2
3	12	2
4	9	2
5	7	2
6	6	2
7	5	2
8	5	2
9	4	2
10	4	2

information about the behaviour of the attractor in infants. We have observed the changes in $S(\tau)$ plots, from a noise like form in T1 toward almost an adult plot (Figure 5.6) in T3, but we can confirm that there is still time needed for the infants to complete this process and reach to the desired adult pattern in case of the postural control and quiet stance behaviour. Our observation in infants' and adult's $S(\tau)$ plots give us critical information regarding the slope of the plots, and their velocity regarding the dimension. regarding the slope, we see that as long as the initial slope is high in infants, the pattern is close to the white noise signal, while the adults $S(\tau)$ has smoother initial slope. On the other hand, from the plots of Sine we can say that the dimension m also affects the slope of the plots such that for small m values, the slopes are steep, while for larger m, it gets sharp. The following plots (figure 5.5) are the $S(\tau)$ plots of an exemplar subject in T1, T2, and T3.

However, figure 5.5 is just the demonstration of an exemplar subject, and the overall behaviour in each subject is different. Thus, the reliable results can be obtained from the statistical analysis.

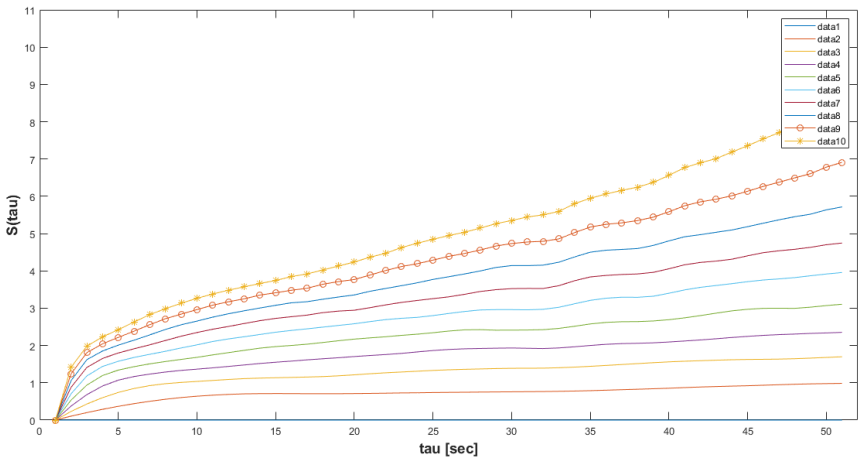

(a) $S(\tau)$ of T1

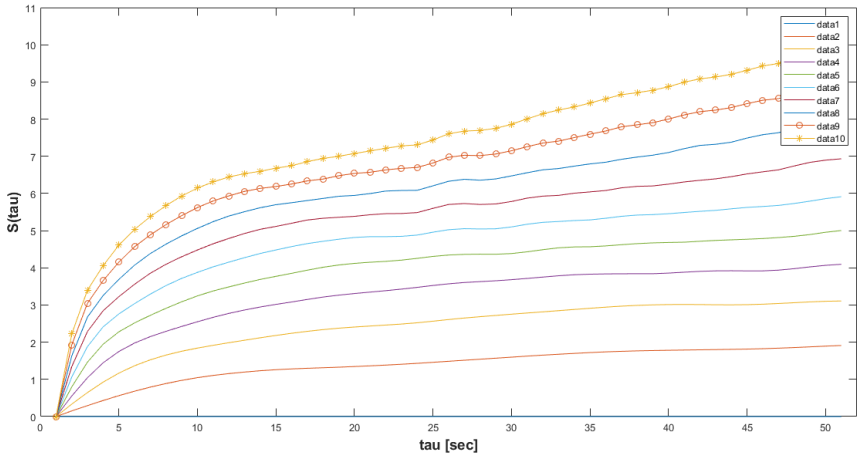

(b) $S(\tau)$ of T2

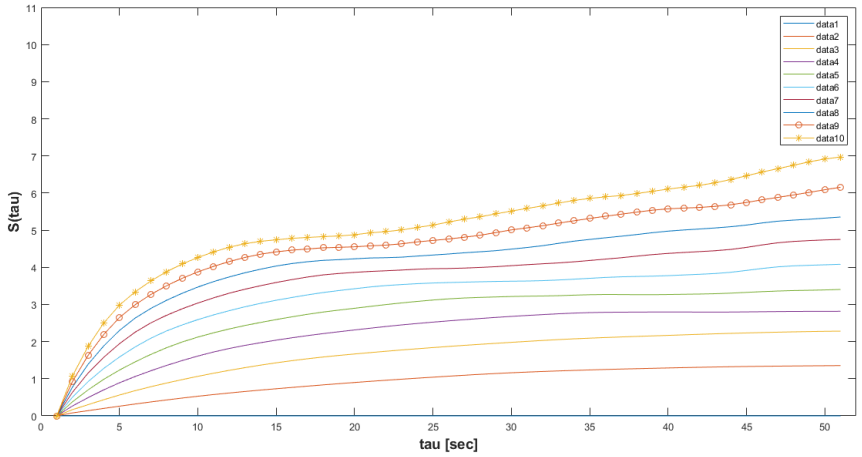

(c) $S(\tau)$ of T3

Figure 5.5: $S(\tau)$ plots of an exemplar female subject in a) T1, b) T2, and c) T3

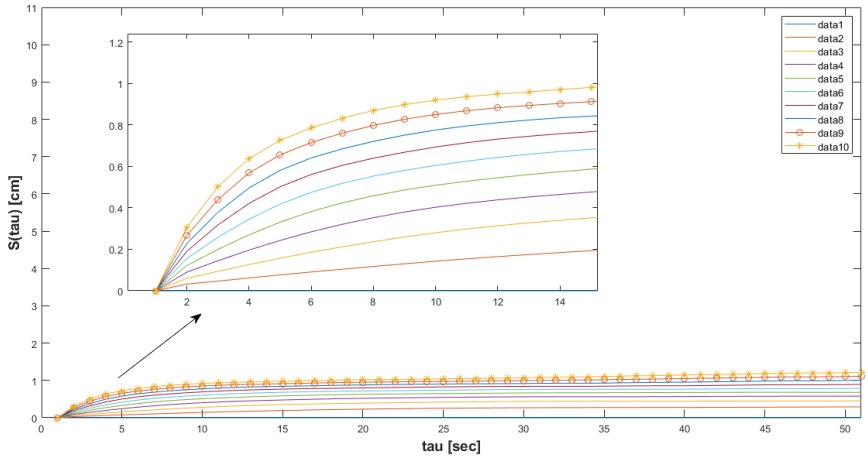

Figure 5.6: $S(\tau)$ plots of and Adult subject

5.3.1 Entropy results of the Five common female subjects

First the entropy was calculated for $\tau = 1$ [57]. Then, we used the obtained τ_c values for the entropy estimation. The approximate entropy (ApEN) values for $\tau = 1$ and $\tau = \tau_c$ are presented in table 5.2. Based on this table, we can see an increase in the entropy for $\tau = \tau_c$, especially regarding T1 to T3. These findings are in close conformity with our hypothesis, in which we mentioned an expectation of an increase in entropy metric as the infants develop their postural control.

5.3.2 Entropy results of the all subjects

The results of the nonlinear analysis for all the subjects (τ_c and entropy), were obtained for $m = 2, ..., 10$. the mean of the entropy for each trimester show an increase in entropy from T1 to T3 (T1=0.72, T2=0.86, and T3=0.88). Moreover, the entropy of an exemplar adult subject were estimated, and it was 0.73.

5.4 Statistical Analysis

In the statistical analysis of this section we want to know if our independent variable which is the three trimester groups and is a categorical variable, has a significant influence on the dependent variable that's the entropy metric. So, the null hypothesis

is that there's not a significant difference in the entropy values of the infants during their first 6 month of post standing (T1, T2, T3), and the alternative hypotheses, which is also known as the research hypothesis or scientific hypothesis, is that there is an increase in the entropy values of the infants during their first 6 month of post standing (T1, T2, T3), and we can follow the spatiotemporal evolution from this analysis. There were two groups of analysis based on the subjects. First, we had repeated measure analysis for our 5 common female subjects, and second, we did General Linear Model Univariate (Multi-factor ANOVA) for 31 subjects.

5.4.1 Repeated Measure ANOVA of Five female subjects

In this method, we compare the entropy results of the 5 common female subjects that have come to all the three trimesters. Therefore, the analysis need to be repeated measure ANOVA with significance level of 0.05. In the repeated measure ANOVA, there is one factor to do the analysis on the within subjects variables (Trimester) for the entropy metric. Results showed a significant increase in entropy from T1 to T3, at p<.001. Figure 5.7 and table 5.3, show the increase and significantly different metrics of the entropy from T1 to T3.

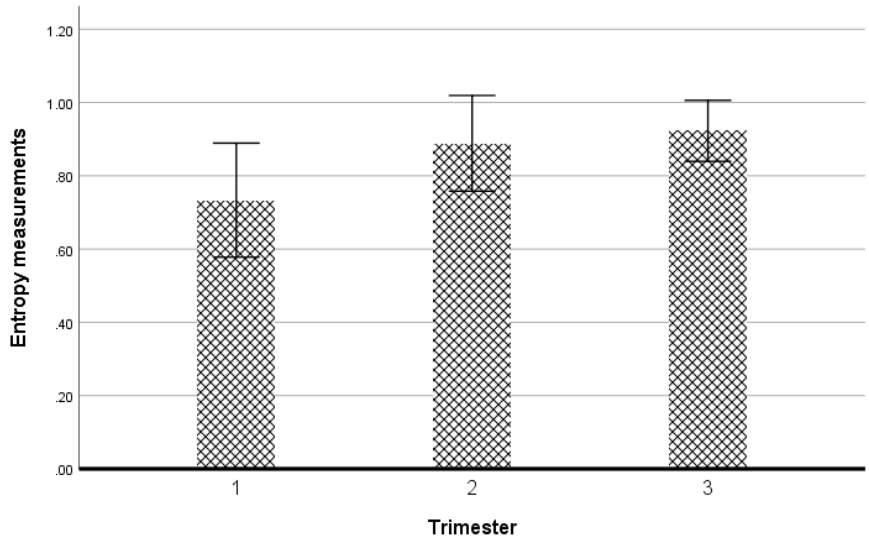

Figure 5.7: Five common Female subjects' Entropy results from T1 to T3

5.4.2 Multi factor ANOVA of all subjects

The multi-factor ANOVA have been analyzed the results of the entropy metric in all the subjects. So, a factorial ANOVA (Univariate) was conducted to compare the main effects of Trimester, and Gender (Independent Variables) as well as their interaction effects on the entropy metric (Dependent Variable). Results showed significantly higher entropy for T2 and T3, comparing to T1. There was no significantly different report for the gender. (Figure 5.8, Table 5.3)

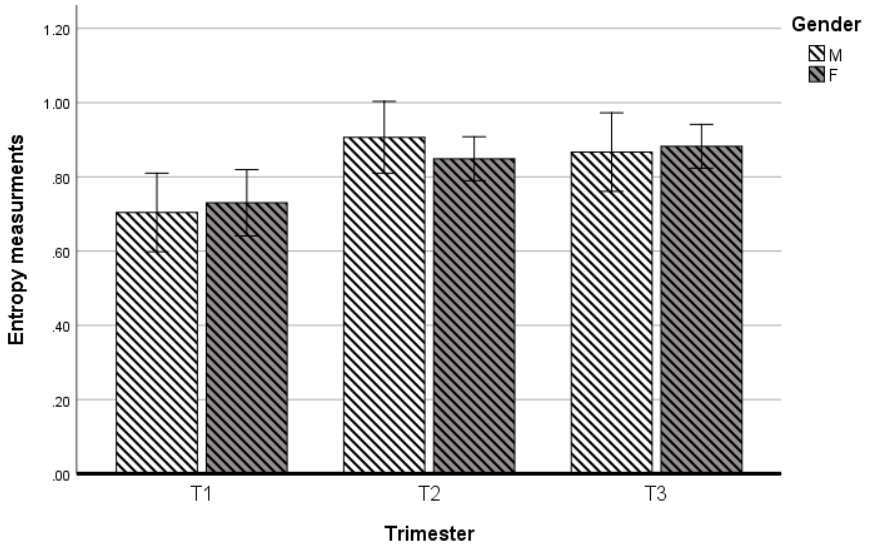

Figure 5.8: All subjects' Entropy results in each gender from T1 to T3

With a comparison between the infants, Adults, and Sine and white noise signals (Figure 5.9), we can see that while the infants entropy increased from 12 to 20 months, the adult entropy is somewhere in between, meaning that the entropy of infants has much more way to path, and it is not reached to the stable, fixed entropy value of adults, yet. On the other hand, we can see that entropy of a sinusoidal signal (periodic signal), is almost 0, meaning that the entropy is minimum and every thing is known, while the entropy of a white noise is larger than 1, meaning that the entropy here is maximum and nothing is known.

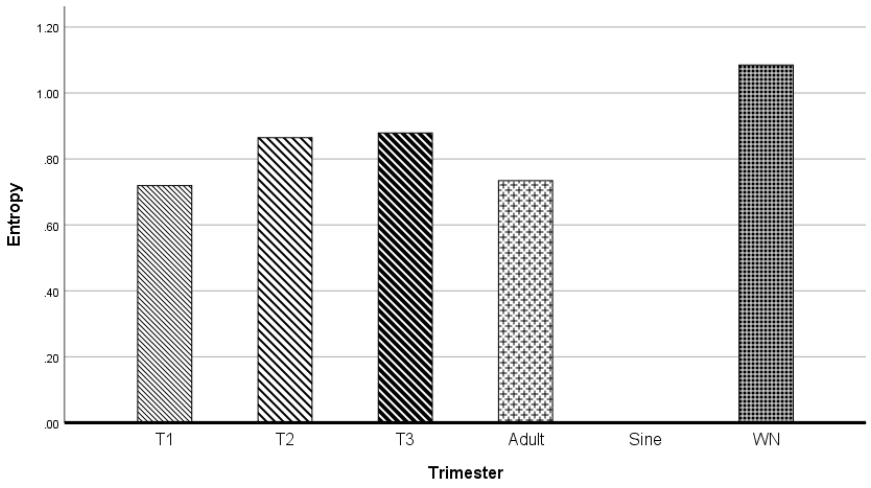

Figure 5.9: Entropy of all the subjects, compared to adults, sinusoidal signal, and white noise.

Table 5.2: τ_c values and approximate entropy (ApEn) of the overall CoPx signals in five common female subjects for $m = 2, .., 10$

CoPx signals in five common female subjects												
Metric / Subject		τ_c									ApEn ($\phi^2 - \phi^3$)	
$m =$		2	3	4	5	6	7	8	9	10	For τ_c	For $\tau = 1$
Subject1	T1	9	6	5	4	3	3	3	3	2	0.81	0.72
	T2	10	7	6	5	4	4	3	3	3	0.95	0.59
	T3	20	14	11	9	7	6	6	5	5	0.97	0.65
Subject2	T1	12	7	6	5	4	3	3	3	3	0.59	0.59
	T2	13	9	6	5	4	4	4	3	3	0.92	0.62
	T3	21	16	12	10	8	7	6	6	5	0.93	0.61
Subject3	T1	10	7	5	4	4	3	3	3	3	0.79	0.62
	T2	12	9	8	6	6	5	5	4	4	0.99	0.70
	T3	18	13	10	8	7	6	6	5	5	0.82	0.52
Subject4	T1	10	8	6	6	6	5	5	4	4	0.86	0.70
	T2	20	15	11	9	8	7	6	6	5	0.73	0.46
	T3	12	9	7	6	6	5	5	4	4	0.99	0.74
Subject5	T1	20	15	11	9	8	7	6	5	5	0.61	0.52
	T2	14	10	8	6	5	5	4	4	4	0.84	0.46
	T3	15	11	8	7	6	5	5	4	4	0.91	0.54

Table 5.3: Mean and Standard deviations of all the significantly different entropy metrics of overall CoPx in Repeated Measure (RP) and Multi Factor (MF) ANOVA

Entropy			
DV / IV		RM (5 subj.)	MF (All subj.)
Trimester	T1	0.73 ± 0.13	0.72 ± 0.08
	T2	0.89 ± 0.11	0.86 ± 0.13^{d}
	T3	0.92 ± 0.07^{e}	0.88 ± 0.11^{e}
a. T1>T2, *b*. T1>T3, *c*. T2>T3 *d*. T2>T1, *e*. T3>T1, *f*. T3>T2			

CHAPTER 6

DISCUSSION AND CONCLUSION

6.1 Discussion and Conclusion on the Results of Linear Analysis

6.1.1 Overall CoPx time domain and frequency domain

- **Stabilogram**: In the stabilogram plots, we see a noticeable shrinkage both in Anteroposterior and Mediolateral directions. The change of this pattern in the stabilogram plots from T1 to T3 is related to self-perception and the way the infant uses his/her space around, beside the demonstration of development of the infant's postural control.(Figure 3.3)

- **Phase Plane**: In the phase plane plots, we see a lot of high and low velocities, demonstrating the way infants have been visited the positions during the quiet stance. There are highly visited positions, as well as rarely visited positions. Also there are high velocity regions beside low velocity regions. The positions that are rarely visited have reached the position threshold, meaning that smaller the position, lower the probability of reaching the threshold. So we can see from the figure that the positions around 0 are frequently visited with all the velocities, while by getting further from the origin, the visited positions decrease and it reaches to the position threshold and it visit those areas with selective high velocities otherwise the subject will fall. As a result, threshold is a function of position. When position is small, threshold is also small, and by expanding the position, threshold also increases [60, 61, 62]. In another words, to fill the space, velocity needs to be low (in the form of lots of dots/data points near each other), but for an empty space, the velocity needs to be high. However, for a newly standing infant, he/she generally visits all positions with all

velocities in order to reach a stable, fixed pattern of quiet stance. (Figure 3.4)

- **Frequency domain plots of overall CoPx and CoPy**: The frequency shift to the left (lower frequencies) means that by growing, infants get more experienced in controlling their balance and posture and as a result the magnitude of the frequency and CoP decrease by time. Thus, it still needs time to achieve to the adult plot, suggesting that the period of 6 month is good but not enough for an infant to progress in the spatiotemporal evolution and reach the final stage of the development [14, 63]. (Figure 3.5)

6.1.2 Regional CoPx and Pressure results in both time and frequency domain and their comparison with adults:

From the time domain statistical analysis results (Multi factor ANOVA) of the pressure signals, the **Mean pressure** of foot regions from the highest to the lowest was Hind, Mid and then Fore foot in all three trimesters in infants, while the mean pressure in the adults from the highest to the lowest was Hind, Fore and then on Mid region. Mean Hind pressure increases while passing from infancy to adults (Figure 3.23). We conclude that the existence of higher pressures in Hind and Mid foot, respectively, and low pressure in Fore foot may point to the fact that Hind region is acting as a support while front region has the least pressure, and may act as the controller [35, 36, 37, 38] (Figure 3.12). Moreover, the figure 3.13 that is presenting the variation of the plantar pressure distribution during the three trimesters, shows that most of the highest pressure is observed in the Hind and medial/lateral side of the Mid foot against to the pressure distribution observed in adults. Because, when the arch of the foot is developed, medial portion of the Mid region of the foot loses its contact with the ground [45]. Beside the development in the heel-toe contact pattern, studies from cross-sectional research show a change in pressure distribution from the Mid foot of newly standing infants to the heel and Fore foot in time [64]. Another study also mentioned an important note regarding the pressure distribution. It has been shown that when pressure variables are taken into account, grouping the growing infants by walking experience does not significantly change relative contact area, arch index, peak pressure, or relative maximum force [65]. From the start of independent walk-

ing until six months later, Bertsch et al. found that the Mid foot's relative contact time decreased from 75.8% to 65.4 percent of the gait cycle and its load decreased from 30% to 20% of the overall impulse on the plantar foot surface [22]. These results have been explained by the medial longitudinal arch's osseous growth [22], beside the decreased need to load the Mid foot for more contact area and muscle control due to an improvement in stability [66].

The **variance of the pressure** in infants signals were significantly high in Hind regions compared to Mid and Fore foot, although there was a slightly decrease in the Hind foot variance from T1 to T3. Variance of Fore foot also has a slight decrease from T1 to T3. Moreover, as a comparison of an infants variance with adult's, we see a noticeable drop in all the foot regions, with Hind foot as the highest and Mid foot as the lowest variance (Figure 3.24). These finding overlap with the following studies on the plantar pressure distribution [41]. As one gains more walking experience, there is a lateral shift in load bearing that occurs along with a shift toward initial heel contact. This is demonstrated by the more lateral deviation in the center of pressure under the growing foot [67]. In comparison to older children, infants walk with modest absolute plantar pressures and high contact areas (relative to body weight). [68, 69, 70]. We also have a finding relative to this section, indicating that the Mid region has a significantly larger frequency band of power (about 2Hz, which is resonance frequency of walking) compared to Fore and Hind regions. Infants who have started walking on their own for 0–2 months have plantar pressures near 25–50% of an adult [67]. Thus, the higher subcutaneous fat on the newborn foot, the smaller body weight to foot contact area ratio, the immature skeleton, and the slower walking speeds in infants have all been implicated in this [22, 67, 71].

The **CFREQ results of pressure** signal in infants decreased from T1 to T3 (toward the lower frequencies), with the regional magnitude ratio of Mid>Fore>Hind. While the adults signal show a smaller CFREQ result in Hind and Fore foot and with the regional magnitude ratio of Mid>Hind>Fore (Figure 3.25). This findings show that while the frequency of pressure decrease in Hind and Fore foot in infants from T1 to T3, and more noticeably in adults, the frequency of pressure in Mid foot is high with respect to the other two regions, both in infancy and adulthood. The reason of this high frequency in Mid foot may be due to the mediolateral adjustment in infancy and

the formation of arch in adulthood [72].

The **CFREQ results of CoPx** signal in infants decreased from T1 to T3 (toward the lower frequencies), with the regional magnitude ratio of Fore>Mid>Hind. The adult results show smaller values in Fore and Hind regions than of the infants' T3, while the Mid region shows a significant increase, being larger than the Mid foot in all the three trimesters (Mid>Fore>Hind). This is due to the role of Mid foot in carrying vibration and transmitting load [72].

The **FD results of pressure and CoPx** signals showed an increase in all the three regions from T1 to T3 in infants. The adult results on the other hand, reveal an increase in Fore and Hind foot with respect to T3, while Mid foot showed a much more slighter increase with respect to T3 [73] (Figure 3.29 and 3.30). We analyzed the complexity issue in the signals better by estimating the entropy measures and/or information dimension later, and found that missing information was higher in infants when compared to adults.

The results of 50% **and** 90% **power frequency of pressure and CoPx** generally revealed that frequency domain characteristics of the spatiotemporal evolution presents power shifts to lower frequencies during infants' developmental periods from 12 to 20 months, and then lower in adults, see figures 3.31, 3.32, 3.33, 3.34. This developmental process manifests through gaining long range correlations in regional CoPx dynamics [74, 75]. Further, we Looked into spatiotemporal evolution of infants' quiet stance, with respect to foot regions. The results showed motility of CoPx in the front region of the foot with significantly larger value than Mid and Hind regions[37, 38].(Figure 3.22)

Talking specifically, in the 90% power frequency of pressure we can follow the change in the role of the Fore foot, which caused a significant decrease in the frequency from T1 to T3 (Fore>Hind) towards adults (Fore<Hind). Also, Mid region have the highest frequency in adults with respect to Fore and Hind (Figure 3.32). The results of the 90% power frequency of CoPx however, showed a continuous decrease of the frequency in Fore and Hind regions from T1 to T3, and Adults, while the Mid foot frequency increased noticeably in adults (3.34).

6.2 Discussion and Conclusion on the Results of Non-Linear Analysis

First the entropy was calculated for $\tau = 1$ [57]. Next, we use the obtained τ_c values for the entropy estimation [76]. we can see high entropy results at T1 to T3, compared to adults. These findings are in close conformity with our hypothesis, in which we mentioned an expectation of an increase in entropy metric as the infants develop their postural control.

Moreover, in the nonlinear analysis the small data collection period causes restrain on the estimations, because the longer the period (3 minuets), the more reliable the results. However, since the study is on the infants, especially at the beginning of independent standing and walking period, it was not possible to collect a longer data from them without getting support.

6.3 Future work:

1. using a more reliable pressure pad for infants with higher sensitivity and lower noise detection
2. Adding kinematic data for Center of Mass (COM) analysis
3. Enlarging the data collection groups to cover all group of ages
4. Study on the copy signals (data is already collected)
5. study through a mathematical model relation between nonlinear dynamics and stochastic noise characteristics.

REFERENCES

[1] D. MÜLLER-KOMOROWSKA, "Komorowska: Data, science, energy."

[2] M. T. Rosenstein, J. J. Collins, and C. J. De Luca, "Reconstruction expansion as a geometry-based framework for choosing proper delay times," *Physica D: Nonlinear Phenomena*, vol. 73, no. 1-2, pp. 82–98, 1994.

[3] J. J. Collins and C. J. De Luca, "Open-loop and closed-loop control of posture: a random-walk analysis of center-of-pressure trajectories," *Experimental brain research*, vol. 95, no. 2, pp. 308–318, 1993.

[4] I. (https://stats.stackexchange.com/users/76937/isbister), "Why does the variance of the random walk increase?." Cross Validated. URL:https://stats.stackexchange.com/q/159650 (version: 2020-12-03).

[5] R. M. Caixeta, D. T. Ribeiro, and J. F. C. L. Costa, "Using multiple random walk simulation in short-term grade models," *REM-International Engineering Journal*, vol. 70, no. 2, pp. 209–214, 2017.

[6] J. H. Argyris, G. Faust, and M. Haase, *An exploration of chaos: an introduction for natural scientists and engineers*, vol. 7. North Holland, 1994.

[7] J. Massion, "Postural control systems in developmental perspective," *Neuroscience & Biobehavioral Reviews*, vol. 22, no. 4, pp. 465–472, 1998.

[8] L. R. Nickel, A. R. Thatcher, F. Keller, R. H. Wozniak, and J. M. Iverson, "Posture development in infants at heightened versus low risk for autism spectrum disorders," *Infancy*, vol. 18, no. 5, pp. 639–661, 2013.

[9] J. Barela, J. J. Jeka, and J. E. Clark, "The use of somatosensory information during the acquisition of independent upright stance," *Infant Behavior and Development*, vol. 22, no. 1, pp. 87–102, 1999.

[10] L. B. Karasik, C. S. Tamis-LeMonda, and K. E. Adolph, "Transition from crawling to walking and infants' actions with objects and people," *Child development*, vol. 82, no. 4, pp. 1199–1209, 2011.

[11] D. Sutherland, "The development of mature gait," *Gait & posture*, vol. 6, no. 2, pp. 163–170, 1997.

[12] E. Thelen, "Motor development: A new synthesis.," *American psychologist*, vol. 50, no. 2, p. 79, 1995.

[13] A. J. Capute and B. K. Shapiro, "The motor quotient: a method for the early detection of motor delay," *American Journal of Diseases of Children*, vol. 139, no. 9, pp. 940–942, 1985.

[14] R. Kliegman, R. Behrman, H. Jenson, and B. Stanton, "Nelson textbook of pediatrics e-book: Elsevier health sciences," *Philadelphia, United States*, 2007.

[15] B. Fritz and M. Mauch, "Foot development in children and adolescents," *A. Luximon A, editor. Handbook of footwear design and manufacture. Woodhead Publishing*, 2013.

[16] C. Price, S. C. Morrison, F. Hashmi, J. Phethean, and C. Nester, "Biomechanics of the infant foot during the transition to independent walking: A narrative review," *Gait & Posture*, vol. 59, pp. 140–146, 2018.

[17] J. Massion, A. Alexandrov, and A. Frolov, "Why and how are posture and movement coordinated?," *Progress in brain research*, vol. 143, pp. 13–27, 2004.

[18] J. J. Jeka and J. R. Lackner, "Fingertip contact influences human postural control," *Experimental brain research*, vol. 79, no. 2, pp. 495–502, 1994.

[19] J. S. Metcalfe and J. E. Clark, "Sensory information affords exploration of posture in newly walking infants and toddlers," *Infant Behavior and Development*, vol. 23, no. 3-4, pp. 391–405, 2000.

[20] L.-C. Chen, J. S. Metcalfe, T.-Y. Chang, J. J. Jeka, and J. E. Clark, "The development of infant upright posture: sway less or sway differently?," *Experimental brain research*, vol. 186, no. 2, pp. 293–303, 2008.

[21] L. J. Claxton, D. K. Melzer, J. H. Ryu, and J. M. Haddad, "The control of posture in newly standing infants is task dependent," *Journal of experimental child psychology*, vol. 113, no. 1, pp. 159–165, 2012.

[22] C. Bertsch, H. Unger, W. Winkelmann, and D. Rosenbaum, "Evaluation of early walking patterns from plantar pressure distribution measurements. first year results of 42 children," *Gait & Posture*, vol. 19, no. 3, pp. 235–242, 2004.

[23] I.-C. Lee, M. M. Pacheco, and K. M. Newell, "The precision demands of viewing distance modulate postural coordination and control," *Human Movement Science*, vol. 66, pp. 425–439, 2019.

[24] B. Day, M. Steiger, P. Thompson, and C. Marsden, "Effect of vision and stance width on human body motion when standing: implications for afferent control of lateral sway.," *The Journal of physiology*, vol. 469, no. 1, pp. 479–499, 1993.

[25] D. N. Lee and J. Lishman, "Visual proprioceptive control of stance.," *Journal of human movement studies*, 1975.

[26] R. J. Peterka, "Sensorimotor integration in human postural control," *Journal of neurophysiology*, vol. 88, no. 3, pp. 1097–1118, 2002.

[27] S. Mitra, "Adaptive utilization of optical variables during postural and suprapostural dual-task performance: comment on stoffregen, smart, bardy, and pagulayan (1999).," 2004.

[28] S. Mitra and E. Fraizer, "Effects of explicit sway-minimization on postural–suprapostural dual-task performance," *Human movement science*, vol. 23, no. 1, pp. 1–20, 2004.

[29] G. E. Riccio, "Information in movement variability about the qualitative dynamics of posture and orientation," *Variability and motor control*, pp. 317–357, 1993.

[30] M. A. Riley, T. A. Stoffregen, M. J. Grocki, and M. Turvey, "Postural stabilization for the control of touching," *Human Movement Science*, vol. 18, no. 6, pp. 795–817, 1999.

[31] J. E. Clark and J. S. Metcalfe, "The mountain of motor development: A metaphor," *Motor development: Research and reviews*, vol. 2, no. 163-190, pp. 183–202, 2002.

[32] O. Alkan, *Statistical analysis of force distribution on the plantar foot during quiet stance*. PhD thesis, Middle East Technical University, 2015.

[33] S. Hassanpour, "Foot somatosensory information contributes to quiet stance," Master's thesis, Middle East Technical University, 2016.

[34] A. Kahveci, B. Cengiz, V. Alcan, S. Gürses, and M. Zinnuroğlu, "Diyabetik periferik polinöropatili hastaların postür özelliklerinin incelenmesi: Kontrollü ve deneysel bir çalışma,"

[35] J. Hicks, "The mechanics of the foot: I. the joints," *Journal of anatomy*, vol. 87, no. Pt 4, p. 345, 1953.

[36] J. Hicks, "The mechanics of the foot: Ii. the plantar aponeurosis and the arch," *Journal of anatomy*, vol. 88, no. Pt 1, p. 25, 1954.

[37] J. Hicks, "The foot as a support," *Cells Tissues Organs*, vol. 25, no. 1, pp. 34–45, 1955.

[38] J. Hicks, "The mechanics of the foot, iv.," *Cells Tissues Organs*, vol. 27, no. 3, pp. 180–192, 1956.

[39] L. A. Kelly, A. G. Cresswell, S. Racinais, R. Whiteley, and G. Lichtwark, "Intrinsic foot muscles have the capacity to control deformation of the longitudinal arch," *Journal of The Royal Society Interface*, vol. 11, no. 93, p. 20131188, 2014.

[40] D. A. Winter, F. Prince, J. S. Frank, C. Powell, and K. F. Zabjek, "Unified theory regarding a/p and m/l balance in quiet stance," *Journal of neurophysiology*, vol. 75, no. 6, pp. 2334–2343, 1996.

[41] T. E. Prieto, J. B. Myklebust, R. G. Hoffmann, E. G. Lovett, and B. M. Myklebust, "Measures of postural steadiness: differences between healthy young and elderly adults," *IEEE Transactions on biomedical engineering*, vol. 43, no. 9, pp. 956–966, 1996.

[42] C. Maurer and R. J. Peterka, "A new interpretation of spontaneous sway measures based on a simple model of human postural control," *Journal of neurophysiology*, vol. 93, no. 1, pp. 189–200, 2005.

[43] J. S. Bendat and A. G. Piersol, *Random data: analysis and measurement procedures*. John Wiley & Sons, 2011.

[44] B. C. Cengiz, "Effect of the vestibular system on search and fall behaviour of human postural sway," Master's thesis, Middle East Technical University, 2017.

[45] P. R. Cavanagh, M. M. Rodgers, and A. liboshi, "Pressure distribution under symptom-free feet during barefoot standing," *Foot & ankle*, vol. 7, no. 5, pp. 262–278, 1987.

[46] E. Morag and P. R. Cavanagh, "Structural and functional predictors of regional peak pressures under the foot during walking," *Journal of biomechanics*, vol. 32, no. 4, pp. 359–370, 1999.

[47] K. Imaizumi, Y. Iwakami, and K. Yamashita, "Analysis of foot pressure distribution data for the evaluation of foot arch type," in *2011 Annual International Conference of the IEEE Engineering in Medicine and Biology Society*, pp. 7388–7392, IEEE, 2011.

[48] K. Imaizumi, Y. Iwakami, K. Yamashita, and Y. Hiejima, "Development of an evaluation system for foot arch types in the elderly using foot pressure distribution data," in *2012 Annual International Conference of the IEEE Engineering in Medicine and Biology Society*, pp. 4859–4862, IEEE, 2012.

[49] R. C. Hilborn *et al.*, *Chaos and nonlinear dynamics: an introduction for scientists and engineers*. Oxford University Press on Demand, 2000.

[50] S. Nakaoka, "Data-driven mathematical modeling of microbial community dynamics," in *Handbook of statistics*, vol. 39, pp. 93–130, Elsevier, 2018.

[51] H. Greenside, A. Wolf, J. Swift, and T. Pignataro, "Impracticality of a box-counting algorithm for calculating the dimensionality of strange attractors," *Physical Review A*, vol. 25, no. 6, p. 3453, 1982.

[52] K. Newell, S. Slobounov, E. Slobounova, and P. Molenaar, "Stochastic processes in postural center-of-pressure profiles," *Experimental Brain Research*, vol. 113, no. 1, pp. 158–164, 1997.

[53] J. P. Keener and J. Sneyd, *Mathematical physiology*, vol. 1. Springer, 1998.

[54] J. Balatoni and A. Renyi, "Uber den begriff der entropie, arbeiten zur informationstheorie i," 1957.

[55] J. D. Farmer, E. Ott, and J. A. Yorke, "The dimension of chaotic attractors," *Physica D: Nonlinear Phenomena*, vol. 7, no. 1-3, pp. 153–180, 1983.

[56] H. G. E. Hentschel and I. Procaccia, "The infinite number of generalized dimensions of fractals and strange attractors," *Physica D: Nonlinear Phenomena*, vol. 8, no. 3, pp. 435–444, 1983.

[57] M. Akay, *Nonlinear Biomedical Signal Processing: Fuzzy Logic, Neural Networks, and New Algorithms*. Wiley-IEEE Press, 1st ed., 2000.

[58] R. Phillips, J. Kondev, J. Theriot, H. G. Garcia, and N. Orme, *Physical biology of the cell*. Garland Science, 2012.

[59] S. M. Pincus, "Approximate entropy as a measure of system complexity.," *Proceedings of the National Academy of Sciences*, vol. 88, no. 6, pp. 2297–2301, 1991.

[60] S. Gürses, *Postural dynamics and stability*. PhD thesis, Ankara, Turkey: Middle East Technical University, 2002.

[61] S. Gurses, "Nonlinear head-neck dynamics at small amplitude perturbations," *Second Chaotic Modeling and Simulation International Conference*, 2009.

[62] S. Gurses, B. Platin, S. Tumer, and N. Akkas, "Characteristic phase plane pattern of human postural sway," *IFAC Proceedings Volumes*, vol. 39, no. 18, pp. 225–230, 2006.

[63] C. Price, J. McClymont, F. Hashmi, S. C. Morrison, and C. Nester, "Development of the infant foot as a load bearing structure: study protocol for a longitudinal evaluation (the small steps study)," *Journal of foot and ankle research*, vol. 11, no. 1, pp. 1–9, 2018.

[64] C. Alvarez, M. De Vera, H. Chhina, and A. Black, "Normative data for the dynamic pedobarographic profiles of children," *Gait & posture*, vol. 28, no. 2, pp. 309–315, 2008.

[65] K. Bosch, J. Gerß, and D. Rosenbaum, "Development of healthy children's feet—nine-year results of a longitudinal investigation of plantar loading patterns," *Gait & posture*, vol. 32, no. 4, pp. 564–571, 2010.

[66] A. Hallemans, D. De Clercq, B. Otten, and P. Aerts, "3d joint dynamics of walking in toddlers: A cross-sectional study spanning the first rapid development phase of walking," *Gait & Posture*, vol. 22, no. 2, pp. 107–118, 2005.

[67] A. Hallemans, K. D'Août, D. De Clercq, and P. Aerts, "Pressure distribution patterns under the feet of new walkers: the first two months of independent walking," *Foot & ankle international*, vol. 24, no. 5, pp. 444–453, 2003.

[68] K. Bosch, J. Gerss, and D. Rosenbaum, "Preliminary normative values for foot loading parameters of the developing child," *Gait & posture*, vol. 26, no. 2, pp. 238–247, 2007.

[69] S. Müller, A. Carlsohn, J. Müller, H. Baur, and F. Mayer, "Static and dynamic foot characteristics in children aged 1–13 years: a cross-sectional study," *Gait & posture*, vol. 35, no. 3, pp. 389–394, 2012.

[70] E. M. Hennig and D. Rosenbaum, "Pressure distribution patterns under the feet of children in comparison with adults," *Foot & ankle*, vol. 11, no. 5, pp. 306–311, 1991.

[71] Y. Hong and R. Bartlett, *Routledge handbook of biomechanics and human movement science*. Routledge New York, NY, USA:, 2008.

[72] M. Giandolini, M. Munera, X. Chiementin, S. Bartold, and N. Horvais, "Footwear influences soft-tissue vibrations in rearfoot strike runners," *Footwear Science*, vol. 9, no. sup1, pp. S25–S27, 2017.

[73] W. Kim and A. S. Voloshin, "Role of plantar fascia in the load bearing capacity of the human foot," *Journal of biomechanics*, vol. 28, no. 9, pp. 1025–1033, 1995.

[74] V. M. Zatsiorsky and M. Duarte, “Instant equilibrium point and its migration in standing tasks: rambling and trembling components of the stabilogram,” *Motor control*, vol. 3, no. 1, pp. 28–38, 1999.

[75] V. M. Zatsiorsky and M. Duarte, “Rambling and trembling in quiet standing,” *Motor control*, vol. 4, no. 2, pp. 185–200, 2000.

[76] S. Gurses and H. Celik, “Correlation dimension estimates of human postural sway,” *Human movement science*, vol. 32, no. 1, pp. 48–64, 2013.

APPENDICES

Appendix A

PATTERNED NOISY DATA PROBLEM

During the time domain analysis of the data collected from force plate, we faced with some noisy pattern graphs, and tried to understand the reason of this pattern. We named it Patterned noisy data and started to investigate the possible causes of this problem.

This problem mostly happened in velocity and phase plane graphs during the analysis of CoPx and CoPy. We reviewed all subjects of first group, we compared the phase plane graphs of each one, and we saw that in some case, there is no patterned noisy data or interruption, in some others there are patterned noisy data on the right side of the graph (the positive side). While on some others the patterned noisy data is on the left (negative) side of the graph. The positive side refers to anterior and the negative side refers to posterior sway. Initially, we thought that this problem occurs wherever the infant spends more time at a position, by looking at more subject's phase planes, we (thought to reject this hypothesis but,) doubted this hypothesis by observing some reversed cases.

After reviewing all the phase plane graphs of CoPx of the subjects of the first group, we chose two subjects based on a good and bad phase plane graph. The one with the most patterned noisy data graphs was named second Subject. The good one, on the other hand, was named first subject. By reviewing the data analysis of the force plate and Pressure pad, we considered the time series, velocity, and phase plane of CoPx for both selected subjects. To see the differences between the data which is collected by force plate and pressure pad, we plot the time series and velocity of both devices (Force Plate (FP) and Pressure Pad (PP)), in one graph. For phase plane graphs, it is better to plot separately to see the differences.

For calling a pressure pad data in MATLAB, first, we need to run the same trial of the subject in Matscan software. After calling the data, regarding which part of the data is needed, we need to open that part of the analysis in Matscan (in this case we need the anterior-posterior graph) and save that part as an excel file to the related folder. Then, in MATLAB and through the same folder, we find that excel file and import it as data. Then, all functions are applicable to this data file in MATLAB. For naming the pressure pad data, since in this part of the analysis we look into the CoPx data, I named the related data as PPAP which refers to Pressure Pad Anterior-Posterior data. The time series plot of CoPx of first subject was smooth data with a small amount of noise. By analyzing the velocity and plotting the phase plane graph of CoPx we noticed a good one with almost no patterned noisy data. And we guess that the small amount of noise is related to the device and is nothing related to the infant. So, this is a resolution problem of the device (see Figure A.1).

The time series plot of CoPx of the second subject was noisier. By analyzing the velocity and plotting the phase plane graph of CoPx we noticed a huge amount of patterned noisy data in force plate analysis (see Figure A.2).

For the velocity plots, to see the patterned noisy data better, we change the marker, marker size, and line style for each graph. Here the blue one indicates the velocity of the force plate and the red one indicates the velocity of the pressure pad. By comparing these two velocities we can see that in force plate velocity, it has been visited limited velocities and there is patterned noisy data problem, however in pressure pad it has been visited almost every velocity. So, the force plate data is jumpier than pressure pad data. To understand this comparison better we can investigate the way each device collects the data. As we know, these velocity data are originally derived from CoPx data, however, the collecting data method is different in each device. The pressure pad measures weighted average of moment arms from distributed load system, pixel by pixel, however, the force plate collects resultant force through the strain gauges on its four bases. therefore, there is a data quality difference base on these two data collection methods, in another word, the data collected by the force plate has some information loss and the data collected by pressure pad is the rich one and has been able to catch all the positions which had been visited by the infant. However, our guess is that this amount of noise and patterned noisy data problem is originated

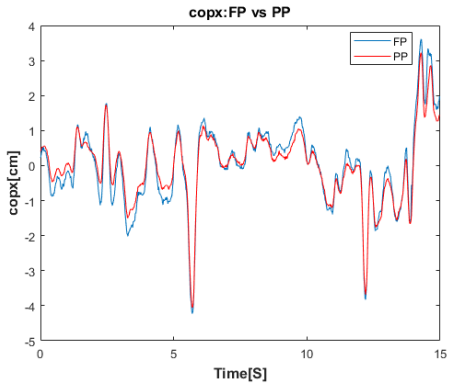

(a) Time Series of CoPx in FP and PP

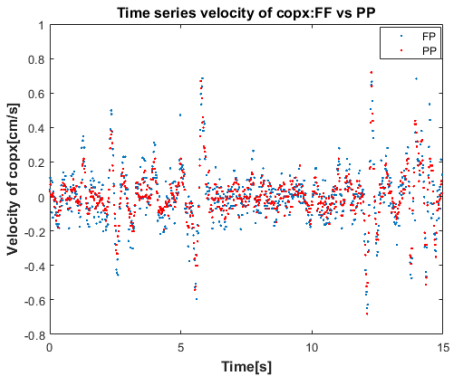

(b) Time Series velocity of CoPx in FP and PP

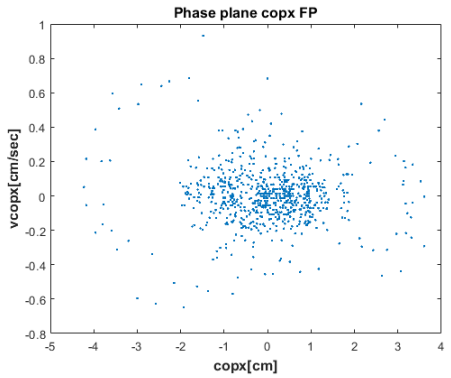

(c) Phase plane of CoPx in FP

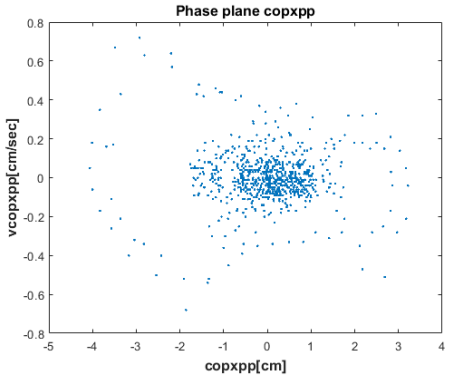

(d) Phase plane of CoPx in PP

Figure A.1: Resolution comparison of the force plate and pressure pad on the first exemplar subject a) Time Series of CoPx in FP and PP, b) Time Series velocity of CoPx in FP and PP, c) Phase plane of CoPx in FP, d) Phase plane of CoPx in PP

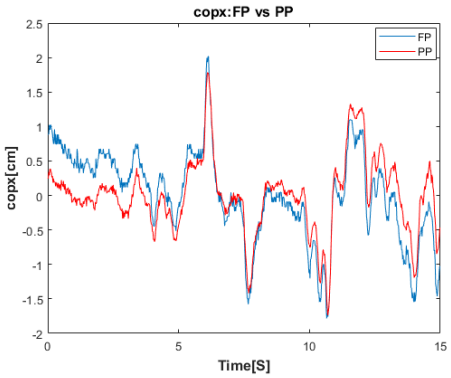

(a) Time Series of CoPx in FP and PP

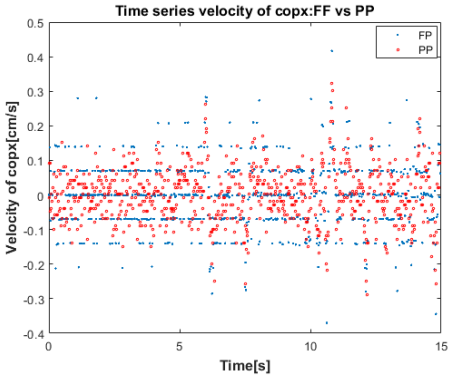

(b) Time Series velocity of CoPx in FP and PP

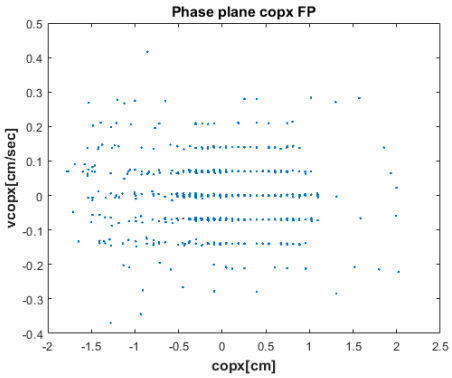

(c) Phase plane of CoPx in FP

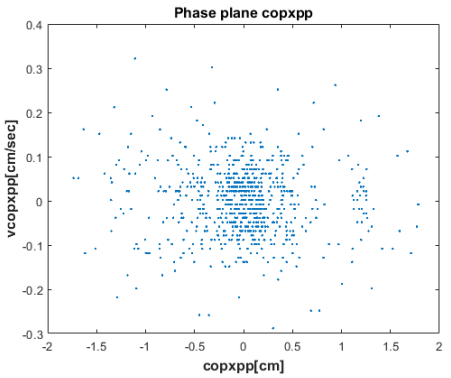

(d) Phase plane of CoPx in PP

Figure A.2: Resolution comparison of the force plate and pressure pad on the second exemplar subject a) Time Series of CoPx in FP and PP, b) Time Series velocity of CoPx in FP and PP, c) Phase plane of CoPx in FP, d) Phase plane of CoPx in PP

form not only the device noise but also the quality of collected data in each case as well as the infant itself. So, this is a resolution problem of the device and data, as well as the human posture of the infant and the way she uses her foot and posture. Therefore, for the human portion, we presumed that this kind of patterned noisy data problem is maybe due to the usage of the forefoot and its role in this variation because in most of the cases the problem occurs in the right (positive) part of the graph which is related to forefoot, and we know that forefoot is more active than Hind foot. However, we need to demonstrate this assumption by entropy measurements and statistical proof.

We also think about the differences between these two subjects, and we assume that maybe this patterned noisy data problem arises when the infant's data is noisy, due to her posture usage. Because in first case, the data was almost smooth and therefore there was no significant patterned noisy data problem in the graphs (velocity and phase plane).

Also, by reviewing Second trimester's (T2) common subjects with T1, one of the important facts is the appearance of patterned noisy data on the highly visited area of the subjects. After monitoring all these results, and the results from two subject's analysis of T1 we consider the negative aspects of filtering as well. Since we believe that in the case of filtering, we may lose some critical information about every posture and motor control development in infants.

Moreover, the amount of measurements per each frame is conceptually different in each device, the resolution, precision, and accuracy of the collected data is different as a result. In another words, while pressure pad can collect for example 80 pixel (spatial sample) per frame form an infant's feet (20 for each region: HR, FR, HL, FL), force plate is able to collect only one resultant at this range of time. Therefore, the difference in the quality of each device's data is predictable. Hence, actually this is the comparison of a poor data with a rich data, and as a result this problem can't be solved by filtering, because not only the problem of the poor data doesn't get better, but also, we may cause more deficiency on it and cut even more information, as the problem is not the matter of noise only, but also is a matter of missing information. Therefore, we decided to use pressure pad generated CoPx signals.

Another hypothesis is that if the search is an explorative dynamic type, the patterned noisy data will not happen. And this needs to be proven by entropy measurements. In the adults there is no exploration and they are acting more exploitatively. And if it is an exploitative one, the is a chance of appearance of this pattern. Moreover, noise is a tricky element here. It sometimes acts in favor of exploration, and sometimes in favor of randomness.

An Additional issue which we wanted to study, was the effect of moments on the appearance of patterned noisy data problem. We wanted to see if the problem is originated form the My or Mx when calculating the CoPx or CoPy equations:

$$CoPx = \frac{-M_y(t)}{F_z(t)} \tag{A.1}$$

$$CoPy = \frac{M_x(t)}{F_z(t)} \tag{A.2}$$

Meaning that, the pattern which we saw in velocity graphs is maybe due to the My signals not the Fz. therefore, we need to prove this fact by running the MATLAB code for My and Mx which are data 5, and data 4 respectively. And we look into these signals the same way we do for velocity signals (changing the marker, marker size, and line style). And here, our hypothesis is that we will see these patterned noisy data problems in the moment signals and not the Fz signal. Because Fz signal is a fixed signal coming from the weight of the subject, so there is a low possibility that this problem is caused by the Fz signal. Another reason for this hypothesis is that, since this patterned noisy data is happened only in the force plate signals, and we know that the data collection method in force plate is different from pressure pad, (the data in pressure pad is being collected from distributed load, however in force plate it is collected from the weighted average moment arms), this can be the main reason of this problem happening in the force plate and not in the pressure pad. One More point here is that we do not expect the appearance of this pattern in the copy signal since the medial-lateral side of the body is not like an unstable pendulum (AP), it is a stable pendulum. However, since infants maybe do not have the ability to use both feet synchronous and simultaneously, there is a chance that ML is also unstable,

and this noise appears in the copy signals as well.

For this purpose, we started with two exemplar subjects from the T1, one of the subjects had a good pattern without any noise (Figure A.3) and the other had a dramatic patterned noisy data problem (Figure A.4). We compared My and Fz graphs for both subjects, to see if the problem originates from the My signal.

By comparing these two figures we can see that this patterned noisy data is in the moment signal and not the other one (Fz). There are jumps in the moment graph, but since this subject's data is the good one, we should see if this problem is a resolution problem or not. By zooming in the graph, we can see that jumpy pattern is obvious in the positions in which the infant has spent more time there. However, since the scales in these two graphs are different, if we zoom in in the Fz signal, we can also see some small jumps. But in this small scale, this jumpy pattern is definitely a resolution problem of the device not the effect of human. Then we continued with the second exemplar subject, which had a dramatic patterned noisy data problem.

In the Fz graph and My graph, there was a significant patterned noisy problem. Then for comparing these two subjects, we created a common axis scale so that each subject's graph is on the same scale. And we can see that in second Subject's My graph there is a behavior pattern which is originated from the human, not the instrument. For proving this statement, we need to show that in the second Subject's My graph if we zoom in, we should find some dots between two jumps so that we prove this is not a resolutions problem of the instrument. However, in this subject, we couldn't find any dot (data) between jumps. Which maybe means that it is an instrument resolution problem for My signal. Yet, we understand that this problem originated from the My signal and it is not related to Fz signal. Because My signal is created by human movements and this is the reason for the problem. And maybe this problem is due to how the instrument collects My signal.

Moreover, the appearance of patterned noisy data in My signals does not mean that our phase plane also has the same pattern. Since we saw that here in the first subject (the good one without any patterned noisy data problem), the My signal had patterned noisy data while the same subject's phase plane graph had nothing but a good pattern without any noise.

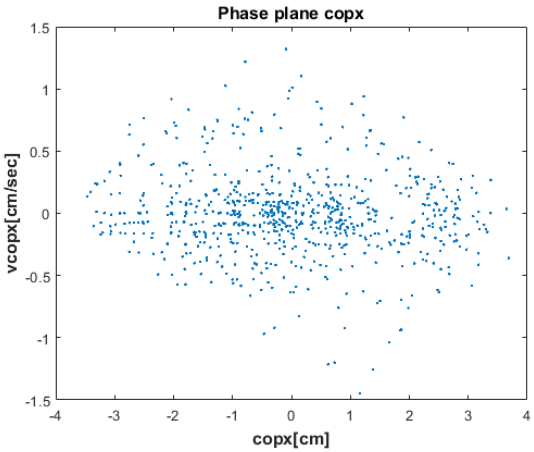

(a) Phase plane of CoPx in FP

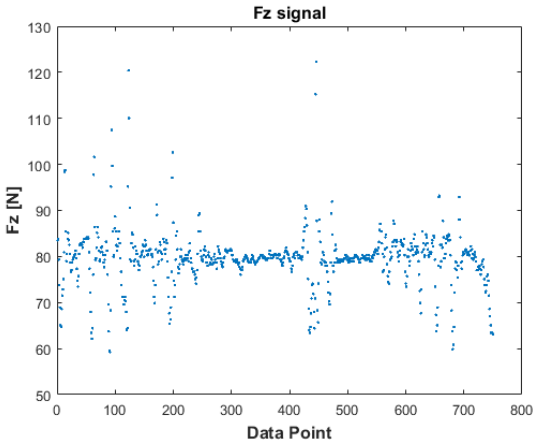

(b) Fz signal of CoPx

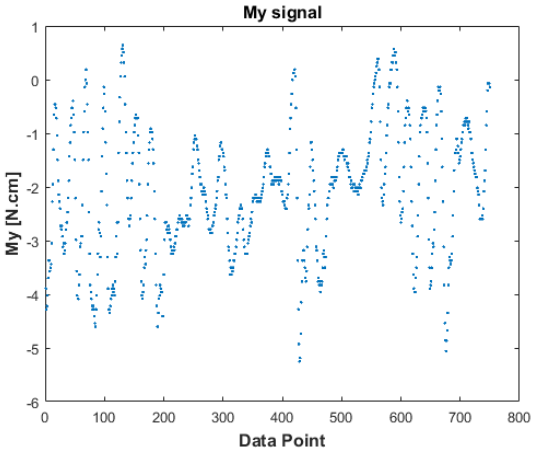

(c) My signal of CoPx

Figure A.3: Resolution comparison of the force plate of the first exemplar subject a) Phase plane of CoPx in FP, b) Fz signal of CoPx, c) My signal of CoPx

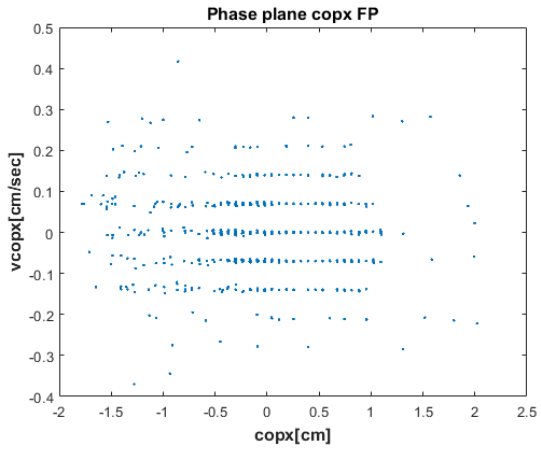

(a) Phase plane of CoPx in FP

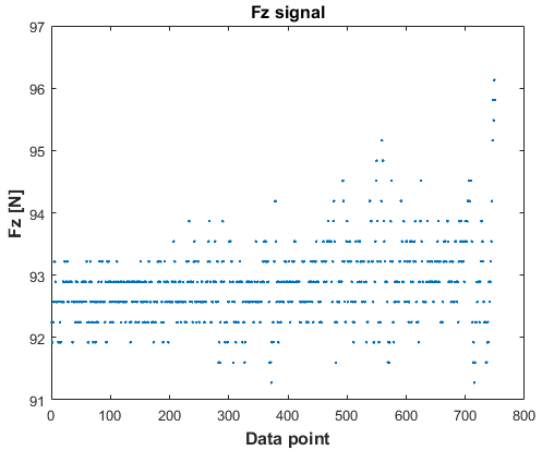

(b) Fz signal of CoPx

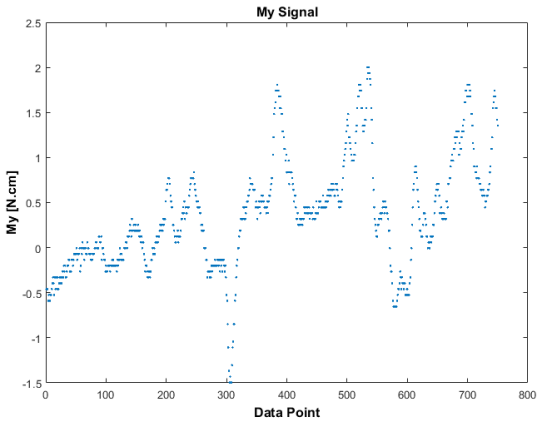

(c) My signal of CoPx

Figure A.4: Resolution comparison of the force plate of the second exemplar subject a) Phase plane of CoPx in FP, b) Fz signal of CoPx, c) My signal of CoPx

Another important hypothesis here is the difference between these two subject's behaviors. By comparing the range of movement in both subjects we can see that when the subject uses a big range of span or sway (6Nm) during the quiet stance, due to the resolution problem of the instrument, the dots in between the jumps can't be seen (subject one, with a good pattern in the phase plane) and we assume that this is only a resolution problem and not the human behavior effect, however, when we study the second subject (subject two, with a patterned noisy data problem in the phase plane), we can see that the second subject uses a smaller range of sway (2Nm) during the quiet stance, so if there were any data in between we were able to locate them, however in this small range it is only the resolution problem that appears and we couldn't find any dot in between. By zooming a bit more, we want to understand the difference between the behavior of these two subjects: In the second subject, we can see that she insisted in one moment for a while, however, the other one did not have the same insistency in a moment for a while. This means that for example in the moment of 0.45 we have several data points in a raw for the second subjects, however, the first subject has visited the 0.45 moment only once and then passed to other moments and has acted more scattered. Our hypothesis here is that the reason for acting jumpy and scattering of the first subject is maybe due to her effort for controlling her balance and it is a try for preventing a fall. However, the second subject has already learned the balance control and is performing a quiet stance by trying to keep her balance in specific moments which are the ones that keep her in the right position. This hypothesis means that our first subject is acting more exploratively and has scattered equilibrium points, and the second one is acting more exploitative and insisted to create her equilibrium point around a specific point. In another word, for the second subject instrument resolution is faced with one moment however for the first subject since there are lots of moments, it has used the same instrument with the same resolution wider and freely in a scattered pattern. So, we assume that if a subject insists on using a limited range of the sway and movements, it puts pressure on the rang of the instrument and as a result resolution problem happens. On the other hand, if a subject uses a larger area of sway and movements with more moments, the instrument collects the data freely and it does not cause any limit or resolution problem. So, for proving this point, we need to control this hypothesis for all the subjects and see if it is true for all of them.

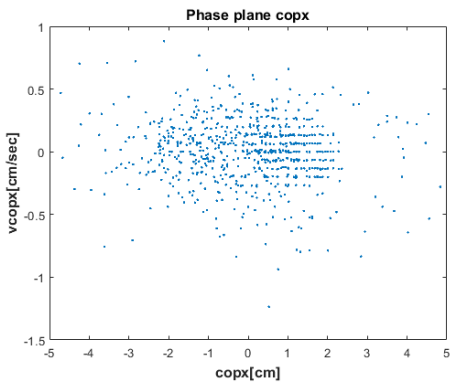

(d) Phase plane of CoPx in FP

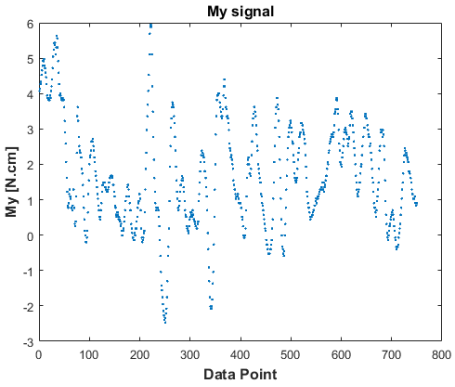

(e) My signal of CoPx

Figure A.5: Resolution comparison of the force plate of a male exemplar subject a) Phase plane of CoPx in FP, b) My signal of CoPx

For providing more proof, we continued with another subject (Male):

By looking at his phase plane graph of the force plate we can see that there are some patterned noisy data on the right side of the graph. By zooming in the graph, we can see that there are some scattered data in between the jumps as well. Then we plot the My signal of this subject's data.

In the My graph, we see that the span length of this subject is large (9Nm) and it is similar to first subject's scale. And it acts explorative in all the graphs. So, based on our previous hypothesis this subject's phase plane graph should be noiseless, while there are some on the right side of the graph, which can be the human intervention, but we are not sure yet. Another guess here is that this subject's behavior is hybrid. Meaning that in some positions he was explorative and sometimes is exploitative. Sometimes he had a search and sometime had tried to stay in one moment. And in positions in which he had tried to stay in one moment and behaved exploitatively, this pattered noisy data appeared.

Now the question is that in the My graph where is the position of exploitative behavior and where is the position of explorative one? And if we find this exploitative part, we can find the position in which the instrument resolution problem happens.

Now, if we want to look into the problem from the physiologic point of view, the

question is that what is the meaning of explorative behavior in physiology? Which strategies are being used in this behavior?

Question: based on the above hypothesis, will this patterned noisy data problem gets worst in the coming months of infants? In another word, does this problem arise when the infant gets professional and reaches her/his best quiet stance skill?

Yes, we expect this. Because we see more exploitative behavior in adults.

So, we find out that the reason for a scattered pattern in My graph is not exactly the same reason of scattered pattern appearance in the phase plane graph. And we cannot be sure about the resolution problem of the force plate by just studying the phase plane graph, and we need the My signal as well.

Another important point that we faced was the amount of time in which region the infant spent. By running the code without detrending we find out that the My signal is negative in anterior and it is positive in the posterior part of the graph, So, by comparing the un-detrended phase plane graph of CoPx with My signal, we can study the regions that infant has spent time there.

Appendix B

DERIVATION OF INFORMATION ENTROPY USING STIRLING'S APPROXIMATION

Based on the information from Chapter 4, we have:

The definition of information can be written as [6]:

$$I \triangleq K \ln R \tag{B.1}$$

Where, $K = \log_2 e$. So:

$$\begin{aligned} I &= \log_2 e \ln R \\ &= \log_2 R \\ 2^I &= R \end{aligned} \tag{B.2}$$

Where, $2^I = R$ is a random walk since this is a binary event with logarithmic base of 2 (points (phase) at the event). "I" is the number of decision making which is known as the information. R is the realization factor (at the reservoir, possible combinations of the points) and can be written as:

$$R(N, n) = \frac{N!}{n!(N-n)!} \tag{B.3}$$

Where, N is the number of decision makings (freedom), and n is the number of outcomes (phase points).

For a binary process via the Stirling's approximation we can rewrite the equation

4.41, by substituting R, as the following:

$$I \triangleq K \ln \frac{N!}{n!(N-n)!} \tag{B.4}$$

Since the information increases with the number N of the realisations and thus with the number of decisions, the mean value is of interest. Therefore, the information per decision is [6]:

$$\bar{I}(p) = \frac{I}{N} \tag{B.5}$$

We can write the binary expression $n!(N-n)!$ by generalizing to k-many events (logarithmic base is $W(\varepsilon)$ in this case, see equation 4.73) as $\Pi n_i!$, where $i = 1, ..., W(\varepsilon)$, and by using the Stirling approximation ($lnN! = NlnN - N$):

$$\begin{aligned}
\bar{I}(p) &= K\frac{1}{N}\ln R \\
&= K\frac{1}{N}\ln\frac{N!}{\Pi n_i!} \\
&= K\frac{1}{N}\left(\ln(N!) - \sum \ln n_i!\right) \\
&= K\frac{1}{N}\left((NlnN - N) - \sum(n_i ln(n_i) - n_i)\right)
\end{aligned} \tag{B.6}$$

By using the fact that the $\sum n_i = N$ (The sum of all items in each box must be equal to the total number of items):

$$\begin{aligned}
&= K\frac{1}{N}\left((NlnN - N) - \sum(n_i ln(n_i) + N\right) \\
&= K\left(\frac{1}{N}(NlnN) - 1 - \frac{1}{N}\sum(n_i ln(n_i) + 1\right) \\
&= K\left(\frac{1}{N}(NlnN) - \frac{1}{N}\sum(n_i ln(n_i)\right)
\end{aligned} \tag{B.7}$$

Now, by using the fact that $p_i = \frac{n_i}{N}$, which is the probability of being in the n_i^{th} box (see equation 4.73), and therefore $n_i = p_i N$:

$$= K\left(\frac{1}{N}NlnN - \frac{1}{N}\sum p_i N lnp_i N\right) \tag{B.8}$$

Using log properties of multiplication we can rewrite as:

$$= K\left(\frac{1}{N}NlnN - (\frac{1}{N}\sum p_i NlnN + \frac{1}{N}\sum p_i Nlnp_i)\right) \tag{B.9}$$

Since $NlnN$ is constant with respect to the summation over i:

$$\begin{aligned}
&= K\left(\frac{1}{N}NlnN - (\frac{1}{N}NlnN\sum p_i + \frac{1}{N}\sum p_i Nlnp_i)\right) \\
&\sum p_i = 1, So \\
&= K\left(\frac{1}{N}NlnN - \frac{1}{N}NlnN - \frac{1}{N}\sum p_i Nlnp_i)\right) \\
&= -\frac{K}{N}\cdot N\sum p_i lnp_i \\
\bar{I}(p) &= -K\sum p_i lnp_i
\end{aligned} \tag{B.10}$$

Appendix C

EXAMPLE OF A 2-D SIGNAL AND ESTIMATING THE INFORMATION AND DIMENSION

lets assume a 2-D signal with spatial tolerance metric of ε. First, we need to partition the space which is deciding on the value of ε. Second, counting the phase points at each box, and third, estimating the dimension. We iterate the above algorithm until finding the required metrics and variables [6]:

- **Counting the phase points at each box:** Based on the two investigated problems ([6]) we solve an example of information and dimension equations (4.52 and 4.53) for 1) fixed point, and 2) limit cycle:

  1) **Fixed point**:

  – For $\varepsilon = \frac{1}{2}$, $W(\varepsilon) = 1$, and $p_k = 1$, see figure C.1 a

$$\begin{aligned} \bar{I}(\varepsilon) &= -K \sum_{k=1}^{W(\varepsilon)=1} p_k \ln p_k \\ &= -K(1)\ln(1) \\ &= 0 \end{aligned} \tag{C.1}$$

$$\begin{aligned} D_I &= \frac{\bar{I}(\varepsilon)}{\ln \frac{1}{\varepsilon}} \\ &= 0 \end{aligned}$$

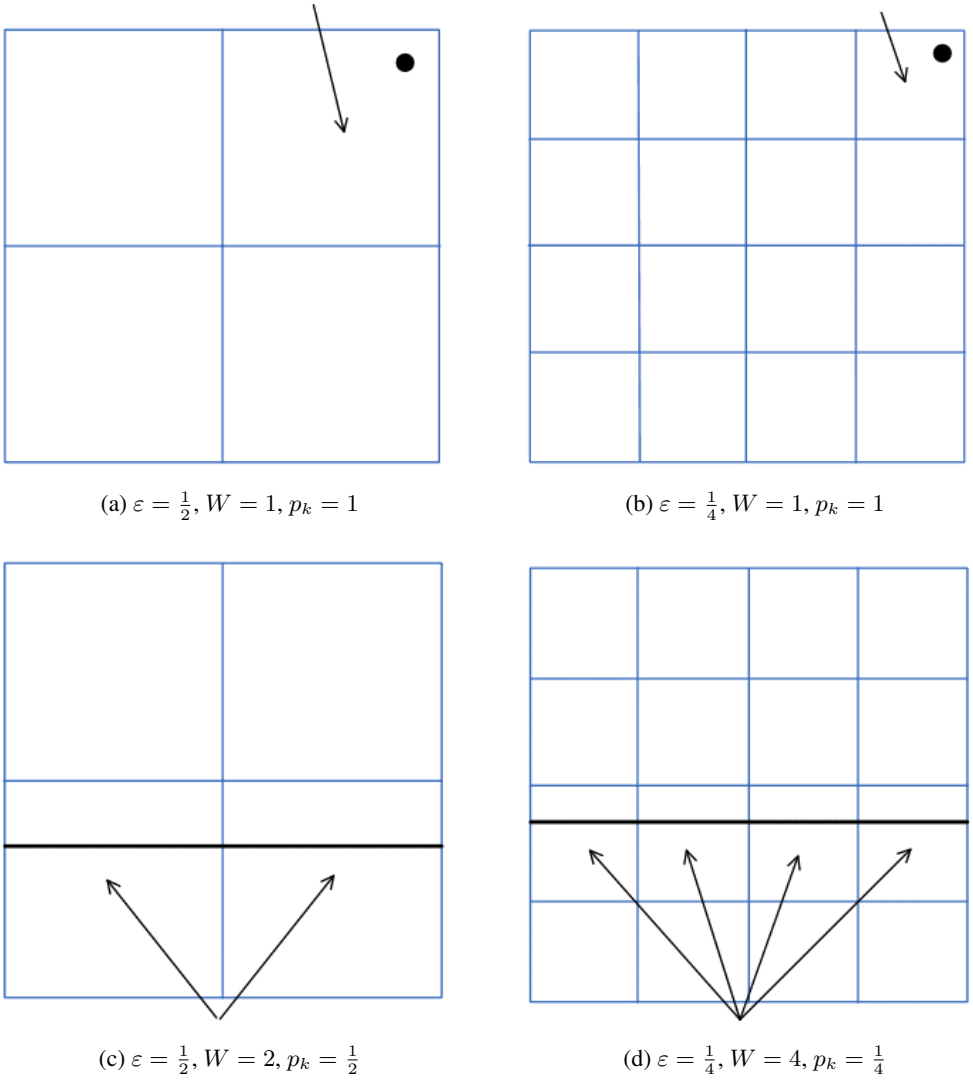

(a) $\varepsilon = \frac{1}{2}, W = 1, p_k = 1$

(b) $\varepsilon = \frac{1}{4}, W = 1, p_k = 1$

(c) $\varepsilon = \frac{1}{2}, W = 2, p_k = \frac{1}{2}$

(d) $\varepsilon = \frac{1}{4}, W = 4, p_k = \frac{1}{4}$

Figure C.1: Estimation of the information and dimension equation of a signal, for a) $\varepsilon = \frac{1}{2}, W = 1, p_k = 1$, b) $\varepsilon = \frac{1}{4}, W = 1, p_k = 1$, c) $\varepsilon = \frac{1}{2}, W = 2, p_k = \frac{1}{2}$, d) $\varepsilon = \frac{1}{4}, W = 4, p_k = \frac{1}{4}$ [6]

– For $\varepsilon = \frac{1}{4}$ and $W(\varepsilon) = 1$, and $p_k = 1$, see figure C.1 b

$$\begin{aligned} \bar{I}(\varepsilon) &= -K \sum_{k=1}^{W(\varepsilon)=1} p_k \ln p_k \\ &= -K(1)\ln(1) \\ &= 0 \\ D_I &= \frac{\bar{I}(\varepsilon)}{\ln \frac{1}{\varepsilon}} \\ &= 0 \end{aligned} \tag{C.2}$$

Thus, no matter how small we select the ε, if the attractor is a fixed point, the missing information and its dimension will be equal to zero (anything is known and the signal is deterministic).

2) **Limit cycle:**

– For $\varepsilon = \frac{1}{2}$ and $W(\varepsilon) = 2$, and $p_k = \frac{1}{2}$, see figure C.1 c

$$\begin{aligned} \bar{I}(\varepsilon) &= -K \sum_{k=1}^{W(\varepsilon)=2} p_k \ln p_k \\ &= -K(\frac{1}{2}\ln(\frac{1}{2}) + \frac{1}{2}\ln(\frac{1}{2})) \\ &= -K(2\frac{1}{2}\ln(\frac{1}{2}) \\ &= -\log_2 e(-\ln 2) \\ &= 1 \end{aligned} \tag{C.3}$$

– For $\varepsilon = \frac{1}{4}$ and $W(\varepsilon) = 4$, and $p_k = \frac{1}{4}$, see figure C.1 d

$$\begin{aligned} \bar{I}(\varepsilon) &= -K \sum_{k=1}^{W(\varepsilon)=4} p_k \ln p_k \\ &= -K(4\frac{1}{4}\ln(\frac{1}{4})) \\ &= -\log_2 e(-\ln 2^2) \\ &= 2 \end{aligned} \tag{C.4}$$

By induction when dividing 1 into N (see equation 4.71):

$$\varepsilon = \frac{1}{N} \tag{C.5}$$

$$\begin{aligned} \bar{I}(\varepsilon) &= -K \sum_{k}^{W(\varepsilon)} p_k \ln p_k \\ &= -K \sum_{k=1}^{W(\varepsilon)=N} \frac{1}{N} \ln(\frac{1}{N}) \\ &= -K \cdot N \cdot \frac{1}{N} \cdot (-\ln N) \\ &= K \ln N = \log_2 e \ln N \\ &= \log_2 N = \log_2 \frac{1}{\varepsilon} \\ \bar{I}(\varepsilon) &= -\log_2 \varepsilon \end{aligned} \tag{C.6}$$

Where, $N = \frac{1}{\varepsilon}$. Next, estimate the Dimension $D(I)$:

$$\begin{aligned} D_I &= \frac{\bar{I}(\varepsilon)}{\ln \frac{1}{\varepsilon}} \\ &= \frac{-\log_2^{\varepsilon}}{\ln \frac{1}{\varepsilon}} \end{aligned} \tag{C.7}$$

By taking the limit of the above function for $\varepsilon \to 0$, the equation will be equal to $\frac{\infty}{\infty}$. Through the L'Hospital's rule we can rewrite it as follow:

$$\begin{aligned} D_I &= \lim_{\varepsilon \to 0} -\frac{\log_2 e \ln \varepsilon}{\ln \frac{1}{\varepsilon}} \\ &= -\frac{\frac{d}{d\varepsilon} \log_2 e \ln \varepsilon}{\frac{d}{d\varepsilon} \ln \frac{1}{\varepsilon}} \\ D_I &= 1 \end{aligned} \tag{C.8}$$

Since it is uniformly distributed along the line (not along 2-D matrix!), missing information (I) and dimension (D) have the maximum entropy along the line (missing information is maximum along the line).

CURRICULUM VITAE

Surname, Name: Pourreza, Elmira
e-mail: e.pourreza@gmail.com
LinkedIn: linkedin.com/in/elmira-pourreza

EDUCATION

Degree	Institution	Year of Graduation
MS	**Middle East Technical University** BioMechanics	2016
BS	**Azad University, Tabriz, Iran** Electric and Electronics Engineering	2011

LANGUAGES

English (Proficient), Turkish (Proficient), Azeri (Native), Farsi (Native)

PUBLICATIONS

1. Pourreza, E., Alshemary, A. Z., Yilmaz, B., Rad, R. M., Tezcaner, A., Evis, Z. Strontium and fluorine co-doped biphasic calcium phosphate: characterization and in vitro cytocompatibility analysis.Biomedical Physics Engineering Express, 3(4), 045004, 2017.
2. Pourreza, E., Cengiz, B. C., Yaradanakul, N.B., Camurdan, A. D., Tas, G. B., Zinnuroglu, M., Gurses, S. "Spatiotemporal Evolution of Infants' Foot Pressure During Learning of Standing." 9th Congress of the European Academy of Paediatric Societies, 7-11 October 2022
3. Pourreza, E., Cengiz, B. C., Camurdan, A. D., Tas, G. B., Zinnuroglu, M., Gurses, S. "Screening Infant Developmental Aspects of Learning During Standing by Measuring Pressure Distribution Beneath the Feet." Orthopedic Proceedings, The British Editorial Society of Bone & Joint Surgery, Vol. 102, No. SUPP 11, pp. 55-55, 2020
4. Pourreza, E., Hassanpour, M., Usual, K. A., Demiroz, F. A., Hohenberger, A., Cakır, M. P. "Eye Movement Analysis in the Simon Task."International symposium on brain and cognitive science, Istanbul, Turkey, 2018